The Dissertation Committee for Josiah D. Couch
certifies that this is the approved version of the following dissertation:

Studies in Holographic Complexity

Committee:

Willy Fischler, Supervisor

Scott Aaronson

Jaques Distler

Can Kilic

Sonia Paban

Studies in Holographic Complexity

by

Josiah D. Couch

DISSERTATION

Presented to the Faculty of the Graduate School of

The University of Texas at Austin

in Partial Fulfillment

of the Requirements

for the Degree of

DOCTOR OF PHILOSOPHY

THE UNIVERSITY OF TEXAS AT AUSTIN

May 2021

Dedicated to the memory of my father, Brian Couch.

Acknowledgments

The number of people who have helped me get to this point and thus write this dissertation is almost certainly larger than my capacity for remembering them. I will nonetheless thank those who come to mind and ask forgiveness of the rest. Firstly, I would like to thank my advisor, Prof. Willy Fischler, for his guidance and for putting up with my tendency towards 'Talmudic exegesis.' Secondly, I would like to thank my esteemed collaborators, who include, in addition to Prof. Fischler, Shira Chapman, Elena Caceres, Stefan Eccles, Yale Fan, Tyler Guglielmo, Juan Hernandez, Ted Jacobson, Robert Myers, Phuc Nguyen, Juan Pedraza, Sarah Racz, Shan-Ming Ruan, Sanjit Shashi, Brian Swingle, Ming-lei Xiao, and Sheng-long Xu. Next, I would like to thank my committee and all the members of the Weinberg Theory Group for their willingness to chat, their many interesting brown bag talks, and their feedback during my talks. I would be remiss not to thank the physics department staff, especially Matt Ervin, Jan Duffy, and AJ Bunyard, for all of their help over the years. Finally, I would like to thank the friends, family, teachers, and advisors who have encouraged me along the way. Among teachers and advisors, Mrs. Lisa Hill, Dr. Andrew Bucki, Dr. Shane Johnson, Prof. Flera Rizatdinova, and Prof. Alexander Khanov come to mind. Many friends have already been mentioned, but I would like to give Georgios Stratis a special thanks for his encouragement during these final stages of my doctoral studies, and to Georgios

as well as Rustam Antia, Abhranil Das, Stefan, Yale, George Miloshevich, and Phuc for feedback on this dissertation and the associated talk. And among my family, I would like to thank my parents, Douglas and Jennifer Woody, my grandparents, Jerry and Eleanor Couch and Orville and Mary Holcomb, my siblings, particularly Ellora, my brother in law Fernie Carmona, and of course my wife Kimberley for supporting and putting up with me through these many years of study. I would also like to thank Kimberley for reading many drafts of my papers and of this dissertation, and for all of her support over the years we've been together.

The work presented in this dissertation was suported by the National Science Foundation through grants PHY-1620610, PHY-1407744, PHY-1708139, and PHY-1820712.

Studies in Holographic Complexity

Publication No. _____

Josiah D. Couch, Ph.D.
The University of Texas at Austin, 2021

Supervisor: Willy Fischler

This dissertation will present the work I have done on the conjectured relationship between various bulk quantities designed to capture the growth of the wormhole in eternal black hole spacetimes and the circuit complexity of the boundary state within the context of the AdS/CFT correspondence, i.e., on the topic of 'holographic complexity.' Four papers are presented here, each focused on the bulk side of this proposed relationship. In these papers, my various co-authors and I seek to improve our understanding of the bulk quantities in question (action of a causal diamond, maximal volume) and test the internal consistency of these proposals and their consistency with our intuition and understanding of the boundary field theory. In particular, the first of these papers focuses on properties of maximal volume slices in black hole spacetimes, along with consequences for the 'complexity = volume' conjecture. The next paper considers whether 'complexity = action' is consistent with the intuition we develop about the time evolution of the boundary circuit complexity in space-times dual to non-commutative field theories. The third paper

deals with a possible relationship between the rate of increase of complexity and the thermodynamic volume of black hole spacetimes. Finally, the last paper deals with restrictions of the 'complexity = action' and 'complexity = volume' conjectures to boundary subregions and their corresponding entanglement wedges and seeks to test the consistency of a conjecture relating these restrictions to the purification complexity of the reduced density matrix.

Table of Contents

List of Tables

List of Figures

Chapter 1

Preliminaries

1.1 Introduction and Structure

This dissertation presents work I have done on the topic of holographic complexity as a Ph.D. student in the Weinberg Theory group at the University of Texas at Austin.

This dissertation will begin with a quick introduction to holography, the AdS/CFT correspondence, the holographic complexity conjectures, and the notion of quantum circuit complexity. The rest of this dissertation will then be dedicated to presenting my own work on the topic of holographic complexity, essentially reproducing [2, 3, 4, 5]. The original appendices to these works are separately reproduced in the appendix to this document.

1.2 The AdS/CFT correspondence

The AdS/CFT correspondence was proposed in 1997 by [6] with [7, 8] following shortly after. The original version of this duality argued that $\mathcal{N} = 4$ super Yang-Mills with gauge group $SU(N)$ in 3+1 dimensions is dual to string theory on an $AdS_5 \times S^5$ background and that the classical weak gravity limit of the string theory (which gives type IIB supergravity) is dual to the strongly

coupled large N limit of the boundary Yang-Mills theory. This correspondence was quickly extended to include many other examples of dualities between d dimensional CFTs (or sometimes QFTs) and d+1 dimensional gravity theories with asymptotically AdS boundary conditions, for instance, the duality between ABJM theory and $AdS_4 \times S^7$ [9]. It has also been extended to dualities between certain other types of field theories and gravity in spacetimes with more general asymptotics. One example of this which will play a role in this dissertation is the duality between non-commutative $\mathcal{N} = 4$ SYM and certain deformed versions of $AdS_5 \times S^5$, first discussed a few years after Maldacena's original paper [10].

In all examples of the AdS/CFT correspondence, the CFT, or boundary theory, can be thought of as living on the timelike asymptotic boundary of the bulk gravity theory. Observables (and other objects of interest) in the bulk and boundary theories are related through the so-called AdS/CFT dictionary. This dictionary relates boundary operators to dual bulk fields (for instance, the boundary stress tensor is dual to the bulk metric), gives a prescription for computing boundary correlation functions from the on-shell bulk action (at large N), and relates thermal states on the boundary to black holes in the bulk (at least above a phase transition). If the correspondence is correct (and all indications are that it is), then any well-formed question about the boundary theory can be answered from bulk information alone and vice-versa. However, it is not always immediately clear what bulk quantity relates to which boundary quantity.

1.2.1 The Ryu-Takayanagi correspondence

One important entry in the AdS/CFT dictionary is the Ryu-Takayanagi(RT) formula [11, 12], which, in the simplest case, relates the entanglement entropy of a boundary region to the area of the minimal surface homologous to that region. The RT surface only works on spatial slices of the bulk about which there is time reflection symmetry but has been generalized in other cases to the Hubeny-Rangamani-Takayanagi (HRT) prescription [13].

1.2.2 subregion-subregion duality and bulk reconstruction

One long-standing goal in the field of AdS/CFT is to determine the bulk geometry dual to a given CFT state from CFT data. While progress has been made on this front, full reconstruction is still elusive. In particular, the parts of the geometry hidden behind horizons have proven particularly tricky to reconstruct.

One of the important questions in AdS/CFT is how to construct the dual bulk geometry given a holographic CFT and a state on that CFT. Much progress has been made towards answering this question by looking at the entanglement structure of the CFT state. This progress was made possible in large part by the RT and HRT formulas and relatedly by the conclusion that a CFT subregion (and a state on it) is dual to the corresponding entanglement wedge in the bulk geometry. However, it is not clear that all bulk regions hidden behind horizons can be reconstructed from entanglement, and likewise, there are aspects of the geometry behind a horizon that seem difficult to cap-

ture in the dual CFT. These facts led Leonard Susskind and collaborators to declare that 'entanglement is not enough' [14] for bulk reconstruction, and ultimately to propose the complexity = volume [14, 15, 16, 17] and complexity = action [18, 19] conjectures.

1.3 Holographic Complexity

1.3.1 Motivation

The two-sided AdS-Schwarzschild black hole is well known in the context of AdS/CFT to be dual to the thermofield double state

$$|TFD\rangle = \frac{1}{\sqrt{Z}} \sum_i e^{-\beta E_i/2} |E_i\rangle_L \otimes |E_i\rangle_R \tag{1.1}$$

on the two CFTs living on the two timelike asymptotic boundaries of the spacetime. Here β is the inverse temperature of the black hole (and the state), the E_i and $|E_i\rangle$ are the energy eigenvalues and eigenkets, the L and R labels refer to the CFT on the left and right boundary respectively, and $\frac{1}{\sqrt{Z}}$ is a normalization factor. There are properties of the two-sided AdS-Schwarzschild geometry for which the CFT dual is highly non-obvious. For example, the spatial 'size' of the portion of the geometry behind the horizon increases indefinitely in time. One way to make this precise to look at the volume of a maximal spatial slice anchored to the left and right asymptotic boundaries at t_L and t_R. As either t_L or t_R is moved to the future, this volume increases indefinitely, as does the portion of the volume that lies behind the horizon. If the AdS/CFT duality holds, there must be some boundary quantity that

captures this growth. Since the boundary theory is simply in the thermofield double state, a 'typical' boundary quantity will tend to be static on time scales much larger than a thermal scale and so won't grow indefinitely. However, the circuit complexity of the state, while it does not grow indefinitely, grows for a time that is exponential in the dimension of Hilbert space. As such, it could provide a good candidate for this growth if we can explain away the discrepancy of the very late time behavior. Susskind argued that on such long time scales, quantum gravity effects become important, and so one should not trust the classical gravity answer in this regime.

1.3.2 Quantum Circuit Complexity

There are two different relevant notions of quantum circuit complexity: that of operator complexity and that of relative state complexity. For both of these, we will need a set of unitary gates $\{g_1, g_2, \ldots, g_n\}$ and a tolerance $\epsilon > 0$. Given such a gate set on a Hilbert space $\mathcal{H}$, a circuit is a finite sequence of gates $Q = g_{i_1} g_{i_2} \ldots g_{i_m}$, and the complexity $\mathcal{C}$ of that circuit is the number of gates that appear in it. To every circuit, we may associate the unitary operator

$$\prod_k g_{i_k} \tag{1.2}$$

which by abuse of notation we will also call Q. Given this, the complexity of an arbitrary unitary operator U is defined as

$$\mathcal{C}(U) = \min_{Q:||U-Q||\leq\epsilon} \mathcal{C}(Q) \tag{1.3}$$

Where we can take $||\cdot||$ to be the operator norm. This, of course, defines operator complexity. Given states $|\psi\rangle$ and $|\phi\rangle$ on $\mathcal{H}$, we can also define the state complexity of $|\psi\rangle$ relative to state $|\phi\rangle$ as

$$\mathcal{C}(\psi|\phi) = \min_{U:U|\phi\rangle=|\psi\rangle} \mathcal{C}(U). \tag{1.4}$$

Often, we will fix a reference state $|r\rangle$, and then the complexity of a state $|\psi\rangle$ will be understood as the complexity relative to the reference state, i.e.

$$\mathcal{C}(\psi) := \mathcal{C}(\psi|r). \tag{1.5}$$

A few notes now on the gate set in the definitions above. First, we will typically assume that the gate set is closed under taking inverses, which gives us the nice property that

$$\mathcal{C}(U) = \mathcal{C}(U^{-1}) \tag{1.6}$$

and likewise that

$$\mathcal{C}(\psi|\phi) = \mathcal{C}(\phi|\psi). \tag{1.7}$$

This further ensures that complexity almost gives us a metric on $U(\mathcal{H})$, in the sense that it provides a metric on the subgroup generated by the gateset[1]. This metric is nothing but the word metric [20] on the relevant finitely generated subgroup. Second, the 'gates' in the gate set are not what are typically referred to as a quantum gate (e.g., the Hadamard gate) because the latter are

[1]It does not give a metric on all of $U(\mathcal{H})$ precisely because this group is not finitely generated, and so we cannot construct every unitary exactly with a circuit. If the gate set is universal, we can construct any unitary to within ϵ, but this is not good enough to get a metric

typically defined on small tensor factors of the whole Hilbert space. Keeping the example of a Hadamard gate H, which is defined on $\mathbb{C}^2$, if our Hilbert space were $\mathcal{H} = \mathbb{C}^{2N}$, then to include the Hadamard gate, our gate set above would have to include all of the operators of the form $\mathbb{I}^{2k} \otimes H \otimes \mathbb{I}^{2(N-k-1)}$ (where $\mathbb{I}^M$ is the identity on $\mathbb{C}^M$), and in our definitions above each of these operators would function as a separate gate.

1.3.3 The conjectures

Complexity = Volume

The *Complexity = Volume* (CV) conjecture [14, 15, 16, 17], developed by Leonard Susskind in collaboration with Douglas Stanford and Ying Zhao, states that the circuit complexity of the CFT state dual to an asymptotically AdS geometry on a time slice σ of the asymptotic boundary of that geometry is proportional to the volume of the maximal volume Cauchy slice of the bulk geometry anchored at σ.

Complexity = Action

The *Complexity = Action* (CA) conjecture [18, 19] was developed as a potential improvement on the CV conjecture by Susskind and Zhao along with Adam Brown, Daniel Roberts, and Brian Swingle. It states that the action, rather than being proportional to a maximal volume slice as in CV, is instead proportional to the bulk action evaluated on the domain of dependence of such a slice, i.e., the *Wheeler-DeWitt patch*.

Chapter 2

Holographic Complexity and Volume

2.1 Introduction

[1]The AdS/CFT correspondence [6, 8, 7] provides a satisfying duality between a black hole in asymptotically anti de-Sitter spacetime and a thermal state of a CFT, in which the entropy of the black hole is dual to ordinary thermal entropy. What remains obscure, however, is the relation between the black hole interior and the physics of the CFT. Aside from its (semiclassical) causal isolation, the interior has two qualitative features that one would like to understand from the viewpoint of the CFT: the curvature singularity, and the growth of space. The latter follows from the well known peculiar fact that the symmetry of time flow outside the horizon becomes a space translation symmetry inside. Under this symmetry flow, exterior time elapses, and the length of a spacelike curve at a fixed interior radius grows, with a rate that increases without bound as the fixed radius approaches the singularity. Susskind observed [15, 14, 16, 18, 19] that this growth should be reflected somehow in the CFT, because it can be captured by a gauge invariant observable of the

[1]This chapter reproduces [2], which I wrote in collaboration with Stefan Eccles, Ted Jacobson, and Phuc Nguyen. My contribution to this work was largely to assist with the computations.

bulk gravity theory. He proposed that it corresponds to the computational complexity of the state of the CFT, which continues to grow, after statistical equilibrium is reached, for a time that is exponential in the entropy.

This proposal was quickly refined to "CV-duality", according to which the complexity at a given boundary/CFT time is proportional to the volume of the maximal slice enclosed within the corresponding "Wheeler-DeWitt patch," i.e., within the domain of dependence of a spacelike bulk hypersurface that asymptotes to the given boundary time slice[2]. Shortly thereafter, the alternative postulate of "CA-duality" was introduced, according to which complexity is equal to the action of the Wheeler-DeWitt patch (see [21, 22, 23, 24, 4] for a selection of recent work on these two proposals [3]). Both of these proposals predict a rate of growth of the complexity at late time that roughly agrees with general expectations.

There is reason to expect that the rate of complexification for a CFT in equilibrium scales as $TS/\hbar$, the product of the temperature T and the entropy S [15]. The entropy counts the number of 'active' degrees of freedom, and $\hbar/T$ is the timescale for thermal fluctuations. If each such fluctuation counts as the execution of a quantum gate on active degrees of freedom, then the number of gates executed per unit time is $\sim TS/\hbar$, which is thus the rate at which the complexity of the state increases. In order to match this rate, the complexity

[2]In this paper, we systematically use the term "slice" to refer to spacelike codimension-1 submanifolds.

[3]See also [25] for the consideration of complexity in a related but somewhat different context involving black holes.

for black holes that are large compared to the AdS radius ℓ should be given in terms of the volume of the maximal slice by [14]

$$\mathcal{C} \sim \frac{V}{\hbar G \ell}. \tag{2.1}$$

In equilibrium, the maximal slice approaches a final maximal cylinder inside the horizon, with fixed cross-sectional area and a proper length that grows in proportion to Killing time. The above formula equates the complexity to this area, measured in Planck units, times the proper length of the cylinder, measured in AdS length units. For black holes small compared ℓ, the complexity should instead be given by[4]

$$\mathcal{C} \sim \frac{V}{\hbar G r_+}, \tag{2.2}$$

so that the proper length of the cylinder is measured in horizon radius units r_+ [14]. Unlike the case for large black holes, this depends upon the black hole size. This discrepancy is a principal reason for preferring CA over CV. The fact that the volume divisor in CV is ℓ for large black holes, but r_+ for small black holes, indicates an apparent lack of universality.

However, in both cases this divisor actually corresponds to an intrinsic property of the black hole: the maximum time τ_f to fall from the horizon to the final maximal cylinder is $\sim r_+/c$ for spherical black holes with $r_+ \leq \ell$ in $D \geq 4$ dimensions, and $\sim \ell/c$ for black holes with $r_+ \geq \ell$.[5] Hence the complexity

[4]For small black holes, the "late time" complexification rate refers to times longer than the thermal timescale but much shorter than the evaporation timescale.

[5]An alternative but related divisor would be the proper time from horizon to final slice along the volume flow. This scales the same way with respect to the black hole parameters as the longest time, but the numerical factor differs.

formulae (2.1) and (2.2) actually coincide, up to an order unity numerical factor, if the length in the denominator is understood as $d_f := c\tau_f$. That is, in computing the complexity, the length of a section of the final cylinder ΔL_f should be measured in units of the maximal time to fall from the horizon to the cylinder. The universal expression for the late time complexity is thus

$$\mathcal{C} \sim \frac{V}{\hbar G \tau_f} = \frac{A_f}{\hbar G} \frac{\Delta L_f}{\tau_f}, \tag{2.3}$$

where A_f is the cross-sectional area of the final slice. It turns out that A_f equal to the horizon area A_H up to an order unity factor, so that $A_f/\hbar G \sim S_{\rm BH}$ can be identified with the black hole entropy, which is dual to the CFT entropy. The remaining factor in (2.3) is then $\Delta L_f/\tau_f$. In Sec. 2.3.4 we will show that, quite generally,

$$\frac{\Delta L_f}{\tau_f} \sim \kappa \Delta t \sim \frac{T_H}{\hbar} \Delta t, \tag{2.4}$$

where κ is the surface gravity, Δt is the elapsed Killing time, and T_H is the Hawking temperature of the black hole, which is dual to the CFT temperature. With these results, the expression (2.3) for complexity thus becomes

$$\mathcal{C} \sim \frac{T_{\rm H} S_{\rm BH}}{\hbar} \Delta t, \tag{2.5}$$

yielding the black hole dual of the expected complexification rate.

While the universality of the divisor τ_f is more satisfying than the previous ad hoc prescription, it should be admitted that we have no rationale for measuring the length of the final slice in units of τ_f, other than that gives the desired result. Another potential drawback is that this prescription only

applies to defining the complexity when the state at late times is thermal equilibrium, so that a 'final' maximal slice exists. In a general dynamical setting, this prescription is inapplicable (although as discussed in Sec. 2.5.4 it *can* be applied in empty AdS, using the boost Killing field to define the notion of equilibrium). That said, as discussed in the next section, the notion of complexity itself is more ambiguous outside of a thermal setting, so it is not clear whether we should expect it to admit a universal holographic definition.

The CV proposal thus remains interesting, as it passes the same checks as does the CA proposal, in some cases (regarding monotonicity on a stationary background) even better as discussed in Sec. 2.4.0.1. The purpose of this paper is to take a closer look at various aspects of the CV proposal, attempting to sharpen it and offer some interpretation of its definition and properties, as well as to extend the tests of it.

For both conceptual and computational reasons, we shall make use of a *volume current*, whose flux through the bulk maximal slices anchored at a boundary foliation is equal to the volume of those slices. This volume current is a unit, timelike, divergence-free vector field orthogonal to the bulk maximal foliation. Our interest in the role of this current was inspired by recent work of Headrick and Hubeny (HH) [26], which established a "min-flow/max-cut" theorem relating volumes of maximal slices to minimal fluxes of timelike, divergence-free, vector fields with norm bounded below by unity ("HH flows"). In Ref. [26], it was remarked that it is natural to relate minimization of the number of gates in defining the complexity of a state, in a dual field theory,

to minimization of the flux of an HH flow in the bulk spacetime, suggesting a "gate-line" picture of holographic complexity. In this picture, our volume current would correspond to a "gate current".

Let us briefly describe here the HH theorem and its relation to our volume current. The theorem states roughly that, given boundary sub-region A, the maximal spatial volume of any slice homologous to A is equal to the minimal flux of an HH flow through the slice or (equivalently) through A. A given minimizing HH flow has unit norm on the corresponding maximal volume slice, and is orthogonal to that slice, but it is not otherwise uniquely determined. By contrast, the volume current we employ is a particular realization of an HH flow, determined by a boundary foliation, and its flux gives the volume of each slice of the corresponding maximal bulk foliation. That volume is not conserved, because there is flux through the cutoff boundary of the bulk region.

Although the HH theorem assumes the spacetime is orientable and time-orientable, and assumes a maximal volume slice exists, its proof does not directly invoke any causality assumption or energy condition on the spacetime. By contrast, the volume current requires the existence of a foliation by maximal slices. We argue in Appendix A.1 that such a foliation exists if i) maximal slices exist, ii) the spacetime satisfies a causality condition, and iii) the strong energy condition and Einstein equation hold. If the foliation is known to exist, then the HH theorem is a simple consequence: the flux of any HH flow is lower-bounded by the maximal volume (for a given boundary Cauchy slice), and the

theorem asserts that this bound is actually saturated. The volume current, when it exists, saturates this bound, so our results can be viewed as providing a *constructive* proof of the HH theorem under certain additional assumptions.

The remainder of this paper is structured as follows. Section II confronts the ambiguity in defining complexity. The notion seems most robust when applied to time evolution of thermal states, and we summarize several reasons for thinking the volume inside a black hole horizon captures the relevant quantity. Section III introduces the volume current, a useful tool for quantifying properties of maximal volumes and their evolution, and obtains several results using it. One of these is evidence for the flow of complexity from UV to IR in holographic CFTs. Section IV deduces a global inequality on maximal volumes, and uses this to establish the monotonic increase of the rate of volume growth on a boost invariant background. Section V probes CV duality in three settings: black hole formation with one or two shells of matter, spinning black holes, and empty AdS viewed as a pair of thermal Rindler wedges. Section VI is a brief conclusion and outlook. In Appendix A it is argued, assuming the existence of maximal slices, a causality condition and the strong energy condition, that a boundary foliation determines a maximal volume bulk foliation. The unit vector field normal to this foliation is the volume current. The remaining three appendices derive useful technical results. For the balance of this paper we use Planck units, with $\hbar = c = G = 1$.

2.2 Volume inside and outside the horizon

The complexity of a pure quantum state is a measure of how many simple unitary operations, or "gates," it takes to produce it, starting with some reference state [27, 28, 29]. Hence, in general, complexity is defined only relative to the choice of reference state and the choice of gates. The original motivation for the proposal of CV duality pertained to time development of complexity at the thermal scale in a finite temperature pure state. In this context, the reference state could presumably be taken to be the thermal microstate at any fixed time, and the gates could be taken to be a fixed collection of gates that act at the thermal energy and length scales, so the rate of change of complexity is intrinsically defined without significant arbitrariness.

However, the CV proposal encounters a divergence in asymptotically AdS spacetime, where the volume of a maximal slice diverges at spatial infinity. This divergence occurs for any state and, according to the usual UV-IR relation in AdS/CFT duality, it would presumably correspond, according to CV duality, to a divergent UV complexity of the CFT vacuum. While the vacuum is simply the ground state of the theory, it is complex if considered as a state to be prepared, starting with a spatially unentangled state, by the application of local quantum gates. Some analysis has suggested that this interpretation of the UV limit of CV duality might be sensible [24], although the volume-complexity relation could be infinitely sensitive to the somewhat arbitrary definition of the reference state and gates, and to sub-leading modifications of the short distance structure of the state [30, 31].

The volume divergence has generally been dealt with in the literature by imposing a cutoff at some large radius, and focusing on the time dependence of the volume, which does not depend on the location of the cutoff. This corresponds, in effect, to taking the reference state to be the vacuum above the cutoff energy scale, and some "unentangled" state below that scale. The rate of change of the volume in a stationary, thermal state at late times is independent of the location of the cutoff, because the volume growth all happens inside the horizon of the black hole. For this reason, and several others, it makes a lot of sense to count only the volume behind the horizon:[6]

- It is only the complexification rate at the thermal scale that appears to have a robust significance, independent of the arbitrary choices of reference state and gates.

- The complexity divisor of the volume, as explained in the introduction, is universal when recognized as a free-fall time from the horizon to the final maximal slice.

- The stationary state volume growth at late time occurs behind the horizon. This was explained in a picturesque way in [14], where it was referred to as "unspooling complexity" from the horizon.

- If the reference state is the vacuum, then only black hole states have complexity that scales as $O(N^2)$ in the CFT. This suggests that holo-

[6]It was also noted in Ref. [17] that the volume divergence can be regulated by counting only the volume behind the horizon.

graphic complexity (with a vacuum reference state) should, at leading order in N, be associated only with black holes, and that the relevant volume in CV duality should be only that located behind a horizon.

- For a two-sided black hole, a natural reference state is the thermofield double, which is dual to the "Euclidean vacuum" for this topology in the bulk [32, 33, 34]. The maximal bulk slice corresponding to this state is a global time slice invariant under time reflection (like the $t = 0$ slice in Schwarzschild coordinates), which does not enter the (future or past) horizon, and therefore has zero volume behind the horizon. The volume behind the horizon thus gives the "right" result: the complexity vanishes, since the reference state by definition has zero complexity, but it grows if the time on one boundary is boosted relative to that on the other.

- A "second law of complexity" [35, 36] follows directly when the horizon is a causal barrier, as discussed in the next section.

- The volume inside a white hole horizon can also contribute to the complexity, as in the shockwave scenario discussed below. This allows for *decreasing* complexity, when such behavior is expected.

When applied in a general, time dependent setting, the proposal that complexity corresponds only to the volume behind the horizon suffers from a major drawback, however, if we use the *event horizon*, because the volume inside can grow *before* anything changes in the CFT, at the boundary of the

maximal slice. This is illustrated by an example in Sec. 2.5.1 We therefore propose to use an "apparent horizon" as the cutoff surface when there is time dependence. We follow the prescription, used previously in the literature, of measuring the volume on leaves of a foliation of the spacetime by spacelike hypersurfaces that maximize the volume inside an outer cutoff boundary. The apparent horizon is then defined as the boundary of the region containing trapped surfaces on each leaf of this foliation. In (quasi)stationary black hole spacetimes, this apparent horizon will (nearly) coincide with the event horizon. A component of the apparent horizon that asymptotes to the event horizon consists of points lying on marginally outer trapped surfaces [37].

When focusing on the volume inside the horizon, we are limited to discussing the growth of complexity in states dual to a spacetime with a horizon. This is not as restrictive as it might seem, since even empty AdS is a thermal state, when viewed as a pair of Rindler wedges. Indeed, the much studied account of complexity increase for the two-sided black hole can be adapted in a straightforward manner to the Rindler case, where the relevant volume is that inside the Rindler horizon. The interpretation in this case appears to be fully consistent with that for black holes, as we explain in Sec. 2.5.

So far we have been referring to the volume inside the black hole horizon, which is relevant for late time equilibrium states. However an important test for any proposed holographic dual of complexity is that it exhibit the switchback effect [16], which brings the white hole horizon into play. The switchback effect refers to a small time-deficit in the growth of complexity,

of order twice the "scrambling time", when a state is evolved backwards in time, perturbed relative to the reference state, and then evolved forwards in time. The calculations in [16] demonstrated that the volume of maximal slices does holographically capture the switchback effect for the thermofield double state, and in particular the maximal volume slices can traverse the black hole region on one side of the shock, and the white hole region on the other side. In the late time approximation used in [16], the portion of the maximal slice outside the horizons does not contribute to the total volume, because it is null, as illustrated in Fig. 2.1. Hence the volume inside the black and white hole

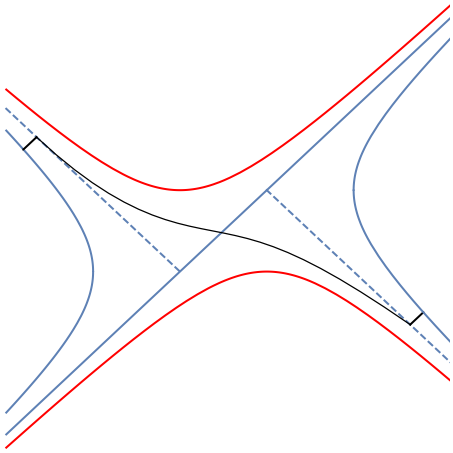

Figure 2.1: Shockwave geometry dual to a perturbed thermofield double state, with a maximal volume hypersurface anchored at late time on the left and early time on the right.

horizons suffices to capture the switchback effect. In general, therefore, our proposal must be taken to include the volume inside the white hole horizon. This appears somewhat natural, considering the fact that the derivation of the switchback effect involves reversed time evolution, and the time reverse of a

black hole is a white hole.

Finally, although it appears difficult to relate the volume outside the horizon to a definition of complexity of the state in a universal manner, the assumption that such a relation exists leads to the interesting picture of complexity flowing from UV to IR, as explained in the following section.

2.3 Volume current

While the volume of maximal slices is a nonlocal construct, there is an associated local object, the "volume current," which can be used to infer the volume growth behind the horizon and the second law of complexity, and which is suggestive the UV to IR flow of complexity. In this section we introduce the volume current, and use it to establish several important properties of the proposed CV duality.

A volume current will be defined given a foliation of spacetime by spacelike hypersurfaces with maximal volume. In the present application, we are interested in asymptotically AdS spacetimes, in which a maximal foliation is determined by a Cauchy foliation of the boundary by slices orthogonal to an asymptotic Killing flow defining time translation. Provided that there is a unique bulk maximal slice that terminates on any fixed boundary Cauchy slice, and provided these bulk slices do not skip over a "gap" in the bulk, the boundary foliation induces a bulk foliation by maximal slices Σ_t, labeled by a parameter t.

We establish the existence of such a bulk foliation by a reasonably convincing—if not mathematically rigorous—series of arguments in Appendix A.1. To rule out the possibility of gaps we will need to assume that the timelike convergence condition (which is equivalent to the strong energy condition modulo the Einstein equation) holds. Whether or not a global foliation exists, our construction can be applied to the portion of spacetime prior to the final slice that is foliated without a gap. The divergence of the unit timelike vector field v orthogonal to the bulk foliation is the trace of the extrinsic curvature K of Σ_t, which vanishes since the slices are assumed to be maximal. This vector field is thus a conserved current, which we dub the *volume current* associated with the maximal foliation. The volume of Σ_t is the flux of this current through Σ_t,

$$V_t = \int_{\Sigma_t} v \cdot \epsilon. \tag{2.6}$$

(Here ϵ is the spacetime volume element, and the dot indicates contraction on the first index of ϵ.) The construction of the volume flow v, starting from a boundary foliation, is illustrated in Figure 2.2.

As discussed in Sec. 2.2, to obtain a finite volume, and hence a finite putative complexity, the integral must be cut off at some outer boundary $\partial\Sigma_t$. We will continue to use the letter "V" for this truncated volume.

2.3.1 Second law of complexity

Since the divergence of v vanishes, the change ΔV from one time slice to another is entirely accounted for by the flux of v through the boundary, or

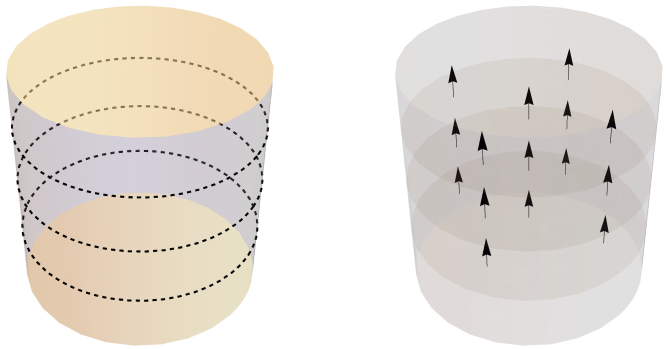

Figure 2.2: Left: Illustration of the boundary foliation $\Sigma(\tau)$ with 3 slices in the foliation. Right: Illustration of the corresponding bulk foliation by maximal slices, and the volume flow.

boundaries, of that slice. If we restrict to the volume inside the horizon, then the change is accounted for by the flux of v through the horizon. Since v is a future pointing timelike vector, the flux through the future event horizon is positive, and it follows that the interior volume can only increase. When considering a spacelike portion of the apparent horizon forming a past boundary of the trapped region, again the flux is positive. CV duality then implies that in these situations, the complexity must increase, in accordance with the second law of complexity [35, 36]. Note that this argument applies in arbitrary dynamical black hole spacetimes, such as a black hole formed by collapse. If, however, the apparent horizon has a timelike section, which can happen when a black hole evaporates, and even when positive energy conditions hold [37], then we cannot rule out a decrease in the volume enclosed. This seems natural: when this horizon is not a causal barrier, there is no reason to expect the

associated complexity to irreversibly increase.

Note that when the region behind the horizon includes the white hole, as with the two-sided black hole with a shockwave of Figure 2.1, the complexity can *decrease* as time increases on the side opposite to the shock [16]. Correspondingly, the volume of the maximal slice inside the white hole decreases, since the volume current can only exit the white hole horizon.

2.3.2 Complexity flow from UV to IR

The flux of the volume current inward across the horizon suggests a picture of complexity flowing from UV to IR, which is further corroborated by examination of the flux through other surfaces. Consider the section of a maximal slice Σ_t stretching between the horizon of a black hole and the outer cutoff boundary in asymptotically AdS spacetime. The rate of complexification of the thermal degrees of freedom should not depend upon where the cutoff surface is placed, because that just changes the constant complexity assigned to the degrees of freedom that are in their ground state. Holographically, this works because at sufficiently large radius, as explained below, v is invariant under the asymptotic Killing flow. The volume between two large radii is thus independent of time, which implies that the flux of v through the boundary is independent of its (large) radius. Moreover, at sufficiently late times, as also explained below, v is invariant under the Killing flow *everywhere*, including on and inside the horizon. The flux of volume through the horizon is therefore equal to the flux through the outer boundary at the UV cutoff. According to

CV duality, *the complexity thus flows from the UV to the IR, and accumulates at the thermal scale*.

This conclusion may be related to the fact that, in a holographic CFT, thermalization proceeds from UV to IR [38, 39]. On the other hand, it seems to be somewhat in tension with the fact that in a thermal state the UV degrees of freedom remain unexcited. If unexcited, how could they participate in the generation of complexity? Perhaps since their excitation is not strictly zero, but only exponentially suppressed, their dynamics could provide the source from which the complexity unfolds. Or is complexity generated purely from the thermal scale fluctuations? And if the latter is the case, then how can we understand the dual flow of the volume current from large to small radii? We leave these questions to be addressed in the future.

2.3.3 Asymptotic and late time volume flow on stationary spacetimes

At sufficiently large radius v is invariant under the asymptotic Killing flow, because the maximal slices must asymptote to the boundary slices defining the maximal foliation, which are taken into each other by the Killing flow. Nevertheless, in the two-sided eternal black hole spacetime, the Killing flow does not push both boundary slices to the future together, so in general the slices of the corresponding maximal foliation are not related by the Killing flow. However, at sufficiently late times the foliation becomes invariant under the Killing flow. This can be seen from the fact that the maximal slices approach

the final maximal slice inside the horizon, and the final slice is taken into itself under the Killing flow. In Appendix A.3, we demonstrate these claims by explicit computation with the AdS-Schwarzschild black hole. Figure 2.3 shows a plot of the volume current for the BTZ black hole, based on the analytical expression derived in A.2.1. This figure illustrates the asymptotic invariance

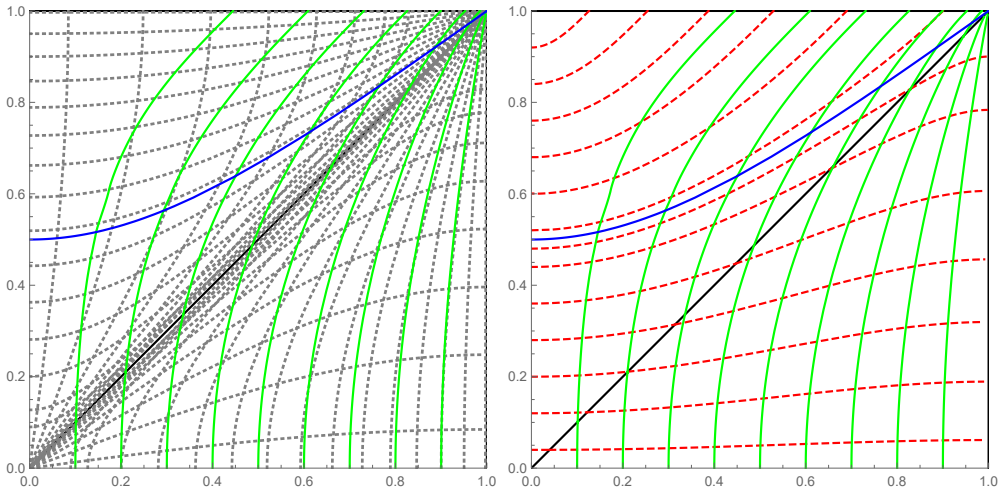

Figure 2.3: Plot of the flow lines of the BTZ volume current (in solid green) on a quarter of a Penrose diagram. Left: the flow lines are shown together with the Schwarzschild coordinate grid lines (dotted black), and the final slice (solid blue). Right: the flow lines are shown together with the maximal slices (dashed red).

under the Killing flow at the boundary and as the final slice is approached.

The late time limit of this flow can be easily found in closed form in spherical symmetry, where it is given by $v = v^t\partial_t + v^r\partial_r$ in Schwarzschild coordinates. The normalization condition $v^2 = -1$ determines v^t in terms of v^r. At late times the components are independent of t, and the divergence free condition implies $v^r = -K/r$ where K is some constant. K can be determined

by the normalization condition $g_{rr}(v^r)^2 = -1$ on the $t = 0$ line in the middle of the black hole interior region since, by symmetry, v^t vanishes there. Because we have assumed the late time limit, this must be done at the "final slice" [16, 14], which is the maximal slice at constant r in the black hole interior. For example, in the non-rotating case of the BTZ black hole treated in Sec. 2.5 we have

$$K = r_f \alpha_f = r_+^2/2\ell. \tag{2.7}$$

where α_f is the norm of the Killing vector ∂_t at r_f.

The constant K gives the rate of volume flow, with respect to Killing time, per unit angle, through any surface of constant r coordinate, e.g. the horizon. To see this, note that the volume flux is given by the integral of $v \cdot \epsilon$ pulled back to the constant r surface. In t, r, ϕ coordinates, $\epsilon = r\, dt \wedge dr \wedge d\phi$, so this pullback is $-rv^r\, dt \wedge d\phi = K\, dt \wedge d\phi$. This conclusion generalizes to spherical black holes in any spacetime dimension.

2.3.4 Asymptotic volume growth and complexity

For the BTZ black hole [40], the K written above can be expressed in terms of the surface gravity $\kappa = r_+/\ell^2$ and the horizon area $A = 2\pi r_+$ as

$$K = \ell\kappa A/4\pi = 2\ell T_{\mathrm{H}} S_{BH}, \tag{2.8}$$

where T_{H} and S_{BH} are the black hole temperature and entropy, respectively. In this way, we can see that the late-time rate of growth is 2ℓ times $T_{\mathrm{H}} S_{BH}$. The factor ℓ is the "divisor," discussed in the introduction, that gives the ratio of volume to complexity.

The fact that $K \propto \ell T_{\rm H} S_{BH}$ is not an accident. It could be anticipated from the first equality in (2.7). In fact, that equality generalizes to a D dimensional spherically symmetric spacetime, where

$$K = r_f^{D-2} \alpha_f, \tag{2.9}$$

and to black holes of any size. This can be used to understand why, as mentioned in the Introduction, the ratio of volume to complexity should be the maximal proper time from the horizon to the final slice for black holes of any size. The factor r_f^{D-2} is the area per solid angle of a cross section of the final slice. It turns out that $r^{D-2}\alpha(r)$ reaches its maximum not far from the horizon, so we have $r_f \sim r_+$. The first factor in (2.9) therefore scales as the horizon area per solid angle, times a numerical constant. The factor α_f is the norm of the Killing vector ∂_t at the final slice. The Taylor expansion for α around the horizon is $\alpha = \kappa\tau + \ldots$, where τ is the proper time from the horizon, in the direction orthogonal to the Killing flow.[7] Thus, for both large and small spherical black holes in any dimension, the volume grows at a rate

$$K \sim \tau_f \kappa A_+ \sim \tau_f T_{\rm H} S_{BH} \tag{2.10}$$

where the symbol $\sim$ denotes equality up to numerical constant that depends on spacetime dimension and is different for large and small black holes. Since complexity is expected to grow in the dual CFT at the rate $\sim TS$, we conclude

[7] Quite generally, $\kappa = |d\alpha|_{\rm horizon}$, where α is the norm of the horizon generating Killing vector. Usually one sees this relation applied to the gradient in the spacelike direction from the bifurcation surface, but it can equally well be applied in the timelike direction as done here.

that the ratio of volume to complexity should be τ_f (i.e. $\hbar G\tau_f$). In section 2.5.3 we show that this reasoning also applies to the Kerr metric (with vanishing cosmological constant).

2.3.5 Maximal time from horizon to final slice

In this subsection we first compute the maximal time τ_f from the horizon to the final slice for hyperbolic, planar, and spherical Schwarzschild-AdS black holes. We next give a general argument, analogous to that used in Hawking's cosmological singularity theorem, showing that for any black hole in a spacetime with negative cosmological constant Λ, and satisfying the strong energy condition for matter other than the cosmological constant, $|\Lambda|^{-1/2}$ sets an upper bound for the value of τ_f.

2.3.5.1 Schwarzschild-AdS black holes

The value of τ_f for Schwarzschild-AdS black holes is given by the proper time from r_+ to r_f along the line $t = 0$:

$$\tau_f = \int_{r_f}^{r_+} \frac{dr}{\alpha(r)}. \tag{2.11}$$

To estimate the value of this integral, we may use the Taylor expansion about the horizon. The line element has the form $ds^2 = -\alpha^2\, dt^2 + \alpha^{-2}\, dr^2 + r^2 h_{ij} dx^i dx^j$, and $(d\alpha^2/dr)_+ = (-2d\alpha/d\tau)_+ = -2\kappa$, so

$$\tau_f \approx \frac{1}{\sqrt{2\kappa}} \int_{r_f}^{r_+} \frac{dr}{\sqrt{r_+ - r}} = \frac{\sqrt{2(r_+ - r_f)}}{\kappa} \sim \frac{\ell r_+}{\sqrt{(D-1)r_+^2 + (D-3)k\ell^2}}, \tag{2.12}$$

where $k = -1, 0, 1$ for hyperbolic, planar, and spherical black holes, respectively. Thus for the BTZ black hole ($D = 3$) or planar black holes, or hyperbolic or spherical black holes with $r_+ \gg \ell$, we have $\tau_f \sim \ell$. If instead $r_+ \ll \ell$ and $D \neq 3$ and $k \neq -1$, then $\tau_f \sim r_+$.

The case of small hyperbolic black holes should be treated separately: this case has an extremal limit, i.e. a lower bound for r_+ of the order of ℓ [41]. The estimate for τ_f above assumes that $r_+ - r_f \sim r_+$ upto some order unity factor, but $r_+ - r_f = 0$ at extremality. A computation expanding around extremality (similar to that for the Kerr case treated below in section 2.5.3) shows that $\tau_f \sim \ell$ for the extremal hyperbolic black hole.

2.3.5.2 Upper bound to τ_f set by the AdS scale

It is interesting to note that an upper bound of the form $\tau_f \lesssim \ell$ follows from a more general result. Consider the future domain of dependence $D^+(S)$ of any achronal spacelike surface S (not necessarily a Cauchy slice for the whole spacetime). $D^+(S)$ is itself a globally hyperbolic spacetime, so Theorem 9.4.5 in [42] tells us that any point p in $D^+(S)$ lies on a curve that maximizes the time to S, and Theorem 9.4.3 implies that this curve is a geodesic that meets S orthogonally, without a conjugate point between p and S. Integration of the Raychaudhuri equation for the congruence of geodesics orthogonal to S then shows that, regardless of the value of the trace of the extrinsic curvature of S (which is the expansion of this congruence evaluated at S), each geodesic must have a conjugate point within a time $\int_{-\infty}^{\infty} d\theta/(\theta^2/2 + R_{ab}u^a u^b)$. To obtain

this we neglect the squared shear term in the Raychaudhuri equation, since it would only make the time shorter. If there is a negative cosmological constant $\Lambda = -(D-1)(D-2)/2\ell^2$, and if the matter stress energy tensor satisfies the strong energy condition and the Einstein equation holds, then by neglecting the matter contribution we obtain the upper bound $\pi\sqrt{D-2}/\sqrt{-\Lambda} = \sqrt{\frac{2}{D-1}}\pi\ell$ to the time. No point inside $D^+(S)$ can lie at a time greater than this from S. For example, this result applies to the domain of dependence of a Cauchy slice for an asymptotically AdS spacetime, also known as the "Wheeler deWitt patch".

To derive an upper bound for τ_f, we can apply this result to the case where the achronal surface S is a spacelike slice just inside the future horizon H of the black hole. As long as the final slice lies inside $D^+(H)$,[8] we obtain the upper bound

$$\tau_f \leq \sqrt{\frac{2}{D-1}}\pi\ell. \tag{2.13}$$

For $D = 3$ this becomes $\tau_f \leq \pi\ell$, which is consistent with the exact result $\tau_f = \pi\ell/4$ obtained in section 2.5.2 for the rotating BTZ black hole.

[8] If $D^+(H)$ does not contain everything inside the event horizon, there is a Cauchy horizon, which is presumably unstable to formation of a singularity, eliminating the Cauchy horizon.

2.4 Global volume inequality and complexification rate monotonicity

In this section we discuss a global inequality relating the volume on different slices, which leads to an inequality on mixed partial derivatives with respect to boundary time. On a boost symmetric background, this allows us to obtain an inequality for the second time derivative of the volume, which implies that the complexification rate grows monotonically on boost invariant black hole backgrounds. We thus recover from a general viewpoint this fact found previously using explicit computations with eternal black holes in AdS. To derive the global volume inequality, we need only use the definition of maximal slices; no energy condition or other additional ingredient is needed. Consider for concreteness a compact box in an eternal black hole spacetime (Figure 2.4), with the vertical sides of the box taken to be some near-boundary cutoff. Let t_1, t_2 be two times on the left cutoff (with $t_1 < t_2$), and t_3, t_4 be two times on the right cutoff (with $t_3 < t_4$). The inequality then says that

$$\mathrm{Vol}(t_1, t_3) + \mathrm{Vol}(t_2, t_4) - \mathrm{Vol}(t_1, t_4) - \mathrm{Vol}(t_2, t_3) \geq 0, \tag{2.14}$$

where $\mathrm{Vol}(t_1, t_3)$ is the maximal volume between time t_1 on the left and time t_3 on the right, etc. Note that, even though each of the four maximal slice volumes diverges as the cutoff is sent to the boundary, the linear combination in (2.14) is UV-finite.

To establish the inequality, observe that the two dashed orange slices in Fig. 2.4 intersect each other, and we can divide them into four segments,

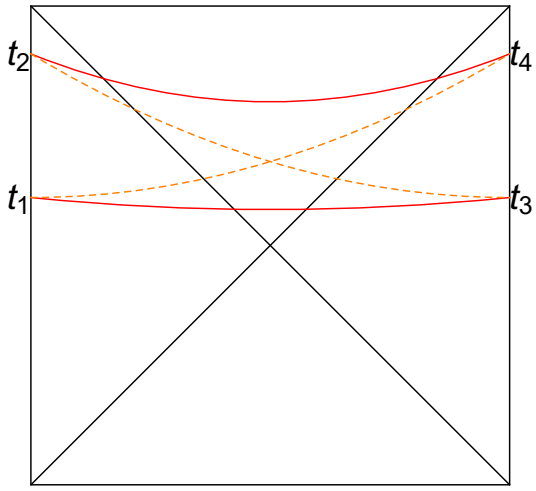

Figure 2.4: An SSA-like inequality is obeyed between the four maximal slices shown (solid red and dashed orange).

each connecting the intersection with one of the four boundary times. By maximality, we know that $\mathrm{Vol}(t_1, t_3)$ is greater than the sum of the volumes of the two lower orange segments. Similarly, we know that $\mathrm{Vol}(t_2, t_4)$ is greater than the sum of the volumes of the two upper orange segments. The sum of these two inequalities yields (2.14).

This example of a global volume inequality can be generalized to a general bulk spacetime, with one or more boundary components. We illustrate this in Figure 2.5 for a spacetime with one boundary. Let σ_1 and σ_2 be two Cauchy slices of the boundary, and let Σ_1 and Σ_2 be the corresponding maximal slices. (As before, we regulate the volume by placing a cutoff surface in the asymptotic region.) Assuming the bulk is time orientable, it admits a foliation by timelike curves, which also extends to the boundary. Each of these curves

intersects each of the Cauchy slices once. On the boundary define two new piecewise smooth Cauchy slices σ_- and σ_+, consisting of the first and second intersection points respectively, and similarly define two new bulk slices (which are also only piecewise smooth), Σ_- and Σ_+. Then the boundary of $\Sigma_\pm$ is $\sigma_\pm$, and $\Sigma_\pm$ is generally not the maximal volume slice with this boundary. Generalizing the previous notation, let $\mathrm{Vol}(\sigma)$ denote the maximal volume for a slice bounded by σ, and now let $\mathrm{Vol}(\Sigma)$ be the volume of the bulk slice Σ. Then we have $\mathrm{Vol}(\sigma_\pm) \geq \mathrm{Vol}(\Sigma_\pm)$, and addition of these inequalities yields $\mathrm{Vol}(\sigma_+) + \mathrm{Vol}(\sigma_-) \geq \mathrm{Vol}(\Sigma_+) + \mathrm{Vol}(\Sigma_-)$. Moreover, $\mathrm{Vol}(\Sigma_+) + \mathrm{Vol}(\Sigma_-) = \mathrm{Vol}(\Sigma_1) + \mathrm{Vol}(\Sigma_2)$, simply because $\Sigma_+ \cup \Sigma_- = \Sigma_1 \cup \Sigma_2$, so it follows that

$$\mathrm{Vol}(\sigma_+) + \mathrm{Vol}(\sigma_-) - \mathrm{Vol}(\sigma_1) + \mathrm{Vol}(\sigma_2) \geq 0. \tag{2.15}$$

To recover the previous case from this generalization, take σ_1 to be the two-boundary slice consisting of the union of the t_1 and t_4 slices, and take σ_2 to be that consisting of the union of the t_2 and t_3 slices.

2.4.0.1 Monotonicity on a boost-symmetric background

We next explain how inequality (2.14) implies monotonic growth in time of the complexification rate.[9] Before showing this, let us discuss the physical significance of this monotonicity property. Black holes are expected to excel at scrambling quantum information and, in particular, should complexify the fastest. Thus, one can expect that their late-time rate of complexification (once

[9]We thank Adam R. Brown for suggesting the following argument.

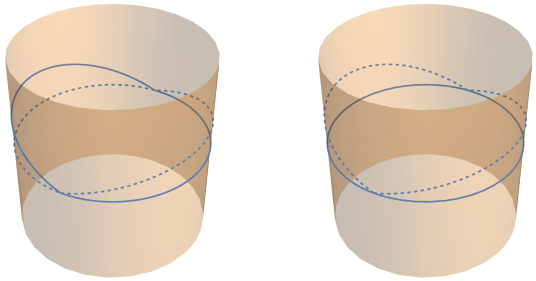

Figure 2.5: On the left are two Cauchy slices, σ_1 (in continuous blue) and σ_2 (in dashed blue), on the boundary of the Poincaré patch of an asymptotically AdS spacetime. On the right the corresponding σ_+ and σ_- are in dashed blue and continuous blue, respectively.

transient effects have died out) saturates quantum-information bounds, and in particular should be greater than the complexification rates at earlier times. The monotonicity property coming out of CV-duality is in agreement with this general expectation. By contrast, CA-duality was recently discovered to violate this monotonicity property [21, 3], perhaps putting into question that particular proposal.

We now take the infinitesimal limit of inequality (2.14), setting $t_1 = t_L$, $t_2 = t_L + \delta t_L$, $t_3 = t_R$, $t_4 = t_R + \delta t_R$. To leading order in small quantities, we find:

$$\mathrm{Vol}(t_L, t_R) + \mathrm{Vol}(t_L + \delta t_L, t_R + \delta t_R) - \mathrm{Vol}(t_L, t_R + \delta t_R) - \mathrm{Vol}(t_L + \delta t_L, t_R) = \frac{\partial^2 \mathrm{Vol}}{\partial t_L \partial t_R} \delta t_L \delta t_R. \tag{2.16}$$

Therefore the global inequality (2.14) implies positivity of the mixed partial derivative:

$$\frac{\partial^2 \mathrm{Vol}}{\partial t_L \partial t_R} \geq 0. \tag{2.17}$$

In terms of the new variables $t_\pm = t_L \pm t_R$, this inequality becomes

$$\frac{\partial^2 \text{Vol}}{\partial t_+^2} - \frac{\partial^2 \text{Vol}}{\partial t_-^2} \geq 0. \tag{2.18}$$

For an eternal black hole, the boost symmetry implies that the maximal volume cannot be a function of t_- [16]. We thus end up with the simple statement:

$$\frac{\partial^2 \text{Vol}}{\partial t_+^2} \geq 0. \tag{2.19}$$

which implies that the first derivative of Vol with respect to t_+ (or equivalently, with respect to either t_L ot t_R with the other one kept fixed) is monotonic. Replacing the volume by the complexity $\mathcal{C}$, this implies the monotonic increase of the complexification rate discussed above.

Note that inequality (2.14) does not imply monotonicity of the complexification rate for a general bulk spacetime, since we used the boost symmetry of a 2-sided black hole to deduce it. Nevertheless, we can take the infinitesimal version of the inequality (2.15) for a generic spacetime, and derive a condition similar to the positivity of the mixed partial derivative (2.17). To this end, consider the case where the two boundary Cauchy slices σ_1 and σ_2 coincide except on two small disjoint bumps to the future, one on σ_1 and one on σ_2. Expanding to leading order in the size of the bumps, we find that the "off-diagonal" part (since the bumps are disjoint) of the second functional derivative of the maximal volume $\text{Vol}(\sigma)$ with respect to σ variations is nonnegative.

2.5 Quenches, rotation and AdS-Rindler: further probes of CV duality

CV duality has been primarily probed in the setting of the eternal black hole, where interesting time dependence is introduced either by examining foliations that are not Killing time slices, or by introducing shockwave perturbations. In this section we extend the set of examples, by considering multiple quenches, where the black hole temperature changes, spinning black holes, where the angular momentum provides an extra parameter on which the dependence can be checked, and AdS-Rindler spacetime, where the time dependence of the vacuum complexity in the Rindler wedge is seen to be equivalent to that in a black hole spacetime.

2.5.1 AdS-Vaidya: event horizon vs apparent horizon

The time dependence of holographic complexity has been studied for quenched systems, i.e. systems into which a finite energy density is injected, using the AdS-Vaidya solution [17, 30, 43, 44]. In this subsection, we compare the growth of the volume inside the horizon for an AdS-Vaidya spacetime in the thin shell limit, using different definitions of the volume cutoff, and we extend existing studies to the case of two infalling shells.

In Section 2.2 we discussed several reasons supporting the notion that volume inside the black hole horizon is perhaps a more robust measure of complexity of the thermal state than is the volume of a global maximal slice with a cutoff at large distances from the black hole. When the black hole forms from

collapse, the degeneracy between different definitions of the horizon is lifted, hence we should examine which (if any) is more appropriate for CV duality. In particular, while the absolute event horizon remains a null hypersurface defined teleologically as the boundary of the past of future null infinity, we shall also consider the apparent horizon, defined here as the boundary of the region containing outer trapped surfaces on the leaves of the maximal foliation An apparent horizon defined this way is an example of a holographic screen [45, 46], i.e. a hypersurface foliated by marginally trapped surfaces. Recent work [47, 48] has shown that the area of a leaf of such a foliation is related to a certain coarse grained holographic entropy, which lends support to the idea that the volume inside such surfaces might be directly related to complexity [49].

When the spacetime is time dependent, the maximal time from the horizon to the final slice (the "complexity divisor" of the volume) in general becomes time dependent, and in that context it might well make more sense to measure the time from the apparent horizon rather than from the event horizon. We shall make no attempt here to determine which precise extension of the concept is more appropriate. Instead, we will just address the case where the black hole is either the BTZ black hole in $D = 3$ dimensions, or in higher dimensions is large enough so that the time $\sim \ell$ is the always the relevant one.

2.5.1.1 Single quench

Consider, then, a black hole formed by an infalling shell in AdS. If the event horizon forms "at the same time" as the time on the boundary when the shell starts to fall in, i.e. the time at which an external agent injects some energy into the CFT ground state, then the maximal slice volume inside the horizon remains zero until the injection time, and starts growing after that. This would be consistent with the general expectation that the CFT state starts to complexify after the energy injection. However, the horizon forms before the injection time if the final horizon radius is greater than the AdS length scale, and after the injection time if it is less [50].

To illustrate this, let us work for simplicity in the in the thin-shell limit, and in three spacetime dimensions. The BTZ-Vaidya metric in (r, v) coordinates reads:

$$ds^2 = -f(r,v)dv^2 + 2dvdr + r^2 d\phi^2 \tag{2.20}$$

$$f(r,v) = 1 + r^2 - \Theta(v)(1 + r_+^2) \tag{2.21}$$

where Θ is the unit step function. This metric describes a spherical shell at $v = 0$ collapsing to form a black hole. To draw the conformal diagram, we need to pass to conformally compactified coordinates (R, T) (see [50] for the coordinate transformation). The metric becomes:

$$ds^2 = \frac{-dT^2 + dR^2}{\cos^2 R} + r(T,R)^2 d\phi^2 \tag{2.22}$$

$$r(T,R) = \begin{cases} \frac{(1-r_+^2)\sin R - (1+r_+^2)\sin T}{2\cos R} & \text{if } R+T > 0 \\ \tan R & \text{if } R+T < 0 \end{cases} \tag{2.23}$$

Fig. 2.6 shows the conformal diagrams for three choices of horizon radius (larger than L, equal to L and smaller than L). The center of AdS is at $R = 0$, the boundary is at $R = \frac{\pi}{2}$, and the singularity is at $(1 - r_+^2) \sin R = (1 + r_+^2) \sin T$. As illustrated in Fig. 2.6, the horizon forms at the same time T as the injection time on the boundary only in the special case when the horizon radius of the final black hole is exactly equal to the AdS length.

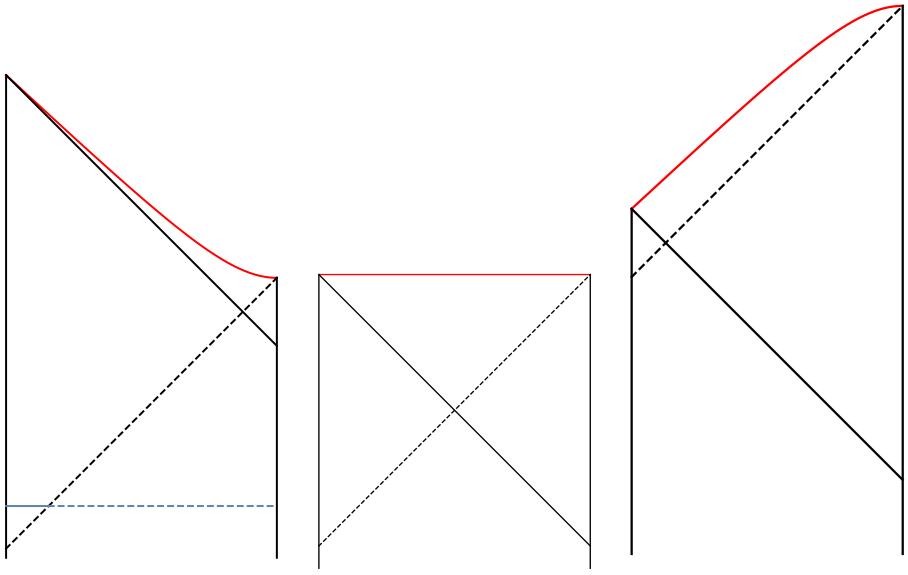

Figure 2.6: Conformal diagram for the BTZ-Vaidya spacetime in the thin-shell limit for three representative choices of the horizon radius r_+ (left: $r_+ = 5L$, center: $r_+ = L$, right: $r_+ = L/5$). For all three panels, the center of AdS, the infalling shell and the boundary are in continuous black, the horizon is in dashed black and the singularity is in red. Moreover, on the left panel, we depict a maximal slice anchored at a boundary time to the past of the infalling shell in blue. The portion inside the event horizon is in continuous blue, and the portion outside the horizon is in dashed blue.

Now consider the large black hole case, and consider a constant T slice

to the past of the infalling shell, where the geometry is locally AdS. This slice is invariant under the T reflection isometry, so it has vanishing extrinsic curvature, hence is maximal. We depict such a maximal slice in blue on the left panel of Fig. 2.6. Clearly the portion inside the horizon starts growing even before the energy injection occurs on the boundary.

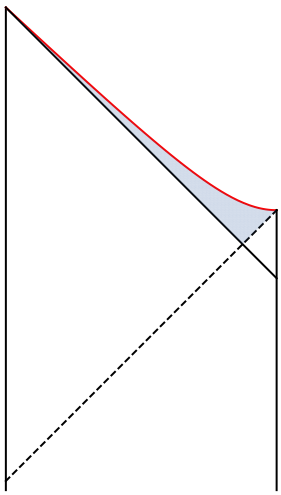

Figure 2.7: The region inside the apparent horizon is shaded in blue.

The apparent horizon for Vaidya-BTZ consists of two segments in the conformal diagram (illustrated in 2.7). One segment is the event horizon $r = r_+$ in the BTZ portion of the spacetime, and the other segment is the infalling shell itself. The interior of the apparent horizon (i.e. the trapped region) is shaded in light blue in Fig. 2.7. It is clear that the volume inside the apparent horizon can grow only after the injection occurs, with a delay because the maximal slice does not have any portion inside the light blue region of Figure 2.7 immediately after injection.

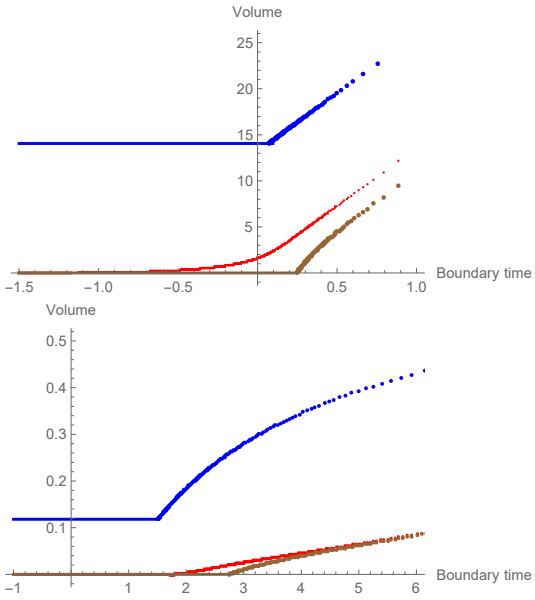

Figure 2.8: Plot of volume versus boundary time, for a large black hole (left) with $r_+ = 5\ell$ and a small black hole (right) with $r_+ = \ell/5$. In both panels, the blue curve is the volume inside some large cutoff, the red curve is the volume inside the event horizon and the brown curve is the volume inside the apparent horizon. The boundary time is measured in units of ℓ.

In Fig. 2.8 we plot the volume inside the horizon as a function of the boundary time, and compare with the volume inside some large cutoff near the boundary, as well as with the volume inside the apparent horizon (see below). The plots on the left are for a large black hole with $r_+ = 5\ell$, while those on the right are for a small black holes with $r_+ = \ell/5$. (To produce this plot, we solved numerically for the maximal slices; the details are explained in Appendix A.4.) Several features of this figure are worth remarking upon:

- The volume inside a near-boundary cutoff is shown as the blue curve. It starts to grow at the injection time. For a large black hole, the volume

inside horizon, shown by the red curve, starts growing before the injection time.

- For a large black hole, the volume inside a near-boundary cutoff (blue curve) grows at essentially the late-time rate as soon as the energy is injected. For a small black hole, the growth rate starts out higher, then decreases to late time rate.

- The growth rates all converge at late time both for large and small black holes. This verifies the expectation that all late time growth of volume occurs inside the horizon for a one-sided black hole, as it does for a two-sided one.

- From a geometrical viewpoint, there are two distinct regimes for the volume inside the event horizon: it may be contained entirely inside the pure AdS part of the spacetime, or it may include a part in the AdS portion and a part in the BTZ portion. There is a critical boundary time at which the former regime transitions to the latter one, on the maximal slice, A priori it seems that the volume curve might have a kink at this transition, however inspection of the red curves suggests that the derivative is actually continuous at the transition.

- The brown curves show the volume inside the apparent horizon, which is always the last to start growing. In particular, no growth occurs before injection, and in fact there is a delay between injection and the onset of growth of the volume inside the apparent horizon. This delay is perhaps

related to a thermalization timescale. As shown in [38, 39] thermalization takes a time on the order of the AdS length scale, with specific behavior depending on the scale at which thermalization is probed.

- The rate of change of the volume inside the apparent horizon starts out higher than the late-time rate, and then approaches the late-time value from above. This is contrary to the monotonic increase expectation; however, since the quench process is far from stationary, that expectation is perhaps not as well justified as in a stationary equilibrium state. This decreasing behavior was also observed in [43]. Moreover, the longest time to the final slice is the same from all points on the outer portion of the apparent horizon (which coincides with the event horizon), and is longer than any other time from inside the horizon, so there is presumably no additional time dependence coming from the divisor τ_f in the complexity formula.

2.5.1.2 Two quenches

In this subsection we consider BTZ-Vaidya with two infalling shells. The field theory picture is that energy is injected twice into the CFT. After the first injection thermalizes, we expect a linear growth of complexity at a rate proportional to the energy injected, since $TS \propto E$. After the second injection, the system now has more energy, so we expect the complexification rate to increase.

If the second injection occurs sufficiently far to the future of the first

one, so that the complexity has enough time to reach the linear growth regime before the second injection, CV duality would imply that the plot of maximal volume versus time will consist of three linear regimes (zero slope, a finite slope, and a bigger finite slope).

The metric is still given by eq. (2.20), except that the function $\Theta(v)$ is no longer a unit step function, but a "double step function":

$$\Theta(v) = a\theta(v) + (1-a)\theta(v-b) \tag{2.24}$$

where a is a real number between 0 and 1, b is a positive real number, and θ is the unit step function. The function $f(r,v)$ becomes:

$$f(r,v) = \begin{cases} 1+r^2 & v<0 \\ r^2 - R^2 & 0<v<b \\ r^2 - r_+^2 & b<v \end{cases} \tag{2.25}$$

with $R^2 \equiv a(1+r_+^2) - 1$. Thus, we have AdS for time $v<0$, and the usual BTZ with horizon radius r_+ for $b<v$. In the intermediate regime, $0<v<b$, we have two qualitatively different cases depending on the sign of R^2 (it need not be positive): If $R^2>0$ we have a BTZ black hole with horizon radius R, while if $-1<R^2<0$ we have a "conical defect" geometry.[10]

We have solved numerically for the maximal slices and their volume with the parameter choice $a=1/2$, $b=1$ and $r_+=2$ (see appendix A.4 for the technical details). The shape of a maximal slice anchored at late time on

[10]This conical defect geometry is also a possibility in the single-shell case. This can be seen as follows: the stress-energy tensor of the single-shell AdS-Vaidya in three dimensions is $T_{vv} = \frac{1+r_+^2}{2r}\Theta'(v)$. If $-1<r_+^2<0$, we do not have a black hole final state, yet the null energy condition is still obeyed. This is the conical defect regime.

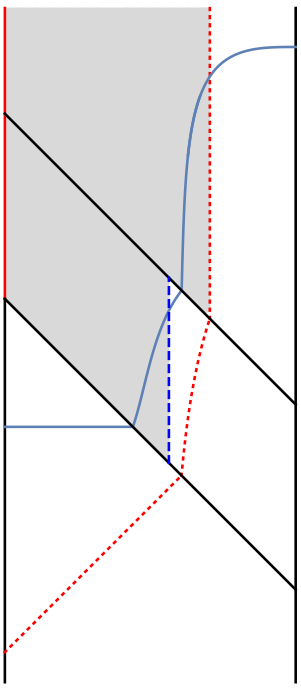

Figure 2.9: Eddington-Finkelstein diagram of the BTZ-Vaidya solution with two infalling shells. The abscissa and ordinate for the plot are $\rho = \arctan(r)$ and $t = v - \rho$, respectively. The two infalling shells, the center of AdS, and the boundary are in thick black, the singularity is in solid red, the constant radius portion of the apparent horizon between the shells is in dashed blue, the event horizon is in short-dashed red, and the maximal slice anchored at late boundary time is shown in continuous blue. The apparent horizon is the boundary of the grey shaded region.

the boundary is depicted using an Eddington-Finkelstein diagram in Fig. 2.9. The effect of the outer shell is to push the slice further from the singularity, which can be explained intuitively as follows: the final slice for the BTZ-Vaidya should approach the final slice of the eternal BTZ black hole (with the same total mass) at late time, which is a constant radius slice with $r \propto r_+$. Since the effect of the outer shell is to increase the horizon radius, it also pushes the

final slice further from the singularity.

In Fig. 2.10, we plot the volume of the portion of the maximal slice lying inside the apparent horizon as a function of the boundary time t_b at which the slice is anchored, with the same parameter choice used for Fig. 2.9. Note that for a brief period of time after the maximal slice crosses the point where the second shell meets the apparent horizon, the slice has two disconnected parts lying inside the apparent horizon, separated by an annular region falling outside the apparent horizon.

It would be interesting to consider similar double quenches but in $D \geq 4$ dimensions, with spherical black holes of different sizes, so that the time dependence of the time to final slice divisor τ_f might come into play.

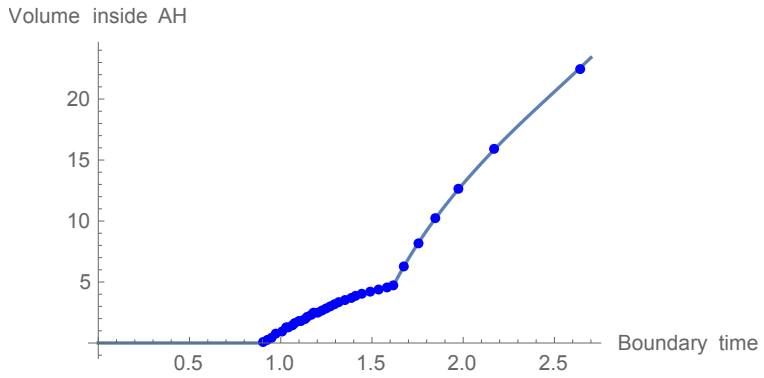

Figure 2.10: Plot of the maximal slice volume inside the apparent horizon in a Vaidya spacetime with two shells. The kinks occur when the maximal slice crosses the points where the first and second shells meet the apparent horizon.

2.5.2 Rotating BTZ black hole

A further probe of CV duality is provided by considering rotating black holes. A rotating black hole is dual to a rotating thermal CFT state. The complexity in such a state should presumably grow, with respect to time in the rotating frame, as the entropy of the state times the temperature $T_{\rm rot}$ in that frame, since that is the frame in which thermal equilibrium is established. That is, one would expect that $d\mathcal{C}/dt_{\rm rot} \sim T_{\rm rot} S$. While the CFT entropy is frame independent, and is thus equal to the dual black hole entropy, $T_{\rm rot}$ is not equal to the dual black hole temperature $T_{\rm BH}$. Considering that the thermal frequency defines a clock in the rotating frame, there is a time dilation shift of the temperature, and we have $T_{\rm rot}\, dt_{\rm rot} = T_{\rm BH}\, dt_{\rm BH}$, where $dt_{\rm BH}$ is the Killing time increment in the asymptotic rest frame of the black hole. It follows that the rate of complexity growth can equally be expressed as $d\mathcal{C}/dt_{\rm BH} \sim T_{\rm BH} S_{\rm BH}$ [11]. We will now show, for the case of a rotating BTZ black hole, that CV duality indeed predicts this complexity growth rate at late times.

[11] It is worth noting here a subtlety concerning the existence of the corotating frame for the CFT. It might seem that in order to co-rotate with the black hole, the frame would need to rotate faster than light at large radii. However, as can easily be checked, for the case of the BTZ black hole the horizon generating Killing vector remains timelike all the way from the horizon to spatial infinity. This is of course necessary in order for there to be a sensible dual rotating CFT equilibrium state. The same feature holds for large rotating black holes in asymptotic AdS in any dimension, but for small black holes in AdS, or for Kerr black holes, it does not. This is related to the instability of those black holes [51]. As explained in the preceding paragraph, the rate of complexification with respect to Killing time is given by $T_{BH} S_{BH}$, which does not refer directly to the corotating CFT frame. This formula can therefore be applied in cases such as the asymptotically flat Kerr geometry, where no physical asymptotic corotating frame exists. However, there is no stable CFT equilibrium state to which these quantities refer, so the holographic interpretation is not clear in that case.

The metric for the rotating BTZ black hole can be written as

$$ds^2 = -\alpha^2 dt^2 + \alpha^{-2} dr^2 + r^2(d\phi - \Omega dt)^2, \tag{2.26}$$

with

$$\alpha^2 = \frac{(r^2 - r_+^2)(r^2 - r_-^2)}{r^2 \ell^2}, \qquad \Omega = \frac{r_- r_+}{r^2 \ell}, \tag{2.27}$$

and the surface gravity is $\kappa = (r_+^2 - r_-^2)/\ell^2 r_+$. The "final slice," i.e. the Killing-invariant maximal slice inside the horizon lies where $(r\alpha)' = 0$, which is at r_f given by $r_f^2 = (r_+^2 + r_-^2)/2$. This is a cylindrical surface, with induced metric $ds^2 = -\alpha_f^2 dt^2 + r^2(d\phi - \Omega_f dt)^2$, and volume (area) form $r_f \alpha_f \, dt \wedge d\phi$, where $\alpha_f := \sqrt{-\alpha(r_f)^2}$. The volume of a dt section of the slice is thus $dV = 2\pi r_f \alpha_f \, dt$, so the rate of change of the total volume inside the horizon, growing at both ends, is $dV/dt = 4\pi r_f \alpha_f$. The longest time path from the outer horizon to the final slice has length

$$\tau_f = \int_{r_f}^{r_+} \alpha^{-1} dr = \pi \ell / 4, \tag{2.28}$$

which is the divisor we use in relating the complexity to the volume. (Note that, unlike in higher dimensions, this time is independent of the horizon radius, even for small black holes. In the next section we consider the Kerr black hole in four dimensions, and find that one still obtains TS even for small black holes, when the time to the final slice is used as the divisor.)

The rate of change of the complexity with respect to t is thus

$$\frac{d\mathcal{C}}{dt} = \frac{4}{\pi \ell} \frac{dV}{dt} = \frac{16 r_f \alpha_f}{\ell} = \frac{8(r_+^2 - r_-^2)}{\ell^2} = 8\kappa r_+ = 32 T_{\rm BH} S_{\rm BH}. \tag{2.29}$$

As explained above, $T_{\rm BH}S_{\rm BH}$ is equivalent to the rate $T_{\rm rot}S_{\rm rot}$, which is what one would expect from a thermal state [15]. This is a nontrivial check, since the rotating black hole possesses another dimensionless parameter, r_-/r_+, on which the result might have depended.

We note also that, in the case of the rotating BTZ black hole, the this complexification rate from "complexity = volume" is interestingly the same as the one found for "complexity = action" [19]: the late-time rate of growth is proportional to $r_+^2 - r_-^2$ in both cases. Here we emphasize the proportionality of this result with $T_{\rm H}S_{\rm BH}$, whereas Ref. [19] emphasizes the proportionality with $M - \Omega J$, noting that the late-time rate of growth is slowed down compared to M, due to the presence of the conserved charge J.

2.5.3 Kerr black hole

Next, we discuss rotating black holes in higher dimensions. This case is substantially more complicated to study than the rotating BTZ one due to the lack of spherical symmetry, and this may be why it has not been studied at all in the literature in the context of CV-duality.[12] We will consider the case of the Kerr solution in four spacetime dimensions, since the asymptotically flat case is somewhat simpler, and since its maximal slices have already been studied to some extent in [53] (see however footnote 10 for a caveat concerning the CFT dual in this case). Our aim is to check whether the complexification

[12]The volume of constant radius slices inside the Kerr horizon has been studied previously in [52].

rate (with the time to the final slice divisor taken into account) continues to be of the order of $T_{\rm H} S_{\rm BH}$.

The Kerr metric for a black hole of mass M and angular momentum aM is given in Boyer-Lindquist coordinates by

$$ds^2 = -\frac{\Sigma\Delta}{B}dt^2 + \frac{B}{\Sigma}\sin^2\theta\left(d\phi - \Omega dt\right)^2 + \frac{\Sigma}{\Delta}dr^2 + \Sigma d\theta^2, \tag{2.30}$$

where

$$\Sigma = r^2 + a^2\cos^2\theta, \quad \Delta = r^2 - 2Mr + a^2, \quad B = (r^2+a^2)^2 - a^2\Delta\sin^2\theta, \quad \Omega = 2aMr/B. \tag{2.31}$$

The inner/outer horizons $r_\pm$ are the roots of $\Delta = (r - r_+)(r - r_-)$, $r_\pm = M \pm \sqrt{M^2 - a^2}$.

A general axially symmetric maximal slice is described by some function $r(t, \theta)$. The final slice is a late time limit, so is t-independent due to t-translation symmetry of the background, and is therefore described by a function $r(\theta)$ which extremizes the volume. The volume element on such a slice between the inner and outer horizons (where $\Delta < 0$) is

$$\sqrt{\Sigma(|\Delta| - r_{,\theta}^2)}\sin\theta\, dt \wedge d \wedge d\theta \wedge d\phi \tag{2.32}$$

As argued in [53], $r(\theta)$ must lie between two values, $r_{\rm min}$ and $r_{\rm max}$, which are the extrema of $\Sigma\Delta$ with respect to r at $\theta = 0$ and $\pi/2$, respectively, and which are very close to each other for all values of the spin parameter a/M. The final slice therefore comes very close to being a slice of constant r.

We will adopt $r_f \equiv r_{\max}$ for that approximate constant value of r, which is given by

$$r_f = \frac{3}{4} M \left[1 + \sqrt{1 - 8a^2/9M^2}\right]. \tag{2.33}$$

This radius is never parametrically different from the horizon radius r_+: for $a = 0$ it is $3r_+/4$, while for extremal spin it is r_+. The volume element on this cylinder is given by

$$\epsilon_f = \alpha_f \, dt \wedge \mathcal{A}_f, \quad \alpha_f = \sqrt{\frac{\Sigma_f |\Delta_f|}{B_f}}, \quad \mathcal{A}_f = \sqrt{B_f} \sin\theta \, d\theta \wedge d\phi. \tag{2.34}$$

The volume of a dt section on the final slice is thus $dV = dt \int \alpha_f \mathcal{A}_f$, where the integral is over a constant t slice of the cylinder.

Next let us evaluate the maximal time to fall from the horizon to the final slice, τ_f. Since the coefficient of dr^2 in the line element (2.30) is negative, while those of the other three terms are positive, the longest time is clearly attained with $dt = d\theta = d\phi = 0$. Moreover, the maximum of these is attained at $\theta = 0$, so

$$\tau_f = \int_{r_f}^{r_+} dr \sqrt{\frac{r^2 + a^2}{|\Delta|}} \tag{2.35}$$

Our proposal for the t derivative of the holographic complexity due to growth on one side of the final cylinder is thus

$$\frac{d\mathcal{C}}{dt} = \frac{\int \alpha_f \mathcal{A}_f}{\tau_f}. \tag{2.36}$$

Since $r_f \sim r_+$, the rate (2.36) will agree with $\sim T_{\rm H} S_{\rm BH}$ provided $\alpha_f \sim \kappa \tau_f$, where κ is the surface gravity. If α_f were the norm of the horizon generating

Killing vector $\partial_t + \Omega_+ \partial_\phi$ as before, then this last relation would again follow as the first order Taylor expansion, as explained in the introduction. However, in fact, α_f is the norm of $\partial_t + \Omega_f \partial_\phi$. Nevertheless, again, because $r_f \sim r_+$, these two vector fields are not so different, and so it is plausible that indeed $\alpha_f/\tau_f \sim \kappa$.

To test this relation at the extreme, we define the parameter $\epsilon = \sqrt{1 - a^2/M^2}$, and expand around extremality, $\epsilon = 0$. Expanding to lowest order in ϵ, using units with $M = 1$, we have $r_\pm = 1 \pm \epsilon$, $r_f = 1 + \epsilon^2$, and $\Delta = (r-1)^2 - \epsilon^2$, hence $\Delta_f = -\epsilon^2$. Thus, in computing the volume to lowest order, we may set $r = 1$ in all expressions other than Δ. In particular, $\alpha_f \mathcal{A}_f \to \epsilon\sqrt{1 + \cos^2\theta}\sin\theta\, d\theta \wedge d\phi$. At this lowest order in ϵ we therefore have

$$dV/dt = 2\pi[\sqrt{2} + \sinh^{-1}(1)]\epsilon, \tag{2.37}$$

and

$$\tau_f = \sqrt{2}\int_1^{1+\epsilon} \frac{dr}{\sqrt{\epsilon^2 - (r-1)^2}} = \frac{\pi}{\sqrt{2}}, \tag{2.38}$$

so our proposal for the complexification rate yields

$$\frac{d\mathcal{C}}{dt} = 2\sqrt{2}[\sqrt{2} + \sinh^{-1}(1)]\epsilon \approx 6.49\epsilon. \tag{2.39}$$

On the other hand, the temperature and entropy of the Kerr black hole are

$$T_{BH} = \frac{1}{2\pi}\frac{\sqrt{M^2 - a^2}}{r_+^2 + a^2}, \qquad S_{BH} = \pi(r_+^2 + a^2), \tag{2.40}$$

so it follows that

$$T_{\rm H} S_{\rm BH} = \frac{1}{2}\sqrt{M^2 - a^2} \to \tfrac{1}{2}\epsilon. \tag{2.41}$$

The important thing is that (2.39) and (2.41) are both $O(\epsilon)$, so that their ratio approaches a nonzero pure number in the extremal limit. While the ratio depends on the spin parameter a/M, it is does not go to zero or infinity as this parameter goes to zero. Finally to exhibit the ratio over the full parameter range, we evaluated it numerically. As expected, the plot in Fig. 2.11 of the ratio of these quantities does not vary substantially over the whole range of a/M [13]. It would be interesting to generalize this analysis to Kerr-AdS, in any spacetime dimension.

2.5.4 Rindler wedge complexity growth

It has previously been observed that many aspects of black hole thermodynamics and horizon entanglement apply to acceleration horizons, and specifically to Rindler horizons in flat or AdS spacetimes. In particular, in the AdS/CFT setting, the CFT can be partitioned in to two equal halves, and in the ground state the corresponding bulk entanglement wedges are Rindler wedges, separated by a horizon and future and past "interior" regions analogous to the two-sided black hole interior. Each half of the CFT vacuum is a

[13] To produce this plot we first derive an analytical expression for the volume V_f of a section of the final slice, by integrating the volume element (2.34) over θ and ϕ and t, which yields

$$\frac{dV_f}{dt} = 2\pi\sqrt{|r_f^2 - 2Mr_f + a^2|}\left[\sqrt{r_f^2 + a^2} + \frac{r_f^2}{a}\text{arctanh}\left(\frac{a}{\sqrt{a^2 + r_f^2}}\right)\right] \tag{2.42}$$

For $T_{BH}S_{BH}$, we use the analytical expression given in equation (2.40) in our paper. Finally, τ_f is given as an integral in equation (2.35), which we evaluate numerically.

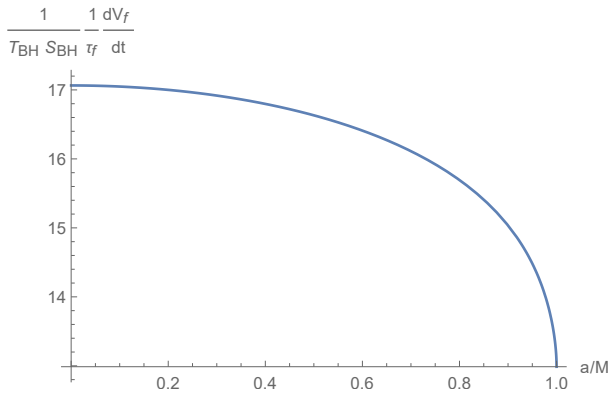

Figure 2.11: Plot of (rate of change of final slice volume $\boldsymbol{\nabla}\cdot$ longest time from the horizon to the final slice) :$(T_{\mathrm{H}}S_{\mathrm{BH}})$, versus the spin parameter for a Kerr black hole in four spacetime dimensions. The ratio is roughly constant over the entire range from nonspinning to maximal spin.

thermal state with respect to the Hamiltonian generating the conformal boost symmetry of its diamond-shaped domain of dependence [54, 55]. The analogy with the two-sided black hole is close enough that we may expect the complexity of the thermal state to grow in time when boosting toward the future on both halves of the partition (as opposed to boosting one side to the future and the other to the past). Moreover, the expected growth rate would be TS, where T is the conformal boost temperature and S is the (entanglement) entropy. We now demonstrate that this is indeed the case for $\mathrm{AdS}_3/\mathrm{CFT}_2$.

The metric of AdS in Rindler coordinates is actually just the BTZ metric (2.26), with $r_- = 0$ and $r_+ = \ell$ [41]. The maximal foliation of interest is defined by constant Rindler time slices of the boundary, and the final slice of this foliation therefore meets the boundary at the Rindler horizon. Fig. 2.12 displays a plot of this slice in global coordinates, which lies at $r_f = r_+/\sqrt{2}$ as

seen in the previous subsection (2.5.2). The results of that section also show that the rate of complexification at late times, measured with respect to the conformal boost time, is $\propto TS$, where $T = 1/2\pi$ is the Unruh temperature, and S is the (infinite) Bekenstein-Hawking entropy of the Rindler horizon. The dual quantities in the CFT are the conformal boost temperature, and the entanglement entropy of the semicircle, as implied by the Ryu-Takayanagi formula. The state on the semicircles is also conformally equivalent to a thermal state on two-dimensional Minkowski space. In higher dimensions it would be conformally equivalent to a thermal state on a static hyperbolic space [56].

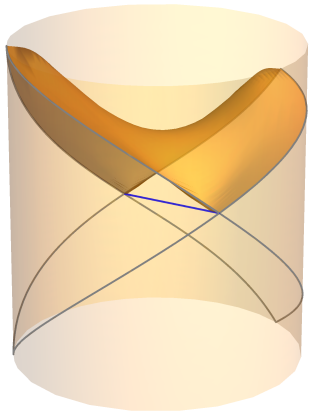

Figure 2.12: A plot of the final slice of AdS-Rindler embedded into global AdS. Here we use global coordinates for AdS, in which the metric reads $ds^2 = L^2(-\cosh^2\rho d\tau^2 + d\rho^2 + \sinh^2\rho d\phi^2)$, except that we have compactified the radial coordinate by applying the *arctan* function (in other words, the boundary of the cylinder is at radius $\pi/2$). The line running across the cylinder is the bifurcation line of the Rindler horizon.

2.6 Conclusion

In this paper, we proposed that the apparent lack of universality in the CV duality for large and small black holes is removed if one identifies the complexity with the volume measured in units of the maximal (free-fall) time τ_f from the horizon to the final slice times Planck area. The distance $c\tau_f$ is $\sim$ the AdS radius for spherical black holes large compared to the AdS radius, and it is $\sim$ the horizon radius for small black holes, thus accounting in both cases for the divisor that had been previously introduced by hand in order for the complexification rate to match the temperature-times-entropy expectation. We also checked that this prescription matches TS for the rotating BTZ black hole, and the Kerr black hole in four dimensions, for all spin parameters. While this does seem an improvement over the previous ad hoc assignment, it should be admitted that we have no reason from first principles for thinking the time τ_f should be relevant, other than that it can be related to the surface gravity and redshift factor at the final slice, as explained in the Introduction and in Sec. 2.3.4. Moreover, τ_f is of course only defined when a horizon and final slice are present, so is of no use otherwise. In this respect, CA duality appears much more universal. However, it is not so clear whether the notion of complexity and its growth should be expected to have a universal meaning, outside of thermal states, because then the dependence on the arbitrary choice of reference state and gates with which to define the complexity may be more severe.

We proposed that to capture complexity at the thermal scale one should

count only the volume inside the horizon, and introduced the "volume current," orthogonal to a foliation of spacetime by maximal slices. This current is a divergence-free vector field, whose flux through the slices of the foliation measures their volume. This flux picture suggests that there is a transfer of the complexity from the UV to the IR in holographic CFTs, which is reminiscent of thermalization behavior decuced using holography. It also naturally gives a second law for the complexity when applied at a black hole horizon. We further showed how the volume current is a useful tool for establishing various properties of the volumes of a maximal foliation, established a global inequality on maximal volumes that can be used to deduce the monotonicity of the complexification rate on a boost-invariant background, and probed CV duality in the settings of multiple quenches, spinning black holes, and Rindler-AdS. Finally, we established the existence of a maximal foliation without gaps (on which the existence of the volume current depends) provided that there exists a maximal slice anchored at each boundary slice, and assuming a causality condition, the strong energy condition, and the Einstein equation.

Taken together, these results demonstrate the mathematical and physical utility of the notion of volume current associated to a maximal foliation. In the setting of CV duality it is tempting to think of the current as a "gate current" [26]. Perhaps this could be given a more concrete meaning in the context of tensor network models of bulk spacetime.

2.7 Acknowledgment

This work is partially supported by NSF grants PHY-1407744, PHY-1708139 and PHY-1620610. We would like to thank Vijay Balasubramanian, Adam Brown, Netta Engelhardt, Matthew Headrick, Veronika Hubeny, Brian Swingle and Aron Wall for helpful discussions.

Chapter 3

Holographic Complexity and Noncommutative Gauge Theory

3.1 Introduction

[1]In the past several years, there has been a growing interest in the topic of "holographic complexity." This interest was originally motivated by the late time growth of the wormhole volume in two sided black holes, which seems to have no correspondence in the boundary which is in thermal equilibrium. It was then conjectured that such a phenomenon should be related to the quantum complexity of the boundary state [15], and this conjecture was strengthened by study of quantum chaos, namely the "switchback effect" [16, 17]. There have since been several conjectures as to the exact quantity dual to complexity on the boundary, all tied to the phenomenon of expanding wormholes in two-sided black holes. The first proposal was that complexity is dual to the volume of a maximal spatial slice with a given boundary [15], and the next [18, 19] was the gravitational action evaluated on the Wheeler-DeWitt (WDW) patch. A third closely related conjecture was later proposed

[1]This chapter is a reproduction of [3], which I wrote with Stefan Eccles, Willy Fischler, and Minglei Xiao. My contribution consisted in developing the intuitive circuit based argument presented to explain our results, as well as to assist with the computations.

in [4], namely that the complexity is dual to the space-time volume of a WDW patch.

Unfortunately, there is little that we know about the concept of quantum complexity in the boundary field theory. The basic definition involves a reference state $|\psi_0\rangle$, a set of quantum gates $G = \{g_i\}$, and a tolerance parameter ϵ. The complexity of a quantum state $|\psi\rangle$ is the minimum number of gates one needs to make up a quantum circuit $Q = \prod_{i=1}^{\mathcal{C}} g_i$ so that $d_f(Q|\psi_0\rangle, |\psi\rangle) < \epsilon$. One can also define the complexity of a unitary operator U to be the minimum number of gates one needs to make up a quantum circuit Q_U so that $||Q_U - U|| < \epsilon$. [2] The holographic complexity is supposed to be the state complexity, while we also use the operator complexity to analyze the characteristic behavior in section 3.3. Even with these definitions, the task of actually computing the relative complexity of two states is notoriously difficult. What is more, in the definition one has to make several choices, and where these choices appear in the holographic prescription is as of yet unclear. It is also a puzzle how one goes from the discretum of quantum circuits to a supposedly continuous quantum field theory. There has been considerable effort defining complexity in the quantum field theory [57, 24, 58, 59, 60, 61], however they are weakly related to the holographic complexity at this point. Therefore, what we are interested in is to utilize our intuitions from quantum

[2] $d_f(\ ,\ )$ is the Fubini-Study metric for quantum state $d_f(\alpha, \beta) = \arccos\sqrt{\frac{|\langle\alpha|\beta\rangle|^2}{\langle\alpha|\alpha\rangle\langle\beta|\beta\rangle}}$. The norm $||A||$ for operators can be defined as the square root of the spectral radius $\rho(A^\dagger A)$, which is the supremum of the eigenvalues of $A^\dagger A$.

mechanics to conjecture some constraints on complexity in general. These constraints are to be tested for both the boundary theory and the holographic theory.

Among the constraints which people have considered is the Lloyd bound [62]. This bound was derived from the Margolus-Levitin theorem [63] under the assumption that each gate will evolve a generic state into an orthogonal state. It states that the time rate change of complexity[3] is constrained by the energy:

$$\dot{\mathcal{C}} \leq \frac{2M}{\pi}, \tag{3.1}$$

where M is the energy of the system. In [18, 19] it was conjectured that neutral black holes should saturate this bound, and this assumption was made in order to set the constant of proportionality between complexity and action. This conjecture originated from the fast scrambling nature of black holes and the related idea that black holes are the fastest possible quantum computers. However, one finds that for neutral black holes, the Lloyd bound is saturated from above [21], which makes the conjecture somewhat suspicious. One can also argue that the Lloyd bound is not an exact bound because the assumption is based on is highly unrealistic. In fact, whether this assumption applies in the case of holographic complexity has recently been questioned in [64].

In light of these difficulties with the Lloyd bound, it is interesting to

[3]We also refer to the time rate change of complexity as the "complexification" rate, which should be considered synonymous as they appear in this paper.

test the holographic complexity conjectures[4] against additional pieces of intuition in novel contexts. One context which might reasonably provide a testbed is the noncommutative field theories. The study of such theories has a long history and has produced many profound results, see for example [65, 66, 10, 67, 68, 69]. One feature of noncommutative field theory which is suggestive of interesting behavior is that it adds a degree of non-locality, which has been shown to lead to interesting effects, e.g. an increase relative to the commutative case in the dissipation rate of scalar modes [70]. Indeed, the holographic entanglement entropy in this context has already been studied in, for example, [71, 72], where non-trivial behavior was found in the limit where the Moyal scale is much larger than the thermal scale. The geometry was obtained in a string theory context by turning on the NS-NS B fields on Dp branes. The non-vanishing B field then induces Dirichlet boundary condition for open strings, and non-zero commutator of the end point coordinates [65]. After decoupling the closed strings, the Dp brane worldvolume becomes a noncommutative space. It was shown that in such setup, although space is coarse-grained by the Moyal scale, which might indicate a reduction in the number of degrees of freedom, it turns out that all thermodynamical quantities are unchanged [67, 66]. This can be understood by looking at the thermal boundary state in the large N limit, which consists of only planar diagrams without external legs. Such diagrams are insensitive to the non-commutativity of the

[4]In this paper we will consider only complexity = action, and discussion of the complexity = volume and complexity = spacetime volume conjectures are left for future work.

spacetime [73]. It thus provides a perfect arena for testing quantum complexity, whose main characteristic is that it is more than thermodynamics. If the holographic complexity can see the difference caused by non-commutativity, it is a sign that we are on the right track.

The remainder of this paper is organized as follows: In section 3.2 we construct the holographic dual of a noncommutative super Yang-Mills (NCSYM) theory and compute the holographic complexity of a state on the boundary using the CA proposal. The complexity growth rate is given as a function of the Moyal scale a, the horizon radius r_H and time t, and at late times its monotonic enhancement with a is shown. In section 3.3, we attempt to give a quantum mechanical explanation of the enhancement of late time complexity growth rate. In section 3.4, we discuss the finite time behavior of our result and compare to the recent independent studies [21]. To make our result more convincing, we explore more examples with non-commutativity in section 3.5. We have a similar setup as in section 3.2 in various dimensions and we have various numbers of pairs of noncommutative directions. In 3.6, we conclude with a brief discussion of our results and make a few remarks of possible directions for future studies. In the appendix B.1, we show the explicit calculation for the WDW patch action. Appendix B.2 talks about the thermodynamic property of the Dp brane solutions.

3.2 Holographic Complexity of 4d $\mathcal{N} = 4$ NCSYM

3.2.1 The holographic dual to noncommutative SYM

We consider the noncommutative field theory widely studied in the context of string theory. It was shown that the non-vanishing NS-NS B field will induce noncommutative space on the D brane that decouples from the closed string excitations [65]. The way to turn on the B field is to perform a T duality, in D3 brane for instance, along x_3 direction, assuming the x_2, x_3 are compatified on a torus. The torus becomes tilted after the T duality, which indicates a D2 brane smearing along x_3 direction. Then one performs another T duality along x_3, to get the following solution ([10, 66]):

$$
\begin{aligned}
&ds^2 = \alpha' \Bigg[\left(\frac{r}{R}\right)^2 \left(-f(r)dt^2 + dx_1^2 + h(r)(dx_2^2 + dx_3^2)\right) + \left(\frac{R}{r}\right)^2 \left(\frac{dr^2}{f(r)} + r^2 d\Omega_5^2\right) \Bigg], \\
&f(r) = 1 - \left(\frac{r_H}{r}\right)^4, \quad h(r) = \frac{1}{1 + a^4 r^4},
\end{aligned}
\tag{3.2}
$$

$$
\begin{aligned}
&e^{2\Phi} = \hat{g}_s^2 h(r), \\
&B_{23} = B_\infty (1 - h(r)), \quad B_\infty = -\frac{\alpha'}{a^2 R^2}, \\
&C_{01} = -\frac{\alpha' a^2 r^4}{\hat{g}_s R^2}, \quad F_{0123r} = \frac{4\alpha'^2 r^3}{\hat{g}_s R^4} h(r).
\end{aligned}
\tag{3.3}
$$

The $\{t, x_1, x_2, x_3\}$ are the D3 brane coordinates, while $\{x_2, x_3\}$ are non-commuting with Moyal algebra

$$
[x_2, x_3] = i a^2. \tag{3.4}
$$

The radius coordinate r has units of inverse length[5], and a is the Moyal scale with units of length. r_H denotes the location of the event horizon, and $\hat{g}_s$ denotes the closed string coupling, which is related to the S^5 radius as $R^4 = \hat{g}_s N$.

Note that the geometry becomes degenerate at $r \to \infty$; thus we have to put the boundary theory on some cutoff surface $r_b < \infty$. It was shown that this natural cutoff plays an important role in the divergent structure of entanglement entropy [71]. However, as will be explained later, our computation is cutoff independent; therefore we don't need to worry about it.

As explained in [66], all the thermodynamic quantities of this solution are the same as in the commutative case. In particular, the temperature and entropy is independent of a, given by

$$\begin{aligned} E &= \frac{3r_H^4 \Omega_5 V_3}{(2\pi)^7 \hat{g}_s^2} \\ T &= \frac{r_H}{\pi R^2}, \\ S &= \frac{4\pi R^2 r_H^3 \Omega_5 V_3}{(2\pi)^7 \hat{g}_s^2} \end{aligned} \tag{3.5}$$

It is then interesting to ask whether the complexity is affected by the non-commutativity because complexity is fine-grained information that knows more than thermodynamics.

We adopt the Complexity equals Action (CA) approach to compute the holographic complexity of the boundary state. It involves evaluating the

[5]In the literature, the coordinate denoted here by 'r' is typically denoted 'u' in order to emphasize that it does not have dimensions of length. We have however chosen to denote it by 'r' to avoid confusion with the Eddington-Finkelstein like null coordinate

action in a bulk subregion, called the Wheeler-deWitt (WDW) patch. Recent work on evaluating gravitational action [74] provided a toolkit that deals with null boundary contributions in the context of Einstein gravity. Hence we are interested in the Einstein frame action of type IIB supergravity:

$$ds_E^2 = \exp(-\Phi/2) ds^2, \tag{3.6}$$

$$2\kappa^2 S_E = \int d^{10}x\sqrt{-g_E}\left[\mathcal{R} - \frac{1}{2}|d\Phi|^2 - \frac{1}{2}e^{-\Phi}|dB|^2 - \frac{1}{2}e^{\Phi}|F_3|^2 - \frac{1}{4}|\tilde{F}_5|^2\right] - \frac{1}{2}\int C_4 \wedge dB \wedge F_3, \tag{3.7}$$

where the notation $|F_p|^2 = \frac{1}{p!}F_{\mu_1\cdots\mu_p}F^{\mu_1\cdots\mu_p}$ is understood. One should keep in mind that the 5-form $\tilde{F}_5$ is self dual while evaluating this action. This requirement actually always makes the term $|\tilde{F}_5|^2 = 0$. [6]

3.2.2 Wheeler-DeWitt Patch Action

The WDW patch is defined to be the union of all spatial slices anchored on a boundary time slice Σ. Regarding representing the boundary state, the WDW patch differs from the entanglement wedge at two points: first, it specifies a specific time slice on the boundary, instead of a covariant causal diamond; second, it probes behind the horizon, which is supposed to contain information beyond thermodynamics. It was conjectured in [18, 19] that the action evaluated in the WDW patch is dual to the relative complexity of the quantum state living on Σ. This conjecture is referred to as 'complexity

[6] We point it out that due to the famous subtlety about type IIB action, that the self-duality condition should be imposed by hand, the treatment we use for the action is only plausible. There are other ways to impose self-duality, for example the PST formulation, but the action computation and the holography there will be subtle.

= action' or CA duality. In our noncommutative geometry setup, we will be interested in the WDW patch for the two-sided black hole, which intersects the left boundary at time t_L, and the right boundary at time t_R. According to CA quality, the action evaluated on such a patch will compute the relative complexity of the quantum state of the boundary CFT living on the (t_L, t_R) slice as

$$\mathcal{C}(t_L, t_R) = kS_{WDW}, \tag{3.8}$$

with the coefficient set to $k^{-1} = \pi\hbar$ by the assumption that AdS-Schwartzchild black hole saturates the Lloyd bound. The complexity computed this way is cutoff dependent, but its time derivative

$$\dot{\mathcal{C}}(t_L, t_R) := \frac{d}{dt_L}\mathcal{C}(t_L, t_R), \tag{3.9}$$

in which we are interested, is cutoff independent. Notice that our choice to differentiate with respect to the left time is arbitrary, as the geometry should be symmetric between left and right. It will prove convenient to utilize radial advanced/retarded null coordinates:

$$dr^* = \frac{R^2 dr}{r^2 f(r)}, \quad u = t + r^*, \quad v = t - r^*. \tag{3.10}$$

Notice that unlike r, r^* has units of length. Suppressing all but the bulk and timelike direction, the contributions to the time rate change of the WDW patch can be visualized in the conformal diagram represented in Figure 3.1.

The calculation of the time rate change of the action is detailed in Appendix B.1. It is convenient to express the result in terms of the radial

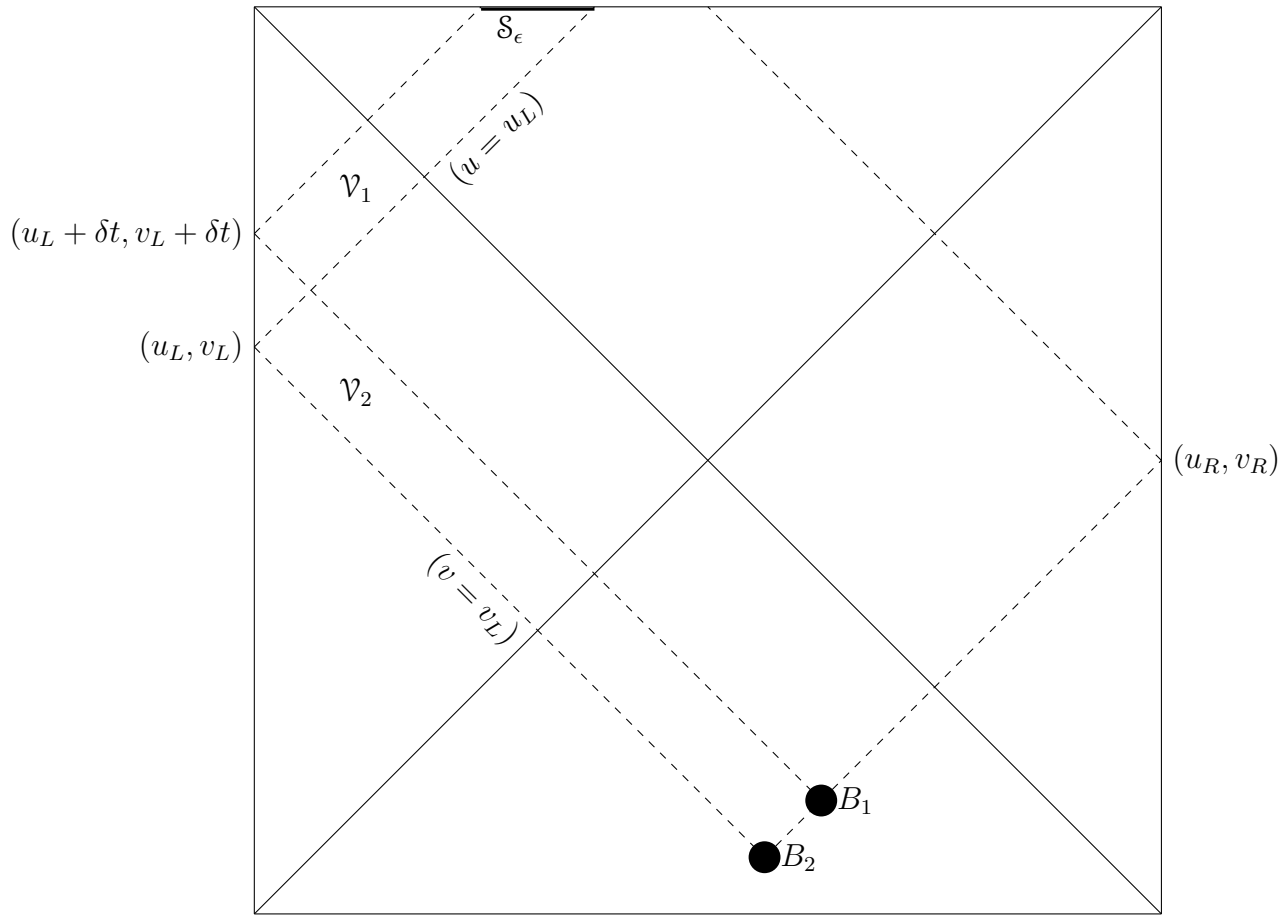

Figure 3.1: Two WDW patches separated by δt. Although the boundary of each patch is really at some large but finite r_b, the choice of r_b drops out in the differences we consider and we do not indicate it explicitly in this graphic.

coordinate r_B of the pastmost joint of the WDW patch (joint B_2 in the diagram 3.1, which coincides with joint B_1 as $\delta t \to 0$.) Note that r_B increases monotonically with t_L from $r_B = 0$ to $r_B = r_H$ as $t_L \to \infty$, and so we will use it to parameterize the time dependence of the complexification rate. [7] We find the following combined result:

$$\dot{S}_{WDW} = \frac{\Omega_5 V_3}{(2\pi)^7 \hat{g}_s^2}\left(\frac{-2\log(1+a^4 r_B^4)}{a^4} + 4r_B^4 + 6r_H^4 + 3(r_H^4 - r_B^4)\log\Big|\frac{c\bar{c}\sqrt{\hat{g}_s}R^2 r_B^2}{\alpha(1+a^4 r_B^4)^{1/4}(r_H^4 - r_B^4)}\Big|\right) \tag{3.11}$$

where c and $\bar{c}$ are arbitrary constants associated with the normalization of boundary null generators entering the computation of δS_{joint}. See Appendix B.1.3, as well as [74], [24] for discussion.

Various aspects of the time dependence (or r_B dependence) of equation 3.11 are unusual in light of the conjectured CA duality. Similar features have been seen in other systems [21]. We discuss the finite time behavior in Section 3.4.

The late time complexification rate is achieved by sending $r_B \to r_H$:

$$\dot{S}\big|_{t\to\infty} \approx \frac{\Omega_5 V_3 r_H^4}{(2\pi)^7 \hat{g}_s^2}\left(10 - 2\frac{\log(1+a^4 r_H^4)}{a^4 r_H^4}\right) \tag{3.12}$$

One can immediately see that if we assume the standard relationship, $\mathcal{C} = kS$ with $k = 1/\pi$, then the system violates the Lloyd bound (3.1) at late times: the ratio $\frac{\dot{S}}{2M}$ should be less than or equal to 1, but at late times

[7] We consider only $t_L > 0$, and fix t_R so that this corresponds to when the joint B has left the past singularity.

it saturates values between 4/3 to 5/3 as we vary a. The relevance of the bound to holographic complexity has been disputed [64], and violations have been found in many other systems. But for purposes of comparison we find it interesting that, even if we had not assumed the standard $k = 1/\pi$, but instead used the logic that commutative black holes should saturate the Lloyd bound, we would set $k = 3/(4\pi)$. Clearly, the associated bound would fail immediately upon considering highly noncommutative black holes. Rather than proposing some different k in the relationship $\mathcal{C} = kS$, we find it plausible that such a choice does not generalize to all systems, at least under the current conventions for computing bulk action.

Overlooking the Lloyd bound for now, the dependence of the late time complexification on the noncommutativity parameter a is rather striking.

As one can see from Figure 3.2, the complexification rate increases with the non-commutativity parameter a, or more specifically the Moyal scale. It's also intriguing that a always appears in the combination ar_H, indicating that the only reference scale in the theory that the Moyal scale is sensitive to is the thermal scale $T^{-1} \sim r_H^{-1}$. When $a \ll T^{-1}$, the complexification rate does not change much. It noticeably changes when a becomes comparable to T^{-1}. When $a \gg T^{-1}$, the complexification rate stops growing and saturates a new bound. It is inspiring to see that it does not grow indefinitely because that will violate the Lloyd bound in any possible sense. On the other hand, the ratio that it increases is an interesting rational number 5/4. It may imply that this enhancement could be understood as some counting problem. With all

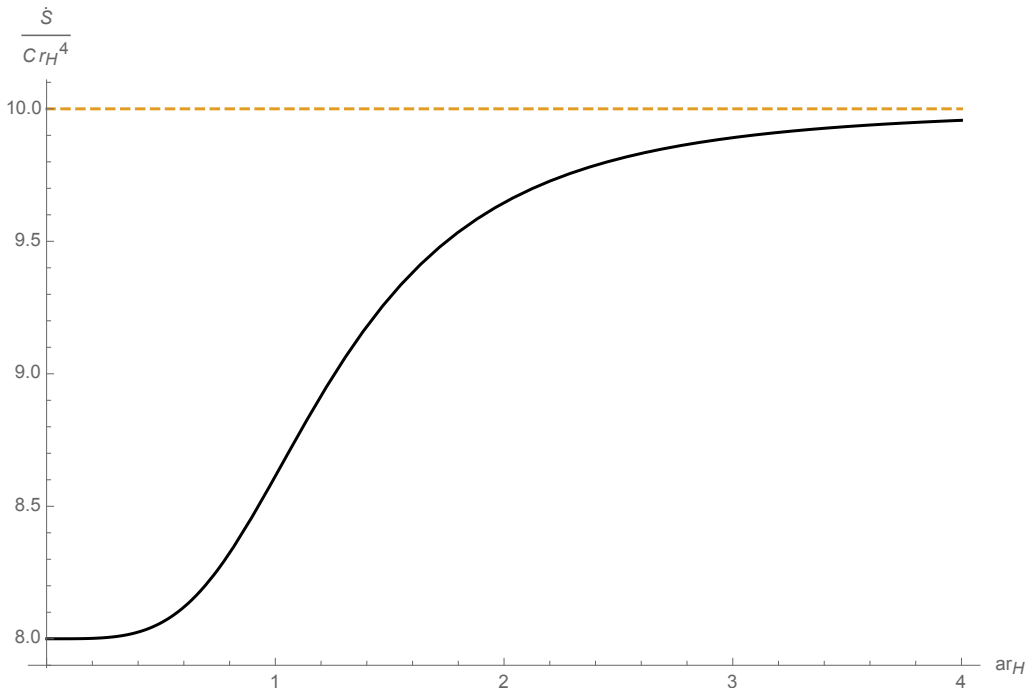

Figure 3.2: Late time action growth rate normalized by $C = \frac{\alpha^4 \Omega_5 V_3}{\hat{g}_s^2}$ and extra r_H dependence, versus ar_H, which is the Moyal scale measured in units of thermal length. It is observed that the complexification rate under the CA conjecture increases significantly when the Moyal scale is comparable to the thermal scale, and saturate a new bound which is 5/4 of the commutative value when the Moyal scale is much larger than the thermal scale.

these interesting features in mind, we want to answer two questions:

1. How might we explain the enhancement from non-commutativity?

2. Are there other examples of noncommutative theories that corroborate these results?

These will provide the content for the next few sections.

3.3 Non-Commutativity Enhancement of Complexification Rate

Why the above enhancement should be exactly 25% is as of yet unclear. We do, however, have a conceptual argument for why there should be a noncommutative enhancement at all.

Consider the following problem: We have a unitary operator U, whose complexity is known to be $\mathcal{C}(U)$, and we want to know what can be said about the complexity of $\mathcal{C}(U^N)$ for some integer N. One thing that can be immediately said is that

$$\mathcal{C}(U^N) \leq N\mathcal{C}(U) \tag{3.13}$$

Because given an optimal circuit Q implementing U, U^N can be implemented by N successive applications of Q, namely Q^N. [8] The bound above

[8] There is a subtlety here in that Q only need implement a unitary that is within some

need not be saturated, however, as there might be a few gates at the beginning of Q which can cancel with some at the end of a successive copy of Q, resulting in a new circuit which (a unitary identical) to Q^N, but which is less complex. If we suppose that every time a new copy of U is added (after the first one of course), we get a cancellation of χ gates, and we suppose that χ doesn't depend on N (or at least asymptotes to a constant as N becomes large), then we have

$$\mathcal{C}(U^N) \approx N\mathcal{C}(U) - (N-1)\chi \tag{3.14}$$

It's easy to show that this formula holds for any $U \to U^n$ with the same χ.

If we are then interested in the (time evolution of the complexity of a family of operators) generated by some hamiltonian H

$$U(t) = e^{iHt}, \tag{3.15}$$

then we may use the above to write

$$\mathcal{C}(t) \equiv \mathcal{C}(U(t)) = \mathcal{C}[U(\delta t)^{t/\delta t}] \approx \frac{t}{\delta t}\left[\mathcal{C}(\delta t) - \chi\right] + \chi. \tag{3.16}$$

This will be true for any t and δt. Therefore we can compute the complexification rate

$$\frac{d}{dt}\mathcal{C}(t) \approx \frac{1}{\delta t}\left[\mathcal{C}(\delta t) - \chi\right]. \tag{3.17}$$

small number ϵ of U, but if this is the case, there is no guarantee that Q^N will be within ϵ of U^N. It is also possible that for particular choices of gate set, some power of Q, say Q^M, may itself be a gate. This would result in "saw tooth" growth in complexity and periodically discontinuous time derivatives. It may be hoped that such issues are rendered obsolete in an appropriate continuum limit (as in the "geometry of complexity" program [36, 35]), and we ignore these subtleties for the present discussion.

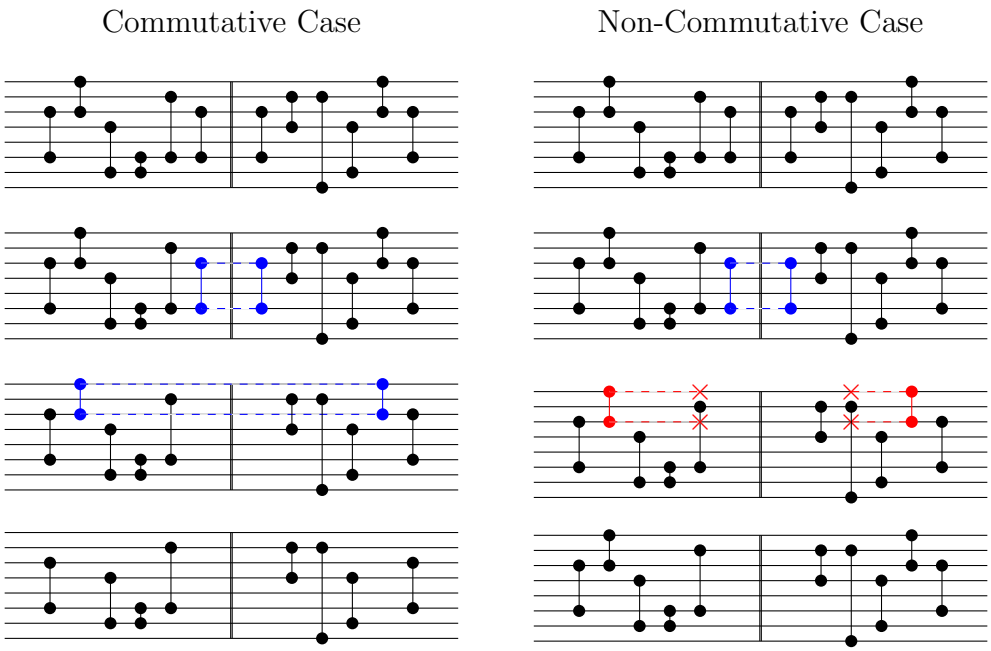

Figure 3.3: This circuit represents the end of one copy of a circuit Q_U implementing a hypothetical unitary U and the beginning of a second copy of Q_U. In this plot horizontal lines are qubits, and the dots connected by vertical lines are gates acting on the pair of qubits they connect. For this illustration, we will consider gates to be their own inverse. Gates from two copies may cancel (illustrated here with dashed blue lines connecting the gates), reducing the complexity of the circuit and providing a more efficient way to compute U^N. This cancellation relies, however, on the ability of gates to commute past each other, so that gates which could cancel can meet. We argue that in the non-commutative case, fewer gates commute and so there are fewer cancelations of this type. In this illustration, we see on the third line that a gate which can commute to cancel in the commutative case is prevented from doing so in the non-commutative case due to mild non-locality. Cartoon inspired by one used in a talk by Adam Brown.

Now, what happens if we turn on non-commutativity in our theory? Let us suppose that our Hamiltonian $H = H_a$ varies continuously with the Moyal scale a, and suppose that our gates vary continuously as well so that the gates in the noncommutative theory can be identified with gates in the commutative theory. Suppose furthermore that for sufficiently small δt, $U_a(\delta t) = e^{iH_a \delta t}$ can be optimally approximated by the same circuit Q, but with each of the original gates g replaced with its noncommutative analog g_a (Call this circuit Q_a). Then it is still true that U_a^N can be implemented by Q_a^N. But now, because of the non-commutativity, it is likely that fewer of the gates at the beginning and end of Q will commute with each other (see figure 3.3). And so we can still write

$$\mathcal{C}_a(t) \approx \frac{t}{\delta t}\left[\mathcal{C}_a(\delta t) - \chi_a\right] + \chi_a \approx \frac{t}{\delta t}\left[\mathcal{C}(\delta t) - \chi_a\right] + \chi_a, \tag{3.18}$$

but because fewer gates cancel, χ_a will be smaller than the original χ. These mean that the complexifaction rate

$$\dot{\mathcal{C}}_a(t) \equiv \frac{d}{dt}\mathcal{C}_a(t) \approx \frac{1}{\delta t}\left[\mathcal{C}(\delta t) - \chi_a\right] \tag{3.19}$$

gets an enhancement due to the suppression of χ_a. Finally we get an enhancement ratio of complexification rate as

$$\dot{\mathcal{C}}_a(t) \approx \frac{\mathcal{C}(\delta t) - \chi_a}{\mathcal{C}(\delta t) - \chi}\dot{\mathcal{C}}(t). \tag{3.20}$$

The same effect could be understood as arising from an increased nonlocality due to the noncommutativity. The dependence of complexity growth

on the locality of gates is explored in [19], where an extension of the Lloyd bound is studied by looking at the "k-locality" of the Hamiltonian and the gate set. A "k-local" operator is one that acts on at most k degrees of freedom: a k-local Hamiltonian consists of interactions coupling at most k degrees of freedom, and similarly a k-local gate set consists of at most k-local operators. [9] For convenience we let the Hamiltonian be "k-local" while the gate set is "j-local." Usually, the Lloyd bound should be satisfied if $j = k$, because one can choose the coupling terms as gates so that the time evolution could be easily implemented by the gates. However if one chooses a different j for the gate set, a bound of the following general form is to be expected

$$\dot{\mathcal{C}} \leq \frac{g(k)}{g(j)} \frac{2M}{\pi}, \tag{3.21}$$

where $g(k)$ is a monotonically increasing function. The interesting connection to our interpretation of non-commutativity is that the Moyal area introduced in non-commutative space can be thought of as an effective k for the Hamiltonian, meaning that non-local interactions couple wider range of degrees of freedom than local interactions. On the other hand, we are not changing j because our holographic prescription is not changed. Then we have an extra factor $g(k)/g(j) > 1$ in the bound, hence an enhanced bound. A similar factor greater than 1 is hence obtained in eq(3.20).

[9] To avoid dependence on the choice of basis, we would like to define k as the maximum rank of the coupling terms, or the maximum rank of the generators of the gates.

3.4 Finite Time behavior

Up to now, we have only discussed the asymptotic behavior of the complexification rate at late times. It is plausible that the early time complexification rate is not as important as the late time limit because there is a thermal scale time resolution for this quantity. One might think of this resolution as the time scale for a new gate to act on the state. In the paper [21] people carefully studied the finite time behavior of the complexification rate and found several interesting features. We will briefly outline the finite time behavior for noncommutative SYM, reproduce those features, and find new features introduced by the non-commutativity.

We will rewrite equation (3.11) using the dimensionless parameters

$$b = ar_H, \quad \rho = r_B/r_H, \quad \gamma = \frac{c\bar{c}\sqrt{\hat{g}_s}R^2}{\alpha' r_H^2}, \tag{3.22}$$

so that we get

$$\frac{\delta S}{\delta t} = \frac{\Omega_5 V_3 r_H^4}{(2\pi)^7 \hat{g}_s^2}\left(\frac{-2\log(1+b^4\rho^4)}{b^4}+4\rho^4+6+3(1-\rho^4)\log\Big|\frac{\gamma\rho^2}{(1+b^4\rho^4)^{1/4}(1-\rho^4)}\Big|\right). \tag{3.23}$$

Note that since $T = r_H/\pi$, we have $b = \pi a T$.

We will now normalize this by the late time commutative result at the same temperature to define

$$\dot{C}_{\rm n}(\rho) = \frac{-\log(1+b^4\rho^4)}{4b^4}+\frac{1}{2}\rho^4+\frac{3}{4}+\frac{3}{8}(1-\rho^4)\log\Big|\frac{\gamma\rho^2}{(1+b^4\rho^4)^{1/4}(1-\rho^4)}\Big| \tag{3.24}$$

Substituting left time in thermal units for ρ, can plot $\dot{C}_n$ vs time at fixed b and γ, yeilding (in the case where we take $b \to 0$ and $\gamma = 80$) the plot in figure 3.4.

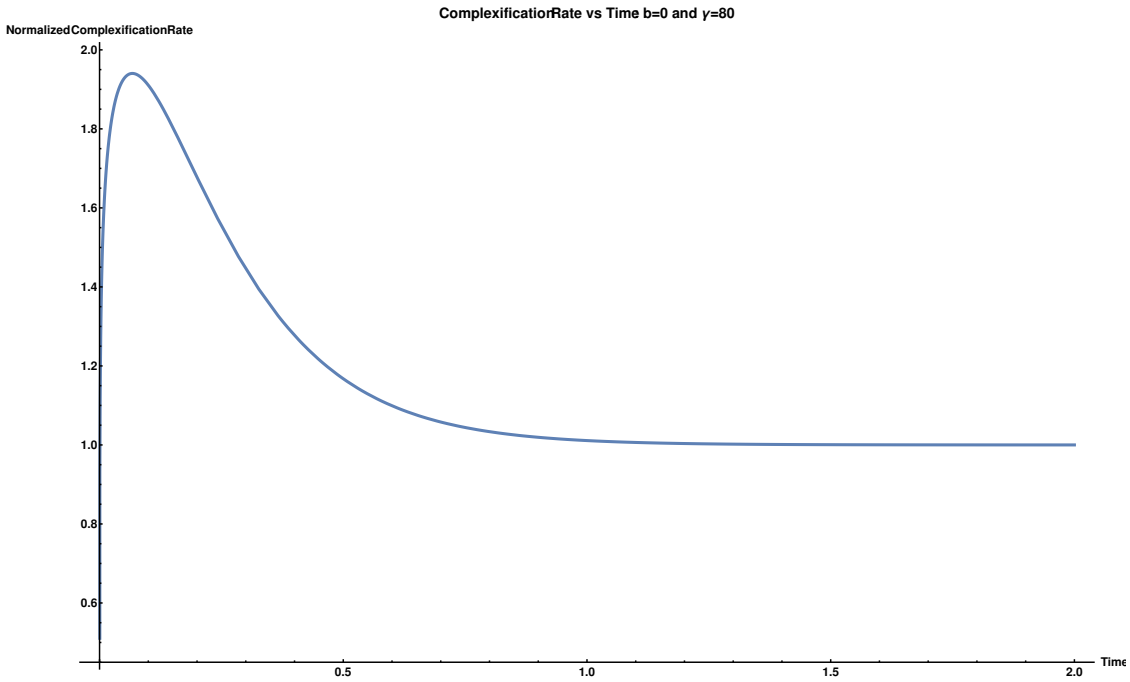

Figure 3.4: Normalized complexification rate versus time in thermal units for $\gamma = 80$ and $b = 0$.

It is clear from this plot that there is a local maximum at early time (around $t = 0.1\beta$, β being the inverse temperature), and then at late times, it approaches the smaller asymptotic value from above. There is also a logarithmic divergence as t goes to zero which comes from the log term in equation (3.24). Both of these features are observed in [21], where they are discussed in great detail. The logarithmic divergence is not important in the sense that if

you take the average complexification rate over a roughly thermal time scale, this divergence will be gone. A small period of decreasing complexity remains, but such behavior is not altogether prohibited. At early times the complexity is highly sensitive to the choice of the reference state, and only at late times is a constant growth rate expected for generic (time-independent) Hamiltonians. Regardless, the issues of the local maximum and the asymptotic approach to the "bound" from above are not resolved in any explanations here. One could average over an artificially long period of time to smooth out the local maximum, but doing so would never eliminate the approach from above, irrespective of the physicality of such a procedure.

Our primary interest here, however, is to discuss how these behaviors change with the noncommutative parameter b. To that end, we will consider what happens when we replot this curve fixing γ but varying b. The result is displayed in figure 3.5.

From figure 3.5 we see that as the non-commutativity is turned up, the local maximum decreases, and the asymptotic value increases. It is obvious that the change happens at $b \sim \pi$, which is when the Moyal scale a is comparable to the thermal scale $T^{-1} = \pi/r_H$. For $b \gg \pi$, it seems that the asymptotic value is approached from below. Strictly speaking, it is not true, because the local maximum always exists, but has a diminishing relative height and is pushed to very late time. We can find the local maximum and plot its ratio to the asymptotic value versus b as in figure 3.6. The fact that the local maximum decays physically rather than by tuning some artificial

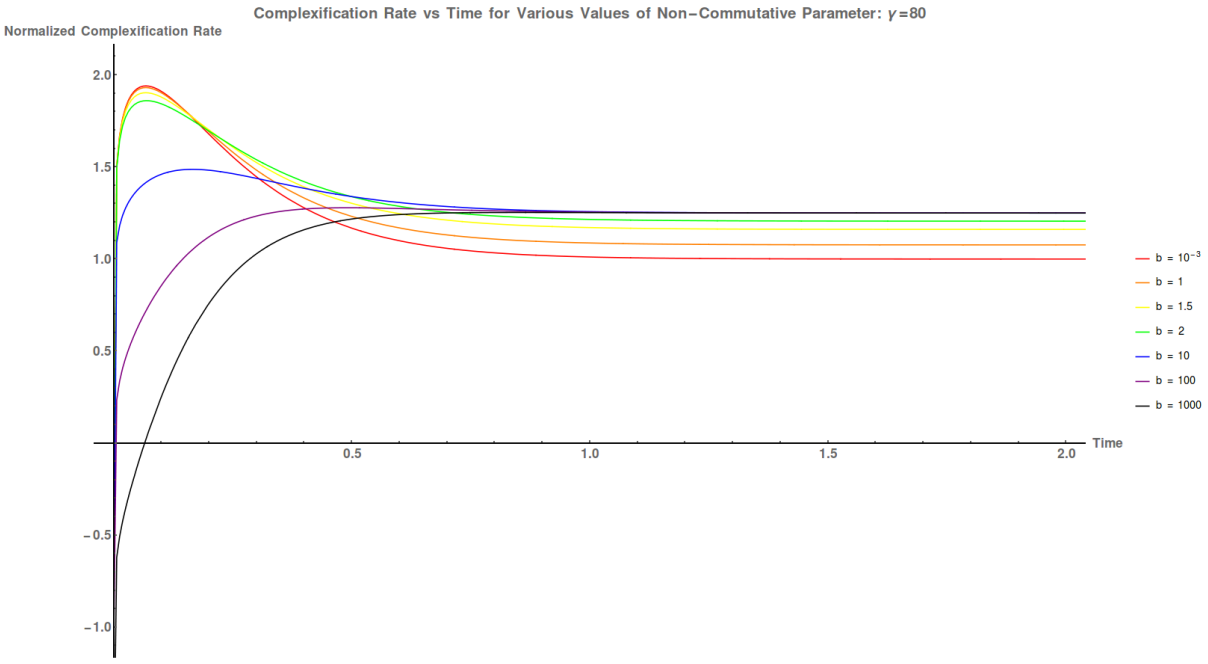

Figure 3.5: normalized complexification rate versus time in thermal units. γ is held fixed at 80 while $b = ar_H$ is varied.

choice is a sign that the noncommutative complexification rate at late time is a more qualified bound for a generic quantum system. We will discuss it in more details in the conclusion.

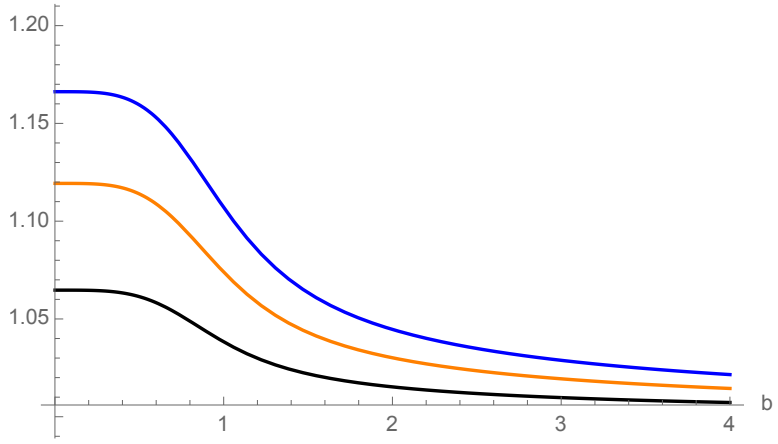

Figure 3.6: The vertical axis is the ratio between the local maximum and the asymptotic late time value of the complexification rate. The black, orange and blue curves correspond to $\gamma = 1, 2, 3$.

It is observed that the complexification rate mainly depends on temperature through the combination b, except an extra logarithmic contribution from γ. Therefore we expect that the variation with respect to temperature is similar to figure 3.5. This can be implemented by varying b while fixing the combination γb^2, i.e., fixing a. When this is done with $\gamma b^2 = 1$ one gets figure 3.7, which is indeed similar to figure 3.5. This check shows that the only scale that the non-commutativity a is sensitive to is the thermal scale.

Finally, one may also be interested in the effect of γ, which at fixed AdS radius and temperature encodes information about the normalization of the

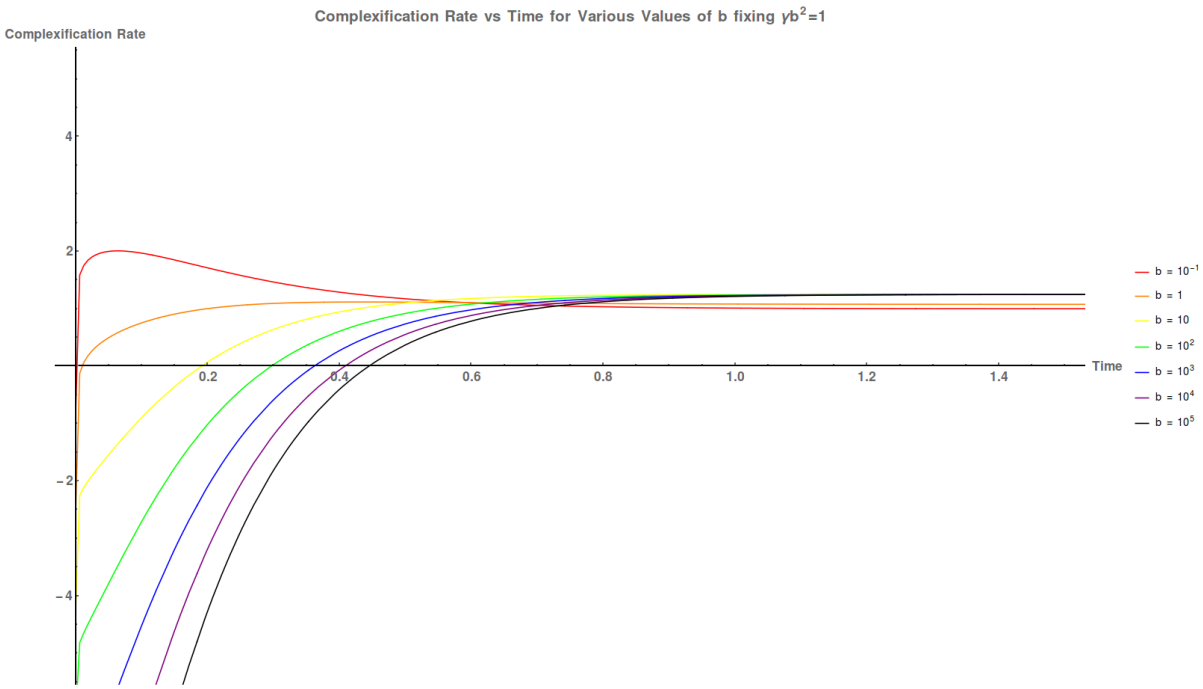

Figure 3.7: normalized complexification rate versus time in thermal units. γb^2 is held fixed at 1 while $b = ar_H$ is varied.

generators of the null boundaries of the WDW patch. It has been suggested that this normalization, which is ambiguous in the action, should correspond to an ambiguity in the definition of complexity on the boundary such as the choice of reference state [24]. In our case, we observe that the dependence on γ does not depend on the non-commutativity at all, which seems to support this idea for a broader class of theories.

3.5 Other noncommutative systems

As a test of the above argument, and to better understand the dependence of the enhancement on various factors, we would like to consider more examples of noncommutative field theories. It's easy to extend the D3 brane solution we discussed in Section 3.2 to other Dp branes, in which we are also able to put more noncommutative pairs of directions. For $p = 4, 5, 6$, we can turn on more than one B field component, making multiple pairs of directions non-commuting. Let us denote the number of non-vanishing B components as m so that B will be a rank-$2m$ matrix. In this section, we will investigate the dependence of late time complexification rate on the dimension of space p and the rank of the B field.

3.5.1 Supergravity solutions and decoupling limit

The general string frame metric for non-extremal Dp branes with m non-commuting pairs of directions are given as

$$\begin{aligned}\frac{ds^2}{\alpha'} = &\left(\frac{r}{R}\right)^{\frac{7-p}{2}} \left(-f(r)dx_0^2 + \sum_{i=1}^{p-2m} dx_i^2 + \sum_{i=1}^{m} h_i(r)(dy_{i,1}^2 + dy_{i,2}^2)\right) \\ &+ \left(\frac{R}{r}\right)^{\frac{7-p}{2}} \left(\frac{dr^2}{f(r)} + r^2 d\Omega_{8-p}^2)\right)\end{aligned} \tag{3.25}$$

where

$$f(r) = 1 - \frac{r_H^{7-p}}{r^{7-p}}, \tag{3.26}$$

$$h_i(r) = \frac{1}{1 + (a_i r)^{7-p}}. \tag{3.27}$$

In NS-NS sector we have

$$\begin{aligned}e^{2\Phi} &= \hat{g}_s^2 \left(\frac{R}{r}\right)^{\frac{(7-p)(3-p)}{2}} \prod_{i=1}^{m} h_i(r), \\ B^{(i)} &= -\frac{\alpha'}{(a_i R)^{\frac{7-p}{2}}}[1 - h_i(r)]dy_{i,1} \wedge dy_{i,2}.\end{aligned} \tag{3.28}$$

We also have many R-R fields turned on via the T-duality. One would expect them by looking at the Chern-Simons term in D brane action

$$S_{CS}^{Dp} = \mu_p \int \left(C \wedge \exp(B + kF)\right)_{p+1}. \tag{3.29}$$

Only rank-$(p+1)$ R-R potential C_{p+1} is turned on without any background field, whereas in the presence of B field, terms like $C_{p+1-2n} \wedge B^{(i_1)} \wedge \cdots \wedge B^{(i_n)}$ can also be sourced, where $n = 0, 1, \cdots, m$. In other words, when $m = 1$, we have C_{p-1} turned on; when $m = 2$, we have C_{p-3} turned on, and so on.

The general formulae for all these R-R fields are

$$\begin{aligned}
C_{p+1} &= -\frac{(\alpha')^{\frac{p+1}{2}}}{\hat{g}_s}\left(\frac{r}{R}\right)^{7-p}\prod_i h_i(r),\\
C^{(j)}_{p-1} &= \frac{(\alpha')^{\frac{p-1}{2}}}{\hat{g}_s}\left(\frac{r}{R}\right)^{7-p}(a_jR)^{\frac{7-p}{2}}\prod_{i\neq j} h_i(r),\\
C^{(j,k)}_{p-3} &= -\frac{(\alpha')^{\frac{p-3}{2}}}{\hat{g}_s}\left(\frac{r}{R}\right)^{7-p}(a_ja_kR^2)^{\frac{7-p}{2}}\prod_{i\neq j,k} h_i(r),\\
C^{(j,k,l)}_{p-5} &= \frac{(\alpha')^{\frac{p-3}{2}}}{\hat{g}_s}\left(\frac{r}{R}\right)^{7-p}(a_ja_ka_lR^3)^{\frac{7-p}{2}}\prod_{i\neq j,k,l} h_i(r).
\end{aligned} \tag{3.30}$$

We are omitting the basis here, but it's clear that these components are along all the directions on Dp brane except for the directions of the B fields indicated by their superscript. We also omitted their (inverse) hodge dual forms which may contribute to the action.

While these are all good solutions for supergravity in the bulk, one has to be careful with its world volume dual theory. The decoupling limit of the world volume theories for $2 \leq p \leq 6$ in the presence of B field is studied in [75], with the conclusion that there is no decoupling limit for D6 branes even for $m > 0$. For $p \leq 5$, decoupling limits do exist, and it's reasonable to talk about the complexity on the world volume theory. One may be worried that for D4 brane we have to up lift to 11 dimensions to compute the M theory action, but the effective string coupling at high energy is

$$e^{\Phi} \sim r^{\frac{(7-p)(p-3-2m)}{4}}, \tag{3.31}$$

which is suppressed by the non-commutativity when $m \geq 1$, indicating that at sufficiently high energy, we don't have to go to M theory.

As such, we will be using type IIB action for odd p and type IIA action for even p. The type IIA action is

$$S^{\rm IIA}_{\rm string} = \frac{1}{2\kappa^2}\int dx^{10}\sqrt{-g}\left[e^{2\Phi}(\mathcal{R}+4|d\Phi|^2-\frac{1}{2}|H|^2)-\frac{1}{2}|F_2|^2-\frac{1}{2}|\tilde{F}_4|^2\right]-\frac{1}{4\kappa^2}\int B\wedge F_4\wedge F_4, \tag{3.32}$$

with the usual conventions:

$$F_2 = dC_1, \qquad F_4 = dC_3, \qquad \tilde{F}_4 = F_4 - C_1\wedge H. \tag{3.33}$$

3.5.2 Complexification Rates

We report the action growth rates with the following p-dependent prefactor,

$$c_p \equiv \frac{\Omega_{8-p} r_H^{7-p}}{(2\pi)^7 \hat{g}_s^2}, \tag{3.34}$$

We also divide out the transverse volume V_p to give a "density of action." The complexification rate will be related to the action growth rate by eq(3.8), where the coefficient k is not specified yet. We will discuss the strategy of choosing k at the end of the section. Both the joint and boundary contributions to the late time complexification rate take a particularly simple form:

$$\begin{aligned} \dot{S}_{\rm joint} &= (7-p)c_p \\ \dot{S}_{\rm boundary} &= \frac{1}{8}(65-14p+p^2)c_p \end{aligned} \tag{3.35}$$

The bulk contributions exhibit more interesting dependencies on the size and number of noncommutativity parameters. These are here reported for each p.

D2 Brane

This is the simplest case, where we have fewest R-R fields and don't need to put the self-duality constraint. We have

$$F_2 = dC_{p-1}, \tag{3.36}$$

$$\tilde{F}_4 = dC_{p+1} - C_{p-1} \wedge H. \tag{3.37}$$

Plugging them in the type IIA action, we obtain the complexity growth rate. Including all contributions, the late time limit becomes

$$\dot{S}_{p=2,m=1} = 12 c_p. \tag{3.38}$$

Surprisingly, we find that the late time complexification rate does not even depend on the non-commutativity parameter a. We may argue that it is the case where the bound is already saturated so that non-commutativity could not enhance it anymore.

D4 Brane

This is the minimal dimension that we can include two pairs of non-commutative directions, hence $m = 2$. The R-R field contents are

$$F_2 = dC^{(1,2)}_{p-3}, \tag{3.39}$$

$$\tilde{F}_4 = \sum_i \left[dC^{(i)}_{p-1} - C^{(1,2)}_{p-3} \wedge H^{(i+1)} \right] + *^{-1} \left[dC_{p+1} - \sum_i \left(C^{(i)}_{p-1} \wedge H^{(i)} \right) \right]. \tag{3.40}$$

Note that mod m is understood in the supercript of the forms.

The complexity growth rate including all contributions has late time limit

$$\dot{S}_{4,2} = \left(5 + \frac{3a_1^3 a_2^3 r_H^6}{(1+a_1^3 r_H^3)(1+a_2^3 r_H^3)}\right) c_p. \tag{3.41}$$

The $p = 4,\ m = 0, 1$ cases can be obtained by taking one or both of the a parameters to zero:

$$\dot{S}_{4,0} = \dot{S}_{4,1} = 5c_4 \tag{3.42}$$

It's striking that turning on a single pair of noncommutative directions does not affect the late time complexification rate at all, but turning on the second pair does increase the rate. It means that we cannot use the argument as for $p = 2$ to explain the zero enhancement here because obviously the bound was not saturated yet.

D5 Brane

It's another case where we need to take into account the self-duality issue. Again we can have $m = 2$, and the R-R field contents are

$$F_3 = dC_{p-3}^{(1,2)} + *^{-1}\left[dC_{p+1} - \sum_i \left(C_{p-1}^{(i)} \wedge H^{(i)}\right)\right], \tag{3.43}$$

$$\tilde{F}_5 = \sum_i \left[dC_{p-1}^{(i)} - \frac{1}{2} C_{p-3}^{(1,2)} \wedge H^{(i+1)} + \frac{1}{2} dC_{p-3}^{(1,2)} \wedge B^{(i+1)}\right] + \text{self dual}. \tag{3.44}$$

The complexity growth rate including all contributions has late time limit

$$\dot{S}_{5,2} = \left(\frac{11}{2} + \frac{a_1^2 a_2^2 r_H^4 - 2}{2(1+a_1^2 r_H^2)(1+a_2^2 r_H^2)} + \frac{a_2^2 \log(1+a_1^2 r_H^2)}{2a_1^2(a_1^2 - a_2^2)} + \frac{a_1^2 \log(1+a_2^2 r_H^2)}{2a_2^2(a_2^2 - a_1^2)}\right) c_5. \tag{3.45}$$

We can also examine the $m = 1$ case by taking $a_2 = 0$ and $a_1 = a$:

$$\dot{S}_{5,1} = \left(5 - \frac{1}{1 + a^2 r_H^2}\right) c_p, \qquad \dot{S}_{5,0} = 4c_p \tag{3.46}$$

In contrast with $p = 4$, turning on the first pair of noncommutative directions already changes the complexity, and turning on the second enhances more.

D6 Brane

Finally we may investigate a case where we can turn on 3 pairs of noncommutative directions, hence D6 brane. For $m = 3$, the R-R field contents are

$$F_2 = dC_{p-5}^{(1,2,3)} + *^{-1}\left[dC_{p+1} - \sum_i \left(C_{p-1}^{(i)} \wedge H^{(i)}\right)\right], \tag{3.47}$$

$$F_4 = \sum_i \left[dC_{p-3}^{(i+1,i+2)} - C_{p-5}^{(1,2,3)} \wedge H^{(i)}\right] + *^{-1}\left[dC_{p-1}^{(i)} - \sum_{j\neq i} C_{p-3}^{(i,j)} \wedge H^{(j)}\right]. \tag{3.48}$$

The complexity growth rate including all contributions has late time limit

$$\dot{S}_{6,3} = \left(4 + \frac{a_1 a_2 \log(1 + a_3 r_H)}{(a_2 - a_3)a_3(a_3 - a_1)r_H} + \frac{a_2 a_3 \log(1 + a_1 r_H)}{(a_3 - a_1)a_1(a_1 - a_2)r_H} + \frac{a_3 a_1 \log(1 + a_2 r_H)}{(a_1 - a_2)a_2(a_2 - a_3)r_H}\right) c_6 \tag{3.49}$$

The three a-dependent terms have the property that no matter how many a's you turn off, their sum is a constant as -1. Thus again, it is a situation where only turning on maximum number of non-commutativity can we increase the non-commutativity, similar to the $p = 4$ case.

$$\dot{S}_{6,0} = \dot{S}_{6,1} = \dot{S}_{6,2} = 3c_6 \tag{3.50}$$

However, this complexity growth rate seems to have no physical meaning, because there is not a world volume theory that is decoupled from gravity. The holographic principle is subtle in this case. We present the result here because the bulk computation can be done in a similar manner without noting the difference. Whether the quantity so computed has any physical meaning is an open question.

3.5.3 Summary of Results

From the above computation, we find that when we turn on non-commutativity on Dp branes, the complexity growth rate either stays the same, or increases. The fact that it does not decrease is encouraging for our argument given in section 3.3. However, the values of the enhancement ratio are not understood.

In the table 3.1, we list all the density of late time action growth rate in unit of c_p, in the limit that all m non-commutativity parameters a_i, $i = 1, .., m$, goes to infinity.

There are no obvious laws that govern these rates in general, but we do observe some interesting features. For both D3 and D5 branes, we have enhancement from each pair of non-commuting directions. In particular, the ratio for the enhancement from the first pair are the same in both cases, and

p	$m=0$	$m=1$	$m=2$	$m=3$	πB_L
2	12	12	-	-	7
3	8	10	-	-	6
4	5	5	8	-	5
5	4	5	6	-	4
6	3	3	3	4	3

Table 3.1: This table lists all the action growth rate at late time for general p and m. They are in unit of the constant c_p defined in eq(3.34). The last column is showing the Lloyd bound B_L also in unit of c_p.

the enhanced amount from the first and second pair are also the same in D5 brane. These two cases seem to provide reasonable behaviors one may naively expect. On the other hand, the type IIA supergravity with even-ps does not always have complexification rate enhancement from non-commutativity. The reason for it may depend on the details of the boundary theory.

In the table 3.1, we also list the Lloyd bound computed from the ADM mass of the geometry (see Appendix B.2). One may set the coefficient k in eq(3.8) to let any of the complexification rate to saturate the Lloyd bound. For instance, if we want to set the commutative $\mathcal{N}=4$ SYM ($p=3$, $m=0$) to saturate the bound, we can take $\pi k_{p=3}=3/4$. However, the consequence is that we can always turn on the non-commutativity and violate this bound. In order that the Lloyd bound is not violated, we need to guarantee that the maximum complexification rate for each p is bounded by B_L, thus

$$k_2 \leq \frac{7}{12\pi}, \quad k_3 \leq \frac{3}{4\pi}, \quad k_4 \leq \frac{5}{8\pi}, \quad k_5 \leq \frac{2}{3\pi}, \quad k_6 \leq \frac{3}{4\pi}. \tag{3.51}$$

If one follows the argument at the end of section 3.3, and get an

enhanced bound for non-commutative field theory, the bound on k_p will be weaker. On the other hand, the Lloyd bound is defined under the assumption that all gates take a generic state to an orthogonal state, which is usually not true. It is argued that we simply should not take this bound seriously [64]. This objection will make it hard to determine what k should be, but for our purpose, k does not affect our main results.

3.6 Conclusion

In this paper, we have considered the effects of non-commutativity on the holographic complexity of SYM according to the complexity = action conjecture. We have done this in the hope that this would produce further evidence about the validity of this conjecture, and of the concept of holographic complexity more generally. Our main result is that the late time complexification rate increases with the non-commutativity in a class of theories.

We computed the holographic complexity for 4D $\mathcal{N} = 4$ non-commutative super Yang-Mills, by evaluating the WDW action in the bulk geometry described by type IIB supergravity with D3 branes. We saw a 5/4 enhancement for late time complexification rate in the non-commutative result over the commutative result. This was striking because it is well known that the thermodynamics of this theory are independent of the non-commutative parameter a. The observed changes to complexity support the idea that complexity is more than thermodynamics, and indicates that the CA prescription is reproducing this feature of complexity. Comparing to the Lloyd bound derived from the to-

tal energy, we discovered that using the coefficient of proportionality $k = 1/\pi$ as in [18] will make the commutative late time complexification rate violate the bound. One could in principle avoid this by arguing that k should not be universal for all kinds of theories, but the commutative black hole still can not saturate the bound because there should be space for enhancement from the non-commutativity.

We presented a quantum argument to explain this enhancement and to argue that we should have expected it. We assume that the time evolution operator is approximated by sequential copies of the same quantum circuit, and the optimization of the total circuit when you combine them will be less efficient in non-commutative theories. We also argue that this expectation matches the k-locality model prediction if we relate the size of Moyal scale to the size of locality k. Then we investigate the finite time behavior of this complexification rate and see that the problematic finite time maximum gets suppressed by non-commutativity.

Finally, we generalized the solution for D3 branes to general Dp branes to get a broader class of noncommutative gauge theories. We presented similar calculations as for $p = 3$ and obtained the late time complexification rates for $2 \leq p \leq 6$ and all allowed ranks of the B field. The results for $p = 5$ are similar to those for $p = 3$ but can have another enhancement of the same magnitude from a second B field component. This is consistent with our heuristic argument. The results for the even p cases are less well understood. We found that there is no enhancement for $p = 2$ and that for $p = 4$ one

must introduce a second B field component to get an enhancement. This result would seem to be in mild tension with the argument of section 3.3. The correct explanation for this behavior is left for future work. Despite not seeing an enhancement in some cases, it is at least encouraging that no decrease was observed, which would have been a much clearer contradiction to the arguments of section 3.3.

Regarding the statement that non-commutativity enhances the complexification rate in general, there are several interesting aspects one can investigate. First, this result is in tension with the often expressed idea that the commutative AdS-Schwarzschild black hole is the fastest possible computer [18]. If non-commutativity can somehow increase the computational speed even further, it would be very interesting to see if it also increases the scrambling process of the black hole. Second, it also would be interesting to compute the complexity of a weakly coupled field theory on a non-commutative manifold in order to test the conclusion of our heuristic argument in a non-holographic context. Such a computation would, in light of this work, provide for a more robust check on the complexity = action conjecture. The work of [24, 57] might prove useful to such an endeavor. Another interesting extension of this work would be to repeat the computations for the complexity = volume, and the complexity = spacetime volume conjectures, which will be both a test for our results and a test for the holographic complexity prescriptions. Finally, it was pointed out to us by Eoin Ó Colgáin that the geometry corresponding to the $D3$-brane case that we have considered here has been discovered to belong

to a larger class of deformations of AdS_5, studied in e.g. [76, 77, 78]. It would perhaps be interesting to extend the results of this paper to the more general case.

We would like to thank Jacques Distler, Hugo Marrochio, Robert Myers, and Phuc Nguyen for useful comments and discussion. This material is based upon work supported by the National Science Foundation under Grant Number PHY-1620610.

Chapter 4

Noether Charge, Black Hole Volume, and Complexity

4.1 Introduction

[1]The laws of black hole thermodynamics, at least in their traditional formulation [79, 80, 81, 82], do not include a pressure-volume conjugate pair. This conspicuous absence is perhaps related to the difficulty of defining the volume of a black hole in a coordinate-invariant way: unlike the area of the horizon, a naïve integration over the interior of a black hole depends on the foliation of spacetime. A number of relativists [83, 84, 85, 86, 87], and more recently high energy physicists [88], have suggested that the pressure should be identified as the cosmological constant. In this framework, dubbed the extended black hole thermodynamics or "black hole chemistry", the ADM mass of the black hole is reinterpreted as the enthalpy H of the system rather than its internal energy U. The volume, then, can be defined in the usual

[1]This chapter is a reproduction of [4], which I wrote with Willy Fishcler and Phuc Nguyen. My contribution was to see how the thermodynamic volume comes into the complexification rate of black holes according to CA, to assist with the calculations, and to develop the 'CV2.0' conjecture in collaboration with the other authors.

thermodynamical way to be:

$$V = \left(\frac{\partial H}{\partial P}\right)_S . \tag{4.1}$$

Fascinatingly enough, in simple cases such as the AdS-Schwarzschild or AdS-Reissner-Nordstrom (AdS-RN) black hole, the thermodynamic volume coincides with a naïve integration over the "black hole interior":

$$V = \frac{4}{3}\pi r_+^3 = \int_0^{r_+} \sqrt{-g} dr d\Omega_2^2. \tag{4.2}$$

In more complicated cases, such as rotating holes or solutions with hair, the thermodynamical volume is less intuitive, and it is an interesting question to ask how the volume arises as an integral of some local quantity over some region of spacetime, in a way similar to (4.2). For a selection of work on or related to this topic, we refer to [89, 90, 91, 92, 93, 94, 95].

Our main goal in this paper is two-fold: on the one hand, we attempt to shed light on the meaning of the thermodynamic volume as a geometrical quantity, which, a priori, is an abstract notion of volume associated to the black hole and does not correspond to the actual volume of any spatial region. On the other hand, we will relate the thermodynamic volume to holography, and in particular to the quantum complexity of the boundary state. Why should we believe that the thermodynamic volume has a role to play in the holographic context? To this question, we will offer four answers, which we list one after another below.

The first reason to believe that the thermodynamic volume has a place in holography is that, as we will demonstrate below, this quantity is derivable from the Noether charge (or Iyer-Wald) formalism [96, 97], or a slight twist thereof. This is the main finding of section 4.2. A powerful way to derive the first law of black hole thermodynamics, the Iyer-Wald formalism has yielded deep insights into the nature of black hole entropy, so it is a natural step to extend the formalism to derive the thermodynamic volume. In recent years, the Iyer-Wald formalism has proved useful to holographers as a means to translate between the geometry in the bulk to quantum information theoretic quantities on the boundary, starting with [98] where the formalism was used to derive the linearized equation of motion in the bulk from the first law of entanglement on the boundary in pure AdS. To give a few more examples, the formalism was used in [99] to relate matter in the bulk to the relative entropy on the boundary, in [100] to relate canonical energy in the bulk to the quantum Fisher information on the boundary, in [101] to relate quantum information inequalities to gravitational positive energy theorems, and finally in [102] in conjunction with the kinematic space program to clarify the emergence of gravity from entanglement.

The second reason to suspect that the thermodynamic volume is relevant to holography is that various notions of volume in the bulk have been identified with quantum information theoretic quantities. In particular, the size of the Einstein-Rosen bridge of a 2-sided eternal AdS black hole is believed to capture the complexity of the thermofield double state [18, 19]. Further-

more, the complexity of subregions of the boundary CFT [103, 104, 105, 106] and the fidelity [107] have been related to the volume of a constant time slice in the bulk enclosed between the Ryu-Takayanagi surface and the boundary. In the light of these ideas, it is suggestive that the thermodynamical volume also admits a quantum information theoretic interpretation, and we will find in this paper that it indeed seems so. In the second part of the paper (sections 4.3 and 4.4), we will relate the thermodynamic volume (and also the Smarr relation) to the complexity as per the proposals in [18, 19].

The third motivation to study the thermodynamic volume in holography is the question of to what extent holography knows about the black hole interior. In [108], the black hole interior was probed with minimal surfaces which cross the horizon, and the notion of "vertical entanglement" as well as a tensor network picture of black hole interiors were formulated. Like the quantum complexity, the vertical entanglement could serve as a useful way to keep track of time in the dual CFT. In the case of the complexity, the key observation is that the size of the ERB grows linearly with the boundary time at late time, a behavior conjectured to be true of the quantum complexity at exponentially late time.

However this linear growth can be observed for various geometrical entities crossing the wormhole, and to correctly pick out one among them is a non-trivial problem. This leads us to the fourth and last motivation of this paper: how to correctly quantify the size of an ERB and capture the complexity? Two ways to achieve this have been considered in the literature [15, 16, 18, 19].

The first way, first proposed in [16] and dubbed "complexity=volume" or CV-duality, postulates that the complexity is dual to the volume of the maximal spatial slice crossing the ERB. This proposal, while capturing the linear growth at late time, has the minor problem that a length scale has to be introduced "by hand", for which there seems to be no unique, natural choice. The second way, first proposed in [18] and dubbed "complexity=action" or CA-duality, postulates that the complexity is dual to the bulk action evaluated on the Wheeler-DeWitt (WDW) patch. This proposal solves the length scale problem of CV-duality and has, in addition, the practical advantage that the WDW patch is easier to work with than the maximal volume. We will see in this paper that the thermodynamic volume is intimately related to the linear growth of the WDW patch at late time. We will also point out a third possibility, dubbed "Complexity = Volume 2.0" in which complexity is identified with the spacetime volume of the WDW patch rather than the action. This is potentially even easier to work with and will be discussed in more detail further in the paper.

The paper is organized as follows: In Section 4.2, we briefly review the Iyer-Wald formalism (with varying cosmological constant) and apply it to derive the thermodynamic volume of two solutions: the charged BTZ black hole and the R-charged black hole. In Section 4.3, we move on to discuss the connection between the extended thermodynamics and the complexity in the simple case of the AdS-Schwarzschild black hole. In Section 4.4, we extend this connection with the complexity to a black hole with conserved charges

(i.e. electrically charged and rotating holes). In Section 4.5, we contrast our proposal for the complexity against CA-duality and show that, in certain cases, our proposal can help fix problems which ail CA-duality. In Section 5.6, we conclude and discuss future work.

4.2 Volume and Iyer-Wald Formalism

In this section we will present a slight generalization of the Iyer-Wald formalism [96, 97, 109] which will allow us to derive the volume. The formalism requires a diffeomorphism invariant action $S = \int \mathbf{L} = \int \mathcal{L}\boldsymbol{\epsilon}$, together with a solution with a bifurcate timelike Killing vector field ξ. We will follow the notation used in [98] [2]. Consider some general variation of the Lagrangian. For an action including a cosmological constant which is allowed to vary, one writes:

$$\delta\mathbf{L} = d\boldsymbol{\Theta} + \sum_{\phi} \mathbf{E}^{\phi}\delta\phi + \frac{\partial \mathbf{L}}{\partial \Lambda}\delta\Lambda, \tag{4.4}$$

[2] In particular, $\boldsymbol{\epsilon}$ denotes the usual volume form in d dimensions:

$$\boldsymbol{\epsilon} = \frac{1}{d!}\sqrt{-g}\ \varepsilon_{a_1..a_d} dx^{a_1} \wedge ... \wedge dx^{a_d} \tag{4.3}$$

We will find it useful to define the additional forms:

$$\boldsymbol{\epsilon}_{\mu} = \frac{1}{(d-1)!}\sqrt{-g}\ \varepsilon_{\mu a_1 ... a_{d-1}} dx^{a1} \wedge ... \wedge dx^{a_{d-1}}$$
$$\boldsymbol{\epsilon}_{\mu\nu} = \frac{1}{(d-2)!}\sqrt{-g}\ \varepsilon_{\mu\nu a_1 ... a_{d-2}} dx^{a1} \wedge ... \wedge dx^{a_{d-2}}$$

where

$$\mathbf{\Theta}(\delta\phi) = \sum_{\phi} \frac{\partial \mathbf{L}}{\partial\left(\nabla_{\mu}\phi\right)}\delta\phi \tag{4.5}$$

is the symplectic potential current,

$$\mathbf{E}^{\phi} = \frac{\partial \mathbf{L}}{\partial\phi} - \nabla_{\mu}\frac{\partial \mathbf{L}}{\partial\left(\nabla_{\mu}\phi\right)} \tag{4.6}$$

is the equation of motion form for the field ϕ, and where the sum over ϕ runs over the entire field content of the theory. In the case where this variation is due to applying a diffeomorphism generated by a vector field ζ, this becomes

$$\delta_{\zeta}\mathbf{L} = d\mathbf{\Theta}(\delta_{\zeta}\phi) + \sum_{\phi}\mathbf{E}^{\phi}\delta_{\zeta}\phi. \tag{4.7}$$

In this case, since our action is diffeomorphism invariant, we may apply Noether's theorem to derive the conserved current

$$\mathbf{J}(\zeta) = \mathbf{\Theta}(\delta_{\zeta}\phi) - \zeta\cdot\mathbf{L} \tag{4.8}$$

and a Noether charge form $\mathbf{Q}(\zeta)$ such that on-shell

$$\mathbf{J}(\zeta) = d\mathbf{Q}(\zeta). \tag{4.9}$$

Replacing our general vector field ζ by the killing vector field ξ, and considering some general other variation $\delta\phi$, we now define

$$\boldsymbol{\chi} = \delta_{\phi}\mathbf{Q}(\xi) - \xi\cdot\mathbf{\Theta}(\delta\phi). \tag{4.10}$$

By an algebraic computation we may see that on-shell

$$d\boldsymbol{\chi} = -\xi\cdot\frac{\partial \mathbf{L}}{\partial\Lambda}\delta\Lambda. \tag{4.11}$$

Applying Stokes' theorem to this form on a region Σ of a constant time slice bounded by the bifurcate killing horizon and the conformal boundary at infinity then yields

$$\int_\Sigma d\boldsymbol{\chi} = -\delta\Lambda \int_\Sigma \xi \cdot \frac{\partial \mathbf{L}}{\partial \Lambda} = \int_\infty \boldsymbol{\chi} - \int_\mathcal{H} \boldsymbol{\chi}. \tag{4.12}$$

In the case of a black hole spacetime, this reduces to the extended first law of black hole thermodynamics upon evaluation of the integrals, where roughly speaking, the second term from the left above gives rise to the VdP.

4.2.1 Application to Einstein-Maxwell: charged BTZ black hole

Next, we apply the above formalism to the Einstein-Maxwell theory:

$$S = \int d^dx\sqrt{-g}\left[(R - 2\Lambda) - \frac{1}{4}F^2\right]. \tag{4.13}$$

After some algebra, we find the symplectic potential current, Noether current and Noether charge to be:

$$\boldsymbol{\Theta} = \Theta^\mu \boldsymbol{\epsilon}_\mu$$

$$\mathbf{J} = J^\mu \boldsymbol{\epsilon}_\mu$$

$$\mathbf{Q} = Q^{\mu\nu}\boldsymbol{\epsilon}_{\mu\nu}$$

with

$$\Theta^\mu = \left[2\left(\nabla_\nu \nabla^{[\nu}\xi^{\mu]} + g^{\mu\nu}R_{\nu\lambda}\xi^\lambda\right) - F^{\mu\nu}\left(\nabla_\nu(\xi^\lambda A_\lambda) + \xi^\lambda F_{\lambda\nu}\right)\right]$$

$$J^\mu = \nabla_\nu\left[2\nabla^{[\nu}\xi^{\mu]} - F^{\mu\nu}\xi^\lambda A_\lambda\right]$$

$$Q^{\mu\nu} = \left[\nabla^{[\nu}\xi^{\mu]} - \frac{1}{2}F^{\mu\nu}\xi^\lambda A_\lambda\right].$$

Let us now specialize to a solution of the Einstein-Maxwell system: the charged BTZ black hole in 3 dimensions. The metric together with the gauge field are given by:

$$ds^2 = -f(r)dt^2 + \frac{dr^2}{f(r)} + r^2 d\phi^2$$
$$f(r) = -2m + \frac{r^2}{L^2} - \frac{1}{2}q^2 \log\left(\frac{r}{L}\right)$$
$$A = -q \log\left(\frac{r}{L}\right) dt.$$

Here we use units where $4G = 1$. This solution has two horizons, an outer horizon at $r = r_+$ and an inner horizon at $r = r_-$. Both outside the outer horizon ($r > r_+$) and inside the inner horizon ($r < r_-$), ∂_t is a bifurcate time-like Killing vector field, whose killing horizons are given by $r = r_+$ and $r = r_-$ respectively. For this choice of Killing vector field, we find that the Noether charge only has one nonzero component:

$$Q^{tr} = \frac{4r^2 - 2L^2q^2 \log\left(\frac{r}{L}\right) - L^2q^2}{16\pi L^2 r} \tag{4.14}$$

and all other independent components of $Q^{\mu\nu}$ vanish. For a perturbation defined by perturbing the AdS length L of the solution above and leaving the other parameters fixed, we find that

$$\Theta^r = \frac{3\left(4r^2 - L^2q^2\right)}{8\pi L^3 r}\delta L \tag{4.15}$$

with the other two components zero. From these we find the only nonzero component of χ to be:

$$\chi^{tr} = \frac{4r^2 - L^2q^2}{16\pi L^3 r}\delta L. \tag{4.16}$$

Integrating this form over any surface of constant t and r yields

$$\int_{r=\text{const}} \boldsymbol{\chi} = \int_0^{2\pi} \sqrt{-g}\chi^{\mu\nu}\varepsilon_{\mu\nu\phi}d\phi = \frac{\delta L}{L}\left[\frac{r^2}{L^2} - \frac{1}{4}q^2\right]. \tag{4.17}$$

Evaluating this on the outer horizon r_+ we can recongnize this as $T\delta S$ after some algebra. On the other hand, the integral of $\boldsymbol{\chi}$ diverges as $r \to \infty$, but putting in a large r cutoff R and adding

$$\delta\Lambda \int \xi \cdot \frac{\delta \mathbf{L}}{\delta \Lambda} = \frac{\delta L}{4\pi}\int_0^{2\pi} d\phi \int_{r_+}^{R} dr\sqrt{-g}\frac{-4}{L^3} = \frac{r_+^2 - R^2}{L^3}\delta L \tag{4.18}$$

we get a cutoff independent result also equal to $T\delta S$. Rewriting this in terms of δP instead of δL, the first law with m and q fixed then becomes

$$T\delta S + \pi\left(r_+^2 - \frac{1}{4}L^2q^2\right)\delta P = 0 \tag{4.19}$$

and so we have the volume

$$V_+ = \pi\left(r_+^2 - \frac{1}{4}L^2q^2\right) \tag{4.20}$$

We could equally well have done this in region inside the inner horizon. Evaluating equation 4.17 at $r = r_-$ once again yields $T\delta S$ for this horizon, and evaluating at the singularity gives $-\frac{q^2}{4L}\delta L$. On the other hand,

$$\delta\Lambda \int \xi \cdot \frac{\delta \mathbf{L}}{\delta \Lambda} = \frac{\delta L}{4\pi}\int_0^{2\pi} d\phi \int_{r_-}^{0} dr\sqrt{-g}\frac{-4}{L^3} = \frac{r_-^2}{L^3}\delta L \tag{4.21}$$

All in all, we obtain the first law:

$$(T\delta S)_- + \frac{\delta L}{L}\left(\frac{r_-^2}{L^2} - \frac{1}{4}q^2\right) = 0 \tag{4.22}$$

where the $(\dots)_-$ is to emphasize that the quantity enclosed pertains to the inner horizon. Once again trading δL for δP we read off the volume for the inner horizon:

$$V_- = \pi \left(r_-^2 - \frac{1}{4} q^2 L^2 \right) \tag{4.23}$$

4.2.2 Application to Einstein-Maxwell-dilaton: the R-charged Black Hole

In this subsection, we consider a more complicated example and derive the volume of the R-charged black hole in 4 dimensions. The thermodynamics of R-charged black holes has been studied in [110]. In (3+1) dimension, the action is given by:

$$L = \left(\frac{R}{16\pi} - \frac{1}{8\pi} \sum_{I=1}^{4} e^{\vec{a}_I \cdot \vec{\phi}} F_{(I)}^2 - \frac{1}{32\pi} \sum_{i=1}^{3} ((\partial \phi_i)^2 - \mathcal{V}(\phi_i)) \right) \varepsilon \tag{4.24}$$

with

$$a_1 = (1,1,1),\ a_2 = (1,-1,-1),\ a_3 = (-1,1,-1),\ a_4 = (-1,-1,1)$$

and

$$\mathcal{V}(\phi_i) = -\frac{g^2}{4\pi} \sum_i \cosh \phi_i \tag{4.25}$$

The metric together with the matter fields are given by:

$$ds^2 = -\prod_{I=1}^{4} H_I^{-1/2} f dt^2 + \prod_{I=1}^{4} H_I^{1/2} \left(\frac{dr^2}{f} + r^2 d\Omega^2 \right) \tag{4.26}$$

$$A^I = \frac{\sqrt{q_I (q_I + 2m)}}{r + q_I} dt \tag{4.27}$$

$$e^{-\frac{1}{2}\vec{a}_I\cdot\vec{\phi}} = \frac{\prod_{J=1}^{4} H_J^{1/4}}{H_I} \tag{4.28}$$

$$f = 1 - \frac{2m}{r} + g^2 r^2 \prod_J H_J \tag{4.29}$$

$$H_J = 1 + \frac{q_J}{r} \tag{4.30}$$

The thermodynamical quantities are:

$$M = m + \frac{1}{4}\sum_{I=1}^{4} q_I \tag{4.31}$$

$$Q_I = \frac{1}{2}\sqrt{q_I(q_I + 2m)} \tag{4.32}$$

$$S = \pi \prod_{I=1}^{4} \sqrt{r_+ + q_I} \tag{4.33}$$

$$T = \frac{f'(r_+)}{4\pi} \prod_{I=1}^{4} H_I^{-1/2}(r_+) \tag{4.34}$$

$$\Phi^I = \frac{\sqrt{q_I(q_I + 2m)}}{2(r_+ + q_I)} \tag{4.35}$$

In the extended phase space, the pressure is the cosmological constant, which is also the bottom of the scalar potential:

$$P = \frac{3}{8\pi} g^2 \tag{4.36}$$

As mentioned in the introduction, the ADM mass is now reinterpreted as the enthalpy and the black hole's volume can be computed using the familiar thermodynamic formula:

$$V := \left(\frac{\partial M}{\partial P}\right)_{Q_I, S} = \frac{\pi}{3} r_+^3 \prod_{J=1}^{4} H_J(r_+) \sum_{K=1}^{4} H_K(r_+)^{-1} \tag{4.37}$$

In particular, the AdS-RN black hole is a special case when all 4 charges coincide $q_1 = q_2 = q_3 \equiv q$. In this case, the above reduces to:

$$V = \frac{4}{3}\pi(q + r_+)^3 \tag{4.38}$$

Also, the radial coordinate has to be redefined by $r \to r - q$ in order to recover the usual Schwarzschild-like form of the AdS-RN metric. We then recognize the volume of the AdS-RN black hole in the form of equation (4.2). A note here is in order about coordinate dependence. While the thermodynamic volume can take different forms depending on the radial coordinate used (as illustrated in the example above), we stress that the volume is coordinate-invariant quantity. The fact that it is not the actual volume of some spatial region, combined with the fact that spatial volumes in General Relativity depend on the foliation, can make this coordinate invariance not so obvious. The cleanest way to see this coordinate invariance is to go back to the definition of V as a partial derivative (4.1). The function $M(S, P)$, which represents an equation of state so to say, is a relation between coordinate invariant quantities (M, S and P), and so is the partial derivative (4.1).

The paper [110] asks the interesting question of what integral over the black hole interior would give rise to the volume (4.37). To answer this question, one can recast the above in the form:

$$V = \int_{S^2} \int_{r_0}^{r_+} V'(r) dr d\Omega_2^2 \tag{4.39}$$

where $V(r)$ is the function defined in equation (4.37) (with r_+ relabeled to r), and r_0 is taken to be the largest root of the equation $V(r) = 0$. We then find

that r_0 is the largest root of a cubic polynomial:

$$4r_0^3 + 3r_0^2 \sum_I q_I + 2r_0 \sum_{i<j} q_I q_J + \sum_{I<J<K} q_I q_J q_K = 0 \tag{4.40}$$

As for the integral $V'(r)$, it was pointed out in [110] that it is essentially the scalar potential:

$$V = -\frac{8\pi}{3g^2} \int_{S^2} \int_{r_0}^{r_+} \mathcal{V} \sqrt{-g} dr d\Omega_2^2 \tag{4.41}$$

Two aspects of this formula are remarkable: first, the fact that the integrand admits a clean interpretation in terms of the scalar potential; and secondly, the integral does not run over the whole of the black hole's interior. As one can generally expect the volume to have something to do with the scalar potential, the second aspect is perhaps a bit more mysterious than the first one. We now proceed to apply the extended Iyer-Wald formalism to compute the volume, and we will see how the formalism sheds light on the two mysterious aspects as described above. The symplectic potential current and Noether charge for this theory are given by:

$$\Theta^a = \nabla_b (g^{ad} g^{bc} \delta g_{cd} - g^{ab} g^{cd} \delta g_{cd}) - \sum_{i=1}^{3} \nabla^a \phi_i \delta \phi_i - 8 \sum_I e^{\vec{a}_I \cdot \vec{\phi}} F_{(I)}^{ab} (\partial_b (\xi^c A_{(I)c}) + \xi^c F_{(I)cb}) \tag{4.42}$$

$$Q^{ab} = -\frac{1}{16\pi} \nabla^{[b} \xi^{a]} + \frac{1}{4\pi} \sum_I e^{\vec{a}_I \cdot \vec{\phi}} F_{(I)}^{ab} \xi^c A_{(I)c} \tag{4.43}$$

Here we only give the on-shell form of these expressions. Next, let us perturb the coupling g^2. By noting that equations (4.27) and (4.28) are g-independent, it is clear that the profiles of the matter fields are unaffected, and only the gravity part contributes to δQ and Θ. Moreover, equations (4.31) and (4.32)

are also g-independent, so neither the ADM mass M nor the charges Q_i are affected by the g-variation. This implies that the (extended) first law of thermodynamics:

$$\delta M = T\delta S + \Phi_I dQ_I + VdP \tag{4.44}$$

simplifies to

$$T\delta S + V\delta P = 0 \tag{4.45}$$

If we now compare with equation (4.12), we can identify the $T\delta S$ term with the integral of χ over the horizon, and the $V\delta P$ term as arising from a combination of the two other terms. The fact that $T\delta S$ corresponds to the integral of χ over the horizon is to be expected from the Iyer-Wald formalism: roughly speaking, it is because the form χ evaluated on the bifurcation surface reduces to the surface binormal, and hence its integral over the bifurcation surface gives the area (or the entropy).

Let us next compute the form χ. After some algebra, we find that the only nonzero component of χ is:

$$\chi^{rt} = -\frac{1}{16\pi}\left(\frac{r}{2}\right)\left(2\sqrt{H_1H_2H_3H_4} + r\partial_r\sqrt{H_1H_2H_3H_4}\right)\delta g^2 \tag{4.46}$$

The integral of χ over infinity diverges. If we regularize by a radial cutoff $r_c >> r_+$, we find:

$$\int_\infty \chi = \left[-\frac{r_c^3}{2} - \frac{3r_c^2}{8}\sum_I q_I - \frac{r_c}{4}\sum_{I<J} q_I q_J - \frac{1}{8}\sum_{I<J<K} q_I q_J q_K\right]\delta g^2 \tag{4.47}$$

Next, let us focus on the $\delta\Lambda$ term in the extended first law. By differentiating the Lagrangian with respect to the coupling g^2, we have:

$$\delta g^2 \int \frac{\partial \mathcal{L}}{\partial g^2} \xi \cdot \varepsilon = -\frac{\delta g^2}{g^2} \int_{S^2} \int_{r_+}^{\infty} \mathcal{V} \sqrt{-g} dr d\Omega_2^2 \tag{4.48}$$

Notice that we have an integral of the scalar potential on the right-hand side! We emphasize here that the extended Iyer-Wald formalism makes this fact manifest, in contrast with the approach described in equation (4.39). As usual, the upper limit of integration above will diverge and we have to regularize by a radial cutoff r_c. Evaluating the integral, we then find:

$$\delta g^2 \int \frac{\partial \mathcal{L}}{\partial g^2} \xi \cdot \varepsilon = \delta g^2 \left[\frac{r^3}{2} + \frac{3}{8} r^2 \sum_I q_I + \frac{1}{4} r \sum_{I<J} q_I q_J \right]_{r_+}^{r_c} \tag{4.49}$$

If we now compare the divergent terms in (4.47) and (4.49), we then find that they cancel pairwise, and we are left with a finite answer which consists of two parts: (1) the finite term in (4.47) and the horizon term (the lower limit of integration) in (4.49). We then obtain:

$$\begin{aligned} V dP &= \int_{\infty} \chi + \delta g^2 \int \frac{\partial \mathcal{L}}{\partial g^2} \xi \cdot \epsilon \\ &= \delta g^2 \left(\frac{r_+^3}{2} + \frac{3}{8} r_+^2 \sum_I q_I + \frac{r_+}{4} \sum_{I<J} q_I q_J - \frac{1}{8} \sum_{I<J<K} q_I q_J q_K \right) \end{aligned} \tag{4.50}$$

and we recover equation (4.37). Notice in particular, that, from the viewpoint of the extended Iyer-Wald formalism, the lower limit of integration r_0 in (4.41) arises from the finite term in the integral of χ at infinity. Moreover, the Iyer-Wald formalism has taught us that the volume of the black hole is perhaps best thought of as arising from an integral over the *exterior* of the black hole

rather than its *interior* [3]. To summarize, the volume arises as the integral of the scalar potential over the whole black hole exterior, but it is regularized by the Iyer-Wald form χ at infinity in a nontrivial way.

4.3 Thermodynamic volume and Complexity: Schwarzschild-AdS

From the viewpoint of the Iyer-Wald formalism, as we have seen above, the black hole volume arises as an integral over the *exterior* of the black hole. This observation naturally begs the question of whether the thermodynamic volume has something to do with the black hole *interior*. Moreover, it remains unclear as to what the information contained in the volume can teach us about the dual CFT. It is generally pointed out in the literature [83, 91, 93, 94, 88, 89, 111, 87] that varying the cosmological constant in the bulk corresponds to varying the rank of $SU(N)$ or the central charge on the field theory side, and that the volume can be thought of as a chemical potential-like quantity corresponding to the degrees of freedom counted by the central charge.

In this section, we bring the two questions above together (the black

[3] We also note here that there exists an alternative approach in the literature to derive the volume, which is based on the Komar formula, see e.g. [86, 110, 83]. As with our approach, the volume also arises from the Komar formula as a integral over the exterior of the black hole, and the integrand is basically the Killing potential.

hole interior and the CFT interpretation) and attempt to answer them through the notion of *complexity* of quantum states. In a series of elegant papers [18, 19], Brown et al. proposed that the complexity of the CFT state is dual to the integral of the bulk action over the so-called Wheeler-DeWitt (WdW) patch. In particular, this quantity grows linearly with time at late time, and we will see in the first half of this section that the thermodynamical volume is a contribution to this growth. In the section half of this section, we switch gear and consider the possibility that it is the *spacetime volume*, rather than the action, of the WDW patch which is dual to the complexity. We will show that the spacetime volume of the WDW patch is intimately related to the thermodynamic volume, and that, in the Schwarzschild-AdS case, the spacetime volume and action behave in very similar fashions and both proposals should work equally well.

4.3.1 Review of Brown et al.

Let us start by reviewing the proposal by Brown et al. in some level of details. The Wheeler-DeWitt patch is a region in the maximally extended black hole spacetime defined with respect to two choices of time, one on each boundary. For simplicity let us first consider the AdS-Schwarzschild black hole in 4 dimensions. We will denote the time on the left boundary as t_L and the time on the right boundary as t_R. From these two points on the boundary (see Figure 4.1 for a depiction), we draw four null rays, and the WdW patch is

the region in the bulk enclosed between rays (and possibly the past and future singularities) [4].

On the CFT side, picking out two times t_L and t_R is equivalent to choosing

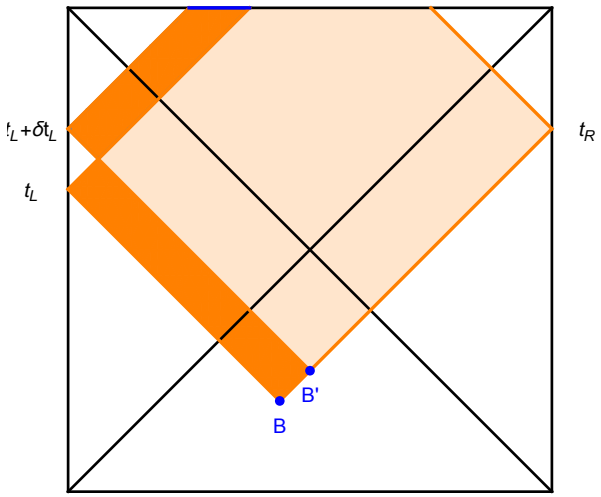

Figure 4.1: The Wheeler-DeWitt patch of the AdS-Schwarzschild black hole (depicted in orange). When t_L is shifted to $t_L + \delta t_L$, the patch loses a sliver and gains another one (depicted in darker orange). The contributions from the Gibbons-Hawking term are in blue.

a quantum state:

$$|\psi(t_L, t_R)\rangle = e^{-i(H_L t_L + H_R t_R)}|TFD\rangle \tag{4.51}$$

[4]The WdW patch as described here extends all the way to the boundary, and therefore the action evaluated on the WdW is divergent. To extract a finite answer, we have to choose a regularization. One could simply cut off the patch at some large radius $r_{\text{cutoff}} >> r_+$. Alternatively, one could move the two corners of the WdW patch on the boundary to r_{cutoff}, as done in [74]. The regularization introduces terms which drop out when we take the time derivative of the complexity, and for this reason, we leave the regularization unspecified.

where H_L and H_R are the Hamiltonian on the left and right boundaries, respectively, and $|TFD\rangle$ is the thermofield double state:

$$|TFD\rangle = Z^{-1/2} \sum_n e^{-\beta E_n/2} |E_n\rangle_L \otimes |E_n\rangle_R \tag{4.52}$$

The thermofield double state has the properties that it is close to being maximally entangled, and that the reduced density matrix on either side is the usual thermal state.

The complexity of a quantum state is, roughly speaking, the minimal number of quantum gates needed to produce the state from some universally agreed-upon starting point. The statement of CA-duality is that:

$$\mathcal{C}(|\psi(t_L, t_R)\rangle) = \frac{\mathcal{A}}{\pi\hbar} \tag{4.53}$$

where $\mathcal{A}$ is the bulk action evaluated on the WDW patch. At late t_L, it follows from CA-duality that the rate of growth of the complexity approaches the mass of the black hole:

$$\lim_{t_L \to \infty} \frac{d\mathcal{C}}{dt_L} = \frac{2M}{\pi\hbar} \tag{4.54}$$

Equation (4.54) is a convincing piece of evidence for CA-duality. This is because it is reminiscent of a conjectured upper bound on the rate of computation by Lloyd ([62]), according to which the rate of computation is bounded above by the energy. Let us briefly review the motivation for the Lloyd bound.

The Lloyd bound takes inspiration from another bound known as the Margolus-Levitin theorem [63]. This latter states that the time $\tau_\perp$ it takes for

a quantum state to evolve into a state orthogonal to it is bounded below by:

$$\tau_{\perp} \geq \frac{h}{4E} \tag{4.55}$$

where E is the average energy of the state. If we take the reciprocal of both sides and re-interpret the left-hand side (which has unit of frequency) as the rate of change of the complexity, we then arrive at the statement that this rate is bounded above by the energy of the system:

$$\dot{\mathcal{C}} \leq \frac{2E}{\pi\hbar} \tag{4.56}$$

which is the Lloyd bound. We point out that, while the Margolus-Levitin theorem can be proved using elementary techniques, the Lloyd bound is a *conjecture*. If we now compare the Lloyd bound with the prediction of CA-duality (4.54) for the late-time complexification rate, we see that the ADM mass of the black hole plays the role of energy in the Lloyd bound and that the bound is *saturated* at late time. That the bound is saturated is another *conjecture* but is appealing: black holes seem to excel at information-related tasks since they saturate the Bekenstein bound [112, 113] and are believed to be the fastest scramblers in nature [114].

4.3.2 CA-duality, through the lens of black hole chemistry

In this subsection, we take a closer look at the gravity calculation of CA-duality to derive equation (4.54). This computation itself, of course, can be found in [18, 19] [5]. Our contribution in this subsection is to show that the

[5] A technical remark is in order here. The method of computation in [18, 19] was questioned by [74], where the calculation was redone with a more careful treatment of the

thermodynamic volume (together with the pressure) arises naturally from the calculation.

First, since the WdW patch is a region with boundary, the action is the sum of the Einstein-Hilbert action and the Gibbons-Hawking(-York) term:

$$\mathcal{A} = \frac{1}{16\pi G}\int_{\mathcal{M}} \sqrt{-g}(R - 2\Lambda) + \frac{1}{8\pi G}\int_{\partial M} \sqrt{|h|}K \tag{4.57}$$

When we shift t_L to $t_L + \delta t_L$, the WdW patch loses a thin rectangle and gains another thin rectangle as described in dark orange in Figure 4.1. Thus, to compute the rate of change of the action we have to evaluate the action above on the two orange rectangles. Observe that all the sides of these two rectangles are null except at the singularity, and the paper [74] gives a detailed argument that the null boundaries do not contribute to the Gibbons-Hawking term. Also, since the boundary is not smooth at the corners of the rectangles, we have to take into account the contributions localized at these corners (named B and B' in Figure 4.1). Thus, we see that the Gibbons-Hawking term contributes at the singularity, at B and at B' (all of which are depicted in blue in Figure 4.1):

$$\delta\mathcal{A} = S_{\mathcal{V}_1} - S_{\mathcal{V}_2} - \frac{1}{8\pi G}\int_S K d\Sigma + \frac{1}{8\pi G}\oint_{B'} a dS - \frac{1}{8\pi G}\oint_B a dS \tag{4.58}$$

boundary of the WDW patch. However the conclusion 4.54 remains unchanged. In this section, we will follow the more rigorous treatment of the boundary term as presented in [74].

Note that $\mathcal{V}_1$ and $\mathcal{V}_2$ denote the upper and lower dark orange slivers from figure 4.1 respectively, and that $a = \ln|k \cdot \bar{k}|$ where k and $\bar{k}$ are the null normals to the corner pieces. Let us consider first the difference between the two rectangles $S_{\mathcal{V}_1} - S_{\mathcal{V}_1}$. Note that the Ricci scalar of the AdS-Schwarzschild solution is a constant:

$$R = \frac{2d}{d-2}\Lambda \tag{4.59}$$

This readily follows from the fact that AdS-Schwarzschild is a vacuum solution of Einstein-Hilbert theory. Thus, if we evaluate the Einstein-Hilbert action on the AdS-Schwarzschild background, we immediately see that we have something proportional to the *spacetime volume*:

$$S_{\mathcal{V}_1} - S_{\mathcal{V}_2} \propto \int_{\mathcal{V}_1} \sqrt{-g} d^4x - \int_{\mathcal{V}_2} \sqrt{-g} d^4x \tag{4.60}$$

Thus, after one evaluates the integrals above, we expect to see something which is schematically the product of a spatial volume and the infinitesimal time interval δt:

$$S_{\mathcal{V}_1} - S_{\mathcal{V}_2} = (\text{some spatial volume})\delta t \tag{4.61}$$

Let now us do the integral for $S_{\mathcal{V}_1} - S_{\mathcal{V}_2}$ explicitly. When we do this, two remarkable things happen. The is that the part of the upper rectangle which is outside the future horizon always cancels with the part of the lower rectangle which is outside the past horizon, and this happens for any t_L thanks to boost symmetry of the black hole [6]. Thus, whatever quantity comes out to be the

[6]Indeed the Schwarzschild-AdS metric in Kruskal coordinates only depends on the coordinates U and V through their product UV, and is therefore invariant under $U \to e^{\beta}U$ and $V \to e^{-\beta}V$.

spatial volume in equation (4.61) only receives contribution from the black hole interior. The second is that the integral evaluates to:

$$S_{\mathcal{V}_1} - S_{\mathcal{V}_2} = -\frac{r_B^3}{2GL^2}\delta t \tag{4.62}$$

where r_B is the r coordinate of the 2-sphere sitting at B. In the late time limit, we can easily see by inspection of Figure (4.1) that r_B tends to r_+. Thus, in the late time limit, the integral above can be interpreted in the language of the extended thermodynamics as:

$$S_{\mathcal{V}_1} - S_{\mathcal{V}_2} = -\frac{r_+^3}{2GL^2}\delta t = -PV\delta t \tag{4.63}$$

where, in the last equality, we used $P = -\frac{\Lambda}{8\pi G}$, $\Lambda = -\frac{3}{L^2}$ and $V = \frac{4}{3}\pi r_+^3$. Thus, we have seen how the thermodynamic volume arises from the action evaluated on the WDW patch. Put differently, the WDW patch provides an interpretation of hte thermodynamic volume as a measure of the black hole interior, and in the same time, relates it to the late-time rate of growth of the complexity.

Let us now evaluate the remaining contributions in (4.58) (The algebraic details are found again in [74]). The contribution of the Gibbons-Hawking term at the singularity is essentially the ADM mass:

$$-\frac{1}{8\pi G}\int_S K d\Sigma = \frac{3}{2}M\delta t \tag{4.64}$$

As for the contribution at the two corners B and B', one finds:

$$\frac{1}{8\pi G}\left[\oint_{B'} a dS - \oint_B a dS\right] = \frac{1}{4G}\left[r^2\frac{df}{dr} + 2rf\log\left(\frac{-f}{K}\right)\right]_{r=r_B}\delta t \tag{4.65}$$

where K is a constant. In the late time limit, where $r_B \to r_+$, the second term above vanishes and:

$$\frac{1}{8\pi G}\left[\oint_{B'} adS - \oint_{B} adS\right] = TS\delta t \tag{4.66}$$

Putting everything together, we find the time derivative of the action at late time to be:

$$\frac{d\mathcal{A}}{dt} = \frac{3}{2}M + TS - PV \tag{4.67}$$

Next, recall the Smarr relation for AdS-Schwarzschild in 4 dimensions:

$$M = 2TS - 2PV \tag{4.68}$$

Using the Smarr relation above, the time derivative of the action simplifies to:

$$\frac{d\mathcal{A}}{dt} = 2M \tag{4.69}$$

If we now turn the logics around, we can reinterpret the following slight rewriting of the Smarr relation:

$$2M = \frac{3}{2}M + TS - PV \tag{4.70}$$

as a way to keep track of the different contributions to the complexity growth: the left-hand side corresponds to the total growth, the term with M on the right-hand side is the contribution from the singularity of the WdW patch, the term with TS is the corner contributions which end up on the horizon at late time, and finally the term with PV is the contribution from the black hole interior away from the singularity.

4.3.3 Complexity = Volume 2.0

As we have learned from (4.63), in the case of AdS-Schwarzschild, the late-time rate of change of the bulk action evaluated on the WDW patch gives the product PV, or equivalently the late-time rate of change of the spacetime volume of the WDW patch is the thermodynamic volume V. These observations beg the question of whether P and V can serve as the basis for a new, alternative proposal for the complexity alongside with CA-duality. In this subsection, we will make the case that a possible holographic dual to the complexity is the spacetime volume of the WDW patch.

As previously noted, what we are looking for in proposing a holographic dual to the complexity is a linear growth at late time, together with consistency with the Lloyd bound. On the information-theoretical side, the linear growth of the complexity at late time is generally believed to be true but is surprisingly hard to prove [7]. It is straightforward to see that the complexity of the thermofield double state is bounded above by a linear function of time:

$$\mathcal{C}(|\psi(t)\rangle) < t \cdot \text{poly}(K) \tag{4.71}$$

almost by definition of the complexity. To see this, recall that the complexity is the smallest number of quantum gates needed to build a state, hence any way to build the state automatically establishes an upper bound on the complexity. In particular, time-evolving the thermofield double state the usual

[7] "Late time" in this statement refers to timescales exponential in the entropy. For much later times (doubly exponential in the entropy), quantum recurrence kicks in, and the complexity periodically returns to zero.

way in quantum mechanics establishes the upper bound (4.71). To establish that the complexity grows linearly at late time, one needs to also bound the complexity from *below* by a linear function of time. This is a highly non-trivial task, but there are two promising directions. One of them is a recently proved theorem by Aaronson and Susskind [29] which establishes a lower bound for the complexity (modulo the possibility that an improbable statement in complexity theory is true). The other direction is Nielsen's idea of the complexity geometry [115] where finding the complexity reduces to the problem of finding geodesics on a curved manifold.

On the gravity side, as noted in the introduction already, one can associate various geometrical quantities to the ERB which all grow linearly in size at late time, so this property of the complexity alone allows for quite some freedom in proposing a holographic dual. A simple illustration of this non-uniqueness phenomenon (given in [16]) is a geodesics in the BTZ black hole anchored at boundary times t_L and t_R. The length of such a geodesic is given by (for the case $r_+ = L$):

$$d(t_L, t_R) = 2 \log \left(\cosh \frac{1}{2}(t_L + t_R) \right) \tag{4.72}$$

If we keep t_R fixed and send $t_L \to \infty$, we find that indeed the leading term is linear in t_L. Another geometrical entity whose size grows linearly at late time is the maximal surface spanning the wormhole. As previously noted, this quantity served as the basis for an earlier proposal by Brown et al known as CV-duality [16].

Taking inspiration from CV-duality and CA-duality, we would like to propose now that the complexity is dual to the spacetime volume of the WDW patch (more precisely the spacetime volume multiplied by the pressure):

$$\mathcal{C} \sim \frac{1}{\hbar} P(\text{Spacetime Volume}) \tag{4.73}$$

In the late time regime, by design we will have:

$$\dot{\mathcal{C}} \sim \frac{PV}{\hbar} \tag{4.74}$$

We will refer to this proposal as "complexity=volume 2.0".

Next, we ask the question of whether "complexity=volume 2.0" satisfies the Lloyd bound. Naively, it might seem that the Lloyd bound favors CA-duality over our proposal, because we have the mass M coming out of CA-duality calculation as opposed to PV, and the Lloyd bound refers to the energy of the system.

However, we can form 3 quantities with the dimension of energy out of the standard thermodynamical variables, by multiplying each variable by its conjugate. Thus we have: M, TS and PV. While M seems to be the "correct" energy from the viewpoint of the Lloyd bound, it is TS which should be identified as the complexification rate from the viewpoint of quantum circuits [16]. To see this, [16] argues that if we think about the CFT as a quantum circuit of K qubits, then the complexity grows linearly in time with slope K:

$$\mathcal{C}(t_L, t_R) = K|t_L + t_R| \tag{4.75}$$

To convert between the quantum circuit picture and the field theory picture, we identify K with the entropy S of the CFT and use the temperature T to convert between the CFT time and the quantum circuit time. Thus, we find after the translation:

$$\mathcal{C}(t_L, t_R) \sim TS|t_L + t_R| \tag{4.76}$$

and

$$\dot{\mathcal{C}} \sim TS \tag{4.77}$$

On the other hand, one could make similar arguments to make the case that the complexification rate should be PV. The complexity should again be proportional to the number of degrees of freedom, which for a discretized CFT is roughly the central charge times the number of lattice sites. Now by the holographic dictionary, we know that the central charge is dual to what we have been calling the pressure. For example, in three bulk dimensions we have the Brown-Henneaux formula [116]

$$c = \frac{3L}{2G} \propto P^{-\frac{1}{2}} \tag{4.78}$$

It furthermore seems reasonable that the volume would roughly encode the number of sites. Thus, one can schematically write down:

$$\mathcal{C} = PV(t_L + t_R) \tag{4.79}$$

and the complexification rate at late time is PV.

We end this section by noting that for most black holes all three quantities M, TS and PV have the same order of magnitude. To see this, we express these quantities as functions of r_+ and L:

$$M = \frac{r_+}{2}\left(1 + \frac{r_+^2}{L^2}\right) \tag{4.80}$$

$$TS = \frac{r_+}{4}\left(1 + \frac{3r_+^2}{L^2}\right) \tag{4.81}$$

$$PV = \frac{r_+^3}{2L^2} \tag{4.82}$$

For $r_+ >> L$ (i.e. large black holes), we then find

$$M \approx \frac{r_+^3}{2L^2} \tag{4.83}$$

$$TS \approx \frac{3r_+^3}{4L^2} \tag{4.84}$$

Interestingly, the two quantities M and TS differ by an $\mathcal{O}(1)$ numerical factor, while M and PV become the same quantity! Thus, for high temperatures at least, it does not make much of a difference whether the rate of growth of the complexity is thought of as M, as TS or as PV. Given that there are ambiguities associated with defining the complexity (such as overall numerical factors), the discrepancies between M, TS and PV seem relatively easy to accommodate.

4.4 Thermodynamic Volume and Complexity: Conserved Charges

Given the clean connection between the Schwarzschild-AdS WDW patch with the thermodynamic volume and the complexity, it is natural to ask whether we can also establish similar connections for charged and rotating solutions. Unfortunately, within the framework of CA-duality, the situation for charged and rotating black holes is not as clean, and the gravity calculation does not respect the Lloyd bound. In this section, however, we will simply present the computation of the complexity according to "complexity=volume 2.0" for a variety of charged black holes, and demonstrate that - like in the uncharged case - the thermodynamic volume and the pressure emerge naturally from the late-time rate of growth. We will relegate the interesting question of consistency with the Lloyd bound to the next section.

On the gravity side, for both charged and rotating black holes, the Penrose diagram is qualitatively the same. In Figure 4.2, we depict their Penrose diagram together with the WDW patch. Note that the WDW patch is qualitatively different from that of the Schwarzschild-AdS solution: the upper part of the patch no longer runs into a singularity, but approaches the inner horizon at late time.

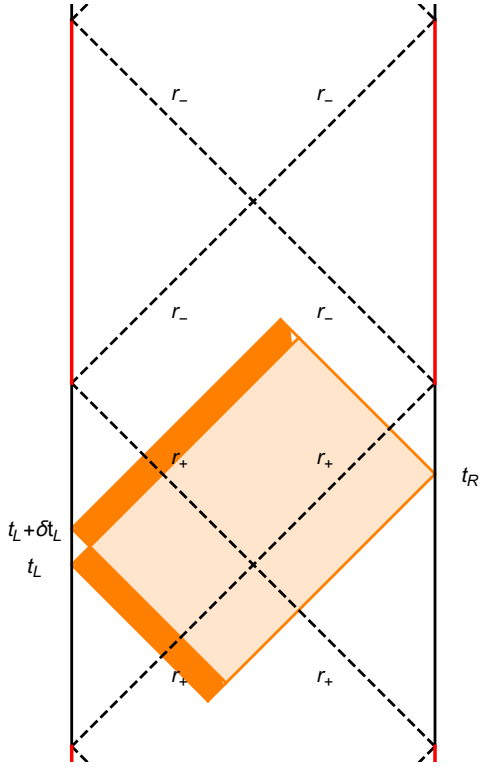

Figure 4.2: The Penrose diagram of a charged and/or rotating black hole and a Wheeler-DeWitt patch (depicted in orange). When t_L is shifted to $t_L + \delta t_L$, the patch loses a sliver and gains another one (depicted in darker orange). The singularity is in red, and the horizons are dashed.

4.4.1 Electrically charged black holes

Let us start with the Reissner-Nordström black hole in $n+2$ dimensions. The metric together with the gauge field are given by:

$$ds^2 = -f(r)dt^2 + \frac{dr^2}{f(r)} + r^2 d\Omega_n^2 \tag{4.85}$$

$$f(r)) = 1 - \frac{\omega^{n-1}}{r^{n-1}} + \frac{q^2}{r^{2(n-1)}} + \frac{r^2}{L^2} \tag{4.86}$$

$$A = \sqrt{\frac{n}{2(n-1)}} \left(\frac{q}{r_+^{n-1}} - \frac{q}{r^{n-1}} \right) dt \tag{4.87}$$

As mentioned in the introduction, the thermodynamic volume is well-known and looks like the geometric volume of a ball in flat space:

$$V_\pm = \frac{\text{Vol}(S_n)}{n+1} r_\pm^{n+1} \tag{4.88}$$

where the subscript $\pm$ of course refers to either horizon. The spacetime volume of the WDW patch takes the form:

$$\text{Spacetime volume} = \frac{\text{Vol}(S_n)}{n} (r_+^n - r_-^n)(t_L + t_R) + \dots \tag{4.89}$$

where the ellipsis stand for terms which are time-independent (and therefore drop out from the time derivative of the complexity) or are exponentially suppressed at late time. We recognize the difference between thermodynamic volumes in the equation above. At late time, then, we have as advertised:

$$\lim_{t_L \to \infty} \dot{\mathcal{C}} = \frac{P(V_+ - V_-)}{\hbar} \tag{4.90}$$

Note the slight difference compared with the Schwarzschild-AdS case: the late-time complexification rate is now proportional to the *difference* between the two thermodynamic volumes. Let us end this subsection by mentioning the 3-dimensional case of the charged BTZ black hole. Here there is potential for some surprise, since the volume takes the somewhat different form:

$$V_\pm = \pi r_\pm^2 - \frac{\pi}{4} Q^2 L^2 \tag{4.91}$$

But in the end, the second term on the right-hand side above drops out of the difference $V_+ - V_-$, and the late-time rate of change of the complexity still takes the form (4.90).

4.4.2 Rotating Black Hole

Next, we move on to discuss rotating holes. Like the Schwarzschild-AdS case, rotating holes are vacuum solutions of the Einstein-Hilbert action, and this again implies that the on-shell Einstein-Hilbert action (ignoring boundary contributions) is proportional to the pressure multiplied by the spacetime volume of the WDW patch:

$$S_{\text{Einstein}-\text{Hilbert}} \propto \frac{1}{L^2}\int d^n x\sqrt{-g} \propto P(\text{Spacetime volume}) \tag{4.92}$$

Thus, like for the Schwarzschild-AdS case, the distinction between the bulk action (i.e. without the boundary term) and spacetime volume is not very important here. In the simple case of the rotating BTZ black hole, the metric reads:

$$ds^2 = -f(r)dt^2 + \frac{dr^2}{f(r)} + r^2\left(d\phi - \frac{J}{2r^2}dt\right)^2 \tag{4.93}$$

The thermodynamic volume can be found to be (see for example [86] for the outer horizon volume):

$$V_\pm = \pi r_\pm^2 \tag{4.94}$$

After some calculation, the late time rate of complexification is again found to be proportional to the difference between the two thermodynamic volumes:

$$\dot{\mathcal{C}} = P(V_+ - V_-) \tag{4.95}$$

Next, we move on to discuss the case of rotating black hole in higher dimensions (the Kerr-AdS). This case is substantially richer and more interesting, as the analysis of the thermodynamics is somewhat different depending on whether

the spacetime dimension is odd or even (see [110]), and there are two possible notions of volume one can identify. For simplicitly, we will focus on the 4-dimensional case. The solution is given by:

$$\begin{aligned} ds^2 &= -\frac{(1+g^2r^2)\Delta_\theta}{1-a^2g^2}dt^2 + \frac{(r^2+a^2)\sin^2\theta}{1-a^2g^2}d\phi^2 + \frac{\rho^2 dr^2}{\Delta_r} + \frac{\rho^2 d\theta^2}{\Delta_\theta} \\ &+ \frac{2mr}{\rho^2(1-a^2g^2)^2}(\Delta_\theta dt - a\sin^2\theta d\phi)^2 \end{aligned} \tag{4.96}$$

$$\Delta_r = (r^2+a^2)(1+g^2r^2) - 2mr \tag{4.97}$$

$$\Delta_\theta = 1 - a^2g^2\cos^2\theta \tag{4.98}$$

$$\rho^2 = r^2 + a^2\cos^2\theta \tag{4.99}$$

Here $a = J/M$ is the ratio of the angular momentum to the mass. The late-time growth of the bulk Einstein-Hilbert action was computed in [117]:

$$\frac{d\mathcal{A}}{dt_L} = -\frac{1}{2G(L^2-a^2)}\left(r_+^3 + a^2r_+ - r_-^3 - a^2r_-\right) \tag{4.100}$$

which again is proportional to the spacetime volume by virtue of the solution being a vacuum solution. As for the thermodynamic volume, we have two different notions of volume depending on whether the analysis is done in a non-rotating or rotating frame at infinity. Following [110], we refer to the volume in the non-rotating frame as the thermodynamic volume and the one in the rotating frame as the geometric volume. The latter admits a geometrical interpretation [8]:

$$V_+ = \frac{1}{3}r_+A_+ \tag{4.101}$$

[8]We also note here that the thermodynamic quantities derived in the rotating frame obey the Smarr relation [110] but not the first law. On the other hand, the thermodynamic quantities derived in the non-rotating frame at infinity do obey a first law (in addition to a Smarr relation) and can be derived from the Iyer-Wald formalism.

where A is the area of the horizon:

$$A_+ = 4\pi \left(\frac{r_+^2 + a^2}{1 - a^2/L^2} \right) \tag{4.102}$$

Putting the two equations above together, we have:

$$V_+ = \frac{4}{3}\pi r_+ \left(\frac{r_+^2 + a^2}{1 - a^2/L^2} \right) \tag{4.103}$$

As in the previous cases, we can define a second volume V_- associated to the inner horizon by the replacement $r_+ \to r_-$ in V_+:

$$V_- = \frac{4}{3}\pi r_- \left(\frac{r_-^2 + a^2}{1 - a^2/L^2} \right) \tag{4.104}$$

Comparing equations (4.100) and (4.103), and converting from the bulk action to the spacetime volume, we finally find:

$$\dot{\mathcal{C}} = P(V_+ - V_-) \tag{4.105}$$

To help gain intuition, in Figure 4.3, we plot the angular momentum-to-mass ratio a versus $V_+ - V_-$ for fixed M and L.

4.5 Action or Volume?

In this paper, we have discussed two different possible holographic identifications of the complexity of the boundary thermofield double state. On could identify this complexity on the one hand with the action of the Wheeler-DeWitt patch, and on the other hand with the spacetime volume of the same. These two quantities behave in a rather similar fashion, and one is naturally

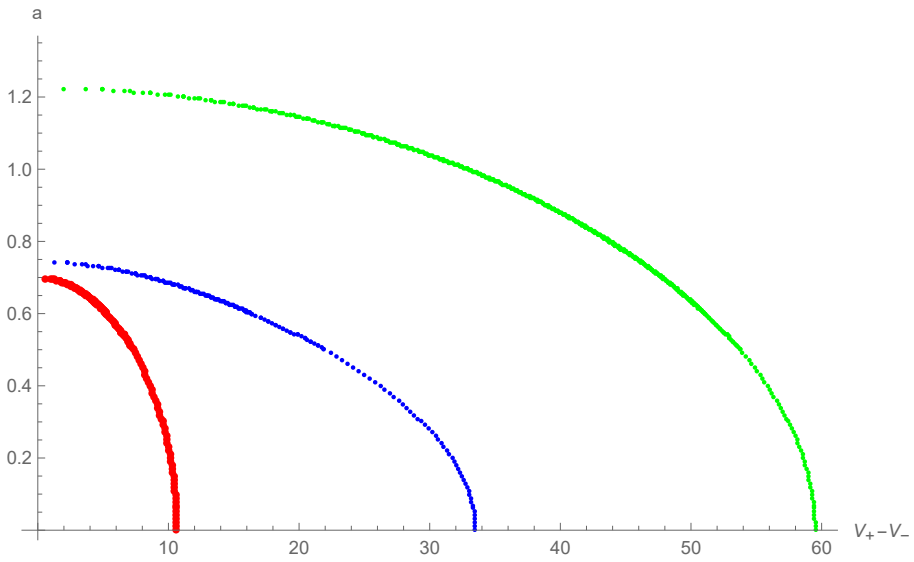

Figure 4.3: Given M and L, we vary the angular momentum to mass ratio a and for each value solve numerically for $V = V_+ - V_-$. Notice that $a = 0$, which reduces to the Schwarzschild case, has the maximal V. As we approach extremality, which here occurs as the plots flatten out on the left (In flat space exremality occurs for $a = 1$, but this is modified by the AdS length dependence of the metric), V tends towards zero. In the plot green is for $M = 5, L = 1$, blue is for $M = 2, L = 3$, and red is for $M = 1, L = 2$.

led to ask whether any advantage can be identified for one or the other. One advantage is that there are no boundary terms, which in higher curvature theories could have problems near a singularity.[9]. In this section, we seek to answer this question as regards the Lloyd bound [62].

[9]We thank Adam Brown for pointing this out to us.

4.5.1 The Lloyd Bound with conserved charge

In this subsection, let us derive the Lloyd bound in the presence of a conserved charge. As argued in [19], the existence of conserved charges puts constraints on the system and implies that the rate of growth of the complexity at late time is slower than in the case without charges. Let us start by generalizing the thermofield double state to include a chemical potential μ:

$$|TFD_\mu\rangle = \frac{1}{\sqrt{Z}} \sum_n e^{-\beta(E_n+\mu Q_n)/2} |E_n Q_n\rangle_L |E_n - Q_n\rangle_R \tag{4.106}$$

This state time-evolves by the Hamiltonian $H_L+\mu Q_L$ on the left, and $H_R-\mu Q_R$ on the right: [10]

$$|\psi(t_L, t_R)\rangle = e^{-i(H_L+\mu Q_L)t_L} e^{-i(H_R-\mu Q_R)t_R} |TFD_\mu\rangle \tag{4.107}$$

Based on this, one would guess that the appropriate generalization of the Lloyd bound is:

$$\dot{\mathcal{C}} \leq \frac{2}{\pi\hbar} (M - \mu Q) \tag{4.108}$$

This however violates our intuition that as zero temperature system, the complexification rate of an extremal black hole should be zero, and that the bound should reflect this. It thus seems appropriate to modify the above to

$$\dot{\mathcal{C}} \leq \frac{2}{\pi\hbar} \left[(M - \mu Q) - (M - \mu Q)_{\text{gs}} \right] \tag{4.109}$$

[10] Note the difference in the sign of μ between H_L and H_R. This is because the electrostatic potential is positive on one side and negative on the other.

where $(M - \mu Q)_{\text{gs}}$ is nothing but $M - \mu Q$ evaluated in the appropriate ground state, which will be either empty AdS or an extremal black hole depending on the case under consideration. If we think of our system as being in the grand canonical ensemble, it is most natural to take the ground state to correspond to the geometry whose chemical potential is the same as the black hole under consideration. As it happens, this is nothing but pure AdS for black holes with $\mu \leq 1$, but for $\mu > 1$, it corresponds to some extremal black hole (In units where $G = 1$).

4.5.2 Bound Violation: Near the Ground State

Now we will check to see whether the Lloyd bound is obeyed by the two proposals at hand. For simplicity, we restrict our attention to 4-dimension and work in units where $G = 1$. First, we consider the case where $\mu > 1$. Expanding the outer horizon radius near extremality, we find that

$$r_+ \approx r_e \left(1 + \frac{\sqrt{3}}{\mu^2\sqrt{\mu^2 - 1}L}\delta M + \mathcal{O}(\delta M^2)\right) \tag{4.110}$$

Where $\delta M := M - M_e$, M is the total mass of the black hole, and r_e and M_e are the radius and mass respectively of an extremal black hole with the same chemical potential as the one we are considering. We likewise may expand the inner horizon as

$$r_- \approx r_e \left(1 - \frac{\sqrt{3}}{\mu^2\sqrt{\mu^2 - 1}\,(2\mu^2 - 1)\,L}\delta M + \mathcal{O}(\delta M^2)\right) \tag{4.111}$$

From these, we can expand $\dot{C}$ under both proposals as

$$\dot{C}_V = P\left(r_+^3 - r_-^3\right) \approx r_e^3 \left[\frac{9\sqrt{3}\sqrt{\mu^2-1}}{4\pi\mu^2\left(2\mu^2-1\right)L^3}\delta M + \mathcal{O}(\delta M^2)\right] \tag{4.112}$$

$$\dot{C}_A = \frac{Q^2}{r_-} - \mu Q \approx \frac{2\left(\mu^2-1\right)}{2\mu^2-1}\delta M + \mathcal{O}(\delta M^2) \tag{4.113}$$

On the other hand, the bound is given by

$$(M-\mu Q) - (M-\mu Q)_e \approx \frac{\sqrt{3}\sqrt{\mu^2-1}}{2\mu^4 L}\delta M^2 + \mathcal{O}(\delta M^3) \tag{4.114}$$

We thus see that both proposals must violate the Lloyd bound near extremality. This is in agreement with [19].

Next we consider $\mu \leq 1$, in which case we expand around empty AdS. Here the bound becomes to lowest order

$$2\left(M-\mu Q\right) \approx \left(1 - \frac{2\mu^2}{\mu^2+1}\right) M = 2\left(\frac{1-\mu^2}{1+\mu^2}\right) M \tag{4.115}$$

But $\dot{C}$ becomes under each proposal

$$\dot{C}_V \approx \frac{3\left(1-\mu^6\right)}{\pi\left(\mu^2+1\right)^3 L^2} M^3 + \mathcal{O}(M^5) \tag{4.116}$$

$$\dot{C}_A \approx 2\left(\frac{1-\mu^2}{1+\mu^2}\right) M + \mathcal{O}(M^3) \tag{4.117}$$

We see immediately that the bound is satisfied in CV-duality sufficiently near extremality, but the bound is far from saturated.The situation with CA-duality is a bit more complex: $\dot{C}_A$ exactly saturates the bound to lowest order in M, and so the lower order behavior becomes important. Expanding the bound violation (i.e. the difference between $\dot{C}_A$ and the bound) directly we find to lowest order

$$\dot{C}_A - 2\left(M - \mu Q\right) \approx \frac{8\mu^2}{\left(\mu^2+1\right)^2 L^2} M^3 + ... \tag{4.118}$$

As this term is positive definite, we see that the bound is violated as we approach empty AdS. This would seem to put CV-duality in a slightly better position than CA-duality, though the expectation that the bound should be saturated, or nearly so is not met in this case.

4.5.3 Bound Violation: Exact Results

In the $\mu \leq 1$ case, one can, in fact, do better. We can find the bound violations as an exact function of the inner and outer horizon. Note of course that these are only valid over the region in r_+, r_- space where $\mu \leq 1$. The exact expressions in 4 dimensions are

$$\dot{C}_V - 2(M - \mu Q) = \frac{2L^2(r_- - r_+) + r_-^3 + 2r_-^2 r_+ + 2r_- r_+^2 - r_+^3}{2L^2} \tag{4.119}$$

$$= -\frac{(r_+ - r_-)^3 + 2L^2(r_+ - r_-) + r_+r_-(r_+ - 5r_-)}{2L^2}$$

and

$$\dot{C}_A - 2(M - \mu Q) = \frac{r_+r_-(r_+ + r_-)}{L^2} \tag{4.120}$$

The second expression is clearly positive definite, and so the under CA-duality the bound is always violated for $\mu \leq 1$. Now the exact expression for the chemical potential is

$$\mu = \sqrt{\frac{r_-(L^2 + r_-^2 + r_-r_+ + r_+^2)}{r_+L^2}} \tag{4.121}$$

From this we may conclude that

$$\mu^2 \leq 1 \Rightarrow r_-(r_+^2 + r_+r_- + r_-^2) \leq L^2(r_+ - r_-) \tag{4.122}$$

and so

$$\dot{C}_V - 2(M - \mu Q) \leq \frac{-(r_+ - r_-)^3 - 2r_-(r_+^2 + r_+r_- + r_-^2) - r_+r_-(r_+ - 5r_-)}{2L^2} \tag{4.123}$$

$$= -\frac{r_+^3 + r_-^3}{2L^2} \leq 0$$

and so we may conclude that C_V respects the bound whenever $\mu \leq 1$.

Generalizing further to arbitrary dimension $d > 3$, we find that

$$\dot{C}_A - 2(M - \mu Q) = \frac{(d-2)\Omega_d r_+^d r_-^d (r_+^2 - r_-^2)}{8\pi L^2 (r_+^d r_-^3 - r_+^3 r_-^d)} \tag{4.124}$$

Which is a positive definite quantity. This in fact recovers a result already derived by [117]. Being, for now, a bit less ambitions with the CV quantity, we find in 5 dimensions

$$\dot{C}_V - 2(M - \mu Q) = -\frac{3\pi \left(2L^2 \left(r_+^2 - r_-^2\right) + r_+^4 - 2r_-^2 r_+^2 - r_-^4\right)}{8L^2} \tag{4.125}$$

and

$$\mu^2 = \frac{3\pi r_-^2 \left(L^2 + r_-^2 + r_+^2\right)}{4L^2 r_+^2} \leq 1 \Rightarrow r_+^2 \geq \frac{3\pi r_-^2 \left(L^2 + r_-^2 + r_+^2\right)}{4L^2} \tag{4.126}$$

from which we get

$$\begin{aligned} \dot{C}_V - 2(M - \mu Q) &\leq -\frac{3\pi \left(2L^2 \left(\frac{3\pi r_-^2 \left(L^2 + r_-^2 + r_+^2\right)}{4L^2} - r_-^2\right) + r_+^4 - 2r_-^2 r_+^2 - r_-^4\right)}{8L^2} \\ &= -\frac{3\pi \left((3\pi - 4)L^2 r_-^2 + (3\pi - 2)r_-^4 + (3\pi - 4)r_-^2 r_+^2 + 2r_+^4\right)}{16L^2} \leq 0 \end{aligned} \tag{4.127}$$

And so CV duality in 5 dimensions respects the bound whenever $\mu^2 < 1$. We conjecture without proof that CV-duality repects the Lloyd bound whenever $\mu^2 \leq 1$ for all AdS-RN spacetimes.

4.5.4 Altering the Bound by a Pre-Factor

We have considered the Lloyd bound in it's usual form,

$$\dot{C} \leq \frac{2E}{\pi\hbar}. \tag{4.128}$$

It would seem, however, due to the arguments leading to this bound, that the bound should only be trusted up to an overall factor. It would be interesting, therefore, to see how robust the above discussion is under the insertion of some pre-factor. For example, under which proposals and sets of circumstances does

$$\dot{C} \leq \frac{\alpha E}{\pi\hbar}. \tag{4.129}$$

hold for various values of α. For example, for $\alpha = 1$ for the AdS-RN case we find:

$$\dot{C}_V - (M - \mu Q) = \frac{r_+ r_-(r_+ + r_-) - L^2(r_+ - r_-)}{2L^2} \tag{4.130}$$

and, using the inequality (4.122) again, we find:

$$\dot{C}_V - (M - \mu Q) \leq -\frac{r_-^3}{2L^2} < 0 \tag{4.131}$$

Hence the value $\alpha = 1$ is also consistent with the bound. We leave further explorations of other values of α to future research.

4.6 Conclusion

Let us summarize the main findings in this paper and sketch out some future directions. In the first part of the paper, we analyzed the notion of thermodynamic volume from the viewpoint of the Iyer-Wald formalism. Using a slight generalization this formalism, we present a systematic way to derive the

volume and illustrate it in two cases: the charged BTZ black hole and the R-charged black hole. In the latter case, our method explains several interesting and intriguing features of the thermodynamic volume, and we believe that it will prove useful to compute the volume of many more complicated black hole solutions in the future. Of particular interest are Lifschitz black holes [118, 119]. Even though the computation of the volume for the R-charged black hole was a bit involved, it is still relatively simple since we saw that perturbing the coupling g leaves all the matter fields unchanged. In comparison, we do not have this luxury in the case of Lifschitz solutions: a generic feature of these spacetimes is the fact that the profiles of the matter fields depend explicitly on the cosmological constant (this property is somehow related to the fact that these spacetimes are not asymptotically AdS), so varying the cosmological constant will affect the matter fields.

In the second part of the paper, we related the thermodynamic volume to the holographic proposals for the complexity. In particular, we showed that the thermodynamic volume (together with its conjugate the pressure) is intimately related to the WDW patch of an eternal AdS black hole, and this holds for a large class of AdS black holes. This intimate relationship can be stated cleanly in two different ways: On one hand, the rate of change of the WDW spacetime volume in the late time limit is precisely the thermodynamic volume (if there is only one horizon) or the difference of thermodynamic volumes (if there are two horizons). On the other hand, the bulk action evaluated on the WDW patch (ignoring boundary contributions) is the sum of "work terms"

involving pressure-volume and charge-potential. The several different ways to arrive at the thermodynamic volume presented in this paper may be a little confusing to the reader, so let us state again the relationship between them: The thermodynamic volume may be defined in the usual thermodynamic fashion as the partial derivative of the ADM mass with respect to the pressure. The volume computed by the Iyer-Wald formalism is by construction the same quantity. We conjecture that this should further correspond to the late-time value of the time derivative of the spacetime volume of the Wheeler-DeWitt patch, and have checked several examples, but have no proof that this holds generally.

How to take this story further? As mentioned in the introduction, a tensor network picture of the black hole interior was introduced by Hartman and Maldacena in [108]. Tensor network is a topic of much recent interest for holographers [120, 121, 122, 123] with an eye on the emergence of spacetime. Thus one can ask the question: can the pressure-volume variables be understood in the language of tensor networks or quantum circuits? Also, according to black hole complementarity [124, 125], the black hole interior is an example of emergent space *par excellence*. Thus, one can hope that the pressure and volume variables can prove helpful to our understanding of quantum gravity in the future.

Chapter 5

Holographic Purification Complexity

5.1 Introduction

[1]In the past several years, quantum complexity has entered into discussions of quantum gravity and holography, starting with a discussion of complexity and the AMPS paradox in [25] and later in [126]. Motivated by these considerations, it was later suggested that in the program of bulk reconstruction, boundary data about entanglement is insufficient to reconstruct a dual geometry and that perhaps something like the quantum circuit complexity of the state could fill the gaps [14]. The complexity $C(|\Psi\rangle)$ of a state $|\Psi\rangle$ is the minimum number of basic unitaries, or 'gates' g, drawn from a pre-established gate set $G = \{g_i\}$, needed to build a circuit $Q = \prod_{i=1}^{C} g_i$ such that $d_f(Q|\Psi_0\rangle, |\Psi\rangle) < \epsilon$, where $|\Psi_0\rangle$ is a pre-established 'reference state', ϵ is the 'tolerance parameter', and $d_f(\cdot,\cdot)$ is the Fubini-Study metric. Out of these ideas arose the 'complexity = volume' conjecture [14, 15] which specu-

[1]This chapter is a reproduction of [5], which I wrote with Elena Caceres, Stefan Eccles, and Willy Fischler. The basic idea of the paper, which was to compare 'subregion complexity' (i.e. the maximal volume of an entanglement wedge or the action of the intersection of an entanglement wedge with the WDW patch) to holographic 'complexity' computations on different geodesically complete geometries into which the entanglement wedge could be isometrically embedded, was substantially mine, though came out of discussions with the other authors. I also assisted with the writing and computations.

lates that the volume of a maximal spatial slice is dual to the quantum circuit complexity of the dual quantum state living on the intersection of that spatial slice with the boundary. For aesthetic reasons, it was eventually suggested to replace 'complexity = volume' (henceforth referred to simply as 'CV') with 'complexity = action' ('CA') [18, 19], and while the bulk of the discussion on the topic is concerned with these two conjectures, at the boundaries at least two other speculations exist, namely 'complexity = spacetime volume' ('CV2.0') [4] and 'CA-2' [127][2]. CA modifies CV by replacing the volume of a maximal spatial slice by the action evaluated on the WDW patch associated with the slice, i.e. the causal development of the (UV-regulated[3]) slice. CV2.0 modifies CA by replacing the action on the WDW patch with the spacetime volume of the WDW patch.

All of these conjectures could be applied to any geometry, including some subregion of the bulk, though we would not expect these quantities computed for a general bulk subregion to have any particular meaning. However, considering that the state on a subregion of the boundary is dual to the entanglement wedge, as argued in [128, 129, 130], it is tempting to say that these proposals applied to an entanglement wedge might be dual to the complexity of the reduced state on the corresponding boundary subregion. This has been suggested by a number of authors [103, 22], and the 'complexity' thus com-

[2]Though in general distinct, CA-2 reduces to CV 2.0 for Einstein-Hilbert gravity with no sources other than a cosmological constant, and as such we will not consider CA-2 separately in this paper.

[3]For a slice not cut-off by some UV-regulator, the WDW patch only corresponds to the causal development of the slice if one forgets the reflecting boundary conditions at infinity.

puted is termed 'subregion complexity.' This, however, raises the question: What is the complexity of a mixed state? There is not a unique way to extend the usual definition of circuit complexity from pure states to mixed states, so which extension are we talking about? To answer this question, the authors of [1] considered a number of possible definitions of mixed state complexity and compared them to what happens in holography. They came to the conclusion that the 'purification complexity,' which is roughly defined as the minimum state complexity among pure states which reduce to the appropriate density matrix on a subsystem, is a good candidate to be dual to subregion complexity in CA. On the other hand, none of the definitions they considered provides a likely dual to subregion complexity in CV. In this paper we further investigate purification complexity, first as defined in [1] but also with minor variations, providing an independent discussion of its behavior for general quantum states and specifically motivating its connection to holographic subregion complexity.

The purification complexity of a holographic mixed state can be bounded from above by considering all its holographic purifications. Beginning with the entanglement wedge dual to the mixed state in question, all holographic geometries which geodesically complete the wedge provide a family of purifications in their boundary dual states. In any such geometry, we argue (supported by an analogy to the entanglement of purification) that different choices of the cut-off surface in the region complement to the original entanglement wedge correspond to different coarse-grainings of the purifying state. By minimization over cut-offs we argue on general grounds that the purification complexity

is bounded above by the subregion complexity in all of CV, CA, and CV2.0. We then prove that so long as we restrict our attention to holographic purifications, this inequality is saturated in CV and CV2.0, because complexity in these proposals is superadditive.

The situation for CA, by contrast, is more complicated. In the absence of a superadditivity property, we must worry that the subregion complexity is not truly minimal among all holographic purifications. To examine this possibility, we consider geodesic completions of the one-side BTZ geometry dual to a thermal state. We find that there are indeed cases where the true minimum is smaller than the subregion complexity, thereby contradicting the conjecture in question.

Our results thus differ here from [1]: we are led to the conclusion that in CV and CV2.0, subregion complexity = purification complexity, whereas in CA it seems either this is not the case, or else that certain asymptotically AdS geometries are not holographic.

The paper is organized as follows: In section 5.2 we define purification complexity and investigate its additivity properties on subsystems of general quantum states. We use this analysis to sharpen our expectations on the behavior of any bulk holographic dual to purification complexity. In section 5.3 we motivate the connection between purification complexity and holographic subregion complexity by analogy with the concept of "entanglement of purification", of which we give a brief overview. We note that for any geodesic completion of the entanglement wedge dual to our mixed state, there will be

one purification which corresponds to a cutoff skirting just outside the entanglement wedge along the HRT surface. This purification will have a complexity equal (up to a possible boundary like the term discussed at the end of the section), to the subregion complexity. In section 5.4 we prove that complexity according to either CV (in its usual form, without a boundary term) or CV2.0 is superadditive. This, in turn, implies that the complexity of the state dual to any geodesic completion of our entanglement wedge, with any choice of cutoff, must be larger than the subregion complexity as ordinarily defined. We are thus led to the conclusion that in CV and CV2.0, the purification found in section 5.3 was indeed optimal among holographic purifications.

In section 5.5 we consider the case of CA, where the purification found in section 5.3 need not be optimal. We consider several families of geodesic completions of the one-sided BTZ geometry. One such family are the n sided genus g generalizations of the two-sided BTZ geometry, where we borrow computations done in [131]. These solutions lead to challenges to the purification complexity interpretation of subregion action, namely that the complexity of certain purifications can be lower than the subregion complexity of the BTZ thermal state, and can even be computed to be negative in some cases, although the issue of the negativity of the action was already raised by [131]. We come to the conclusion that if one is not to abandon the proposal that subregion complexity is dual to purification complexity in CA, one must impose even stricter limits on the geometries considered. We further find that one must impose a limit on the cutoffs considered.

5.2 Purification Complexity: Quantum Expectations

In this section, we will explore some aspects of purification complexity as defined in [1]. We first define the quantity as well as discuss ambiguities and variations on the definition which could lead to qualitatively different behavior on subsystems. We then discuss the expected behavior of purification complexity on subsystems. It should be noted that Agón et al. give a compelling but inconclusive argument that purification complexity should be subadditive for the left and right factors of the thermofield double state, and plausibly more generally. We here give an independent discussion indicating that purification complexity is neither superadditive nor subadditive in general. We then place this discussion in the context of the decomposition into basis and spectrum complexities utilized by [1], and discuss how this breakdown is sometimes insufficient for discerning additivity properties. We then conclude this section with a discussion of how these expectations ought to manifest in holographic states, listing some basic consistency checks which must be obeyed by any bulk quantity dual to purification complexity.

5.2.1 Definition and Refinements

Purification complexity $C^P(\rho)$ of a density matrix ρ is defined in [1] to be the minimum pure state complexity over all its purifications, subject to the constraint that every additional qubit of the purifying system ends up entangled with the original "physical" qubits. That is,

$$C^P(\rho) = \min_{|\psi\rangle \in \mathcal{P}} C(|\psi\rangle) \tag{5.1}$$

where $\mathcal{P}$ is the set of all purifications $|\psi\rangle$ of ρ which have no separable factors which are also purifications, i.e. there is no decomposition $|\psi\rangle = |\psi_1\rangle \otimes |\psi_2\rangle$ such that $|\psi_1\rangle$ also purifies ρ. This last condition is necessary so that purification complexity reduces to ordinary state complexity on pure states. If $|\phi\rangle$ is a pure state, then any 'purification' of it results in a separable state $|\psi\rangle = |\phi\rangle \otimes |\psi'\rangle$, but since $|\phi\rangle$ is pure and hence a purification of itself, no $|\psi\rangle$ with non-trivial $|\psi'\rangle$ is in our set $\mathcal{P}$, and hence $C^P(\rho_\phi) = C(|\phi\rangle)$ (where $\rho_\phi = |\phi\rangle\langle\phi|$). If we however included such purifications in our minimization, we can at best say that $C^P(\rho_\phi) \leq C(|\phi\rangle)$. In purifications satisfying this criterion, we say that the state on the ancillary Hilbert space is 'fully entangled' with the original state $|\psi\rangle$, and we'll refer to such purifications as 'valid' purifications.

It is easy to imagine alternatives to the above definition which share the same spirit as minimization over purifications, but restricting by more or less the allowed class of purifications. At one extreme we could consider 'unrestricted' purification complexity, with the minimum taken over all possible purifications. Such a procedure will not reproduce the usual definition of complexity of pure states, but it does provide a different, competing definition, which in principle could be the one relevant for holography (though we are not making that claim here). On the other hand we could place more stringent conditions on the purifying states, or instead, constrain the ancillary Hilbert space used to purify. As an example of the latter type of constraint, we could dictate that only a Hilbert space of minimal dimension may be used, this being fixed by the rank of the density matrix in question. This last possibility is

also compatible with the usual pure state definition, and in fact, discussions of section 5.3 indicate that such a restriction may be relevant for subregion complexity.

All of these definitions implicitly assume that a notion of pure state complexity has been defined, not only for the original Hilbert space but for every allowed dimension and form of the purifying Hilbert space. A reference state and gate set must be chosen which scale unambiguously with these Hilbert spaces. Mixed state complexity thus inherits all the same ambiguities as any pure state complexity, and in a sense even more. Though at first disconcerting, this feature is perhaps appropriate considering the holographic conjectures; these presumably employ some natural reference and gate set, each suitably adjustable to any cutoff scale[4].

For developing intuition with N-qubit systems, one plausible procedure is to take the "all zeros" state as the reference, regardless of N. For the gate set, one could specify a universal gate set on two-qubit systems and then allow the same logical operations on any pair of qubits. This is referred to as a two-local gate set. With any k-local gate set (defined analogously), the same prescription scales unambiguously as the Hilbert space adds or eliminates degrees of

[4]The need to define mixed state complexity has been most keenly appreciated with the intent to generalize the holographic prescriptions to subsystems, but even considering CFT states at finite cutoff, having traced out some UV degrees of freedom one might wonder if even the original holographic complexity conjectures already require a notion of mixed state complexity to be well-defined. However, at leading order in $1/N$, total states have no entanglement entropy even at finite cutoff and can be thought of as a pure state living on the reduced Hilbert space. In this paper, we restrict ourselves to this limit, where 'total state' entails 'pure state'.

freedom, though the rate at which new gates proliferate with additional degrees of freedom depends on the specifics of these choices. This leads only to the restriction that subsystems should not be considered below k qubits.

We hold such prescriptions loosely in mind, but with the exception of a few comments, we will henceforth remain agnostic about the choice of gate set and reference state. Instead, we seek to identify features of purification complexity which transcend these ambiguities and therefore inform our expectations about any holographic dual ever before such specifics are understood.

5.2.2 Additivity Properties

First, we focus on states which are fully entangled between two subsystems A and B. [5] For these states, purification complexity can easily be seen to obey

$$\mathcal{C}(\rho_A) \leq \mathcal{C}(\rho_{AB}) \qquad \text{(fully entangled subsystems)} \tag{5.2}$$

by noting that any valid purification of AB is also a valid purification of A (or B), and so the minimum complexity over valid purifications of A (or B) is upper bounded by that of AB. This inequality immediately leads to another which we dub 'weak superadditivity':

$$\mathcal{C}_A + \mathcal{C}_B \leq 2\mathcal{C}_{AB} \qquad \text{(fully entangled subsystems)} \tag{5.3}$$

where we introduce the notation of using a subscript to denote the subsystem, e.g. $C^P(\rho_A) = C^P_A$.

[5] Here again, by 'fully entangled' we mean that no subsystem of either A or B factorizes from the full system, i.e., A is fully entangled with B and B is fully entangled with A.

The proof given above for weak superadditivity breaks down when we consider states which factorize on any subsystem of A or B, owing to the constraint that in valid purifications the ancilla system must end up fully entangled with the system it purifies. For example, consider a separable pure state on AB. While such a state is undoubtedly a purification of the states on A and B respectively, it is not a valid purification.

In fact, for pure states which are factorizable on any number of subsystems, purification complexity is demonstrably subadditive over these separable factors. To see this, note that the complexity of each subsystem is an ordinary state complexity (because the state on each subsystem is pure), obtained using gates which act unitarily within that subsystem. The circuits which are individually optimal for these subsystems may also be used together to prepare the full product state, but for that purpose, it may not be optimal since circuits over the whole system may additionally utilize gates which couple the subsystems. [6] This composite circuit's state complexity is the sum of the individual state complexities, and it puts an upper bound on the total state complexity. A nearly identical proof guarantees subadditivity for factorizable systems, regardless of whether or not they are pure:

[6]It may first seem that if we start with an unentangled reference state, then gates which couple unentangled subsystems should play no role in the optimal circuit because these gates create entanglement. However, though such gates are necessary to create entanglement between the two subsystems, they do not always do so. It is easy to find factorizable states and gate sets where the optimal circuit utilizes these gates without ever creating entanglement between the subsystems, even at intermediate stages.

$$\mathcal{C}_A + \mathcal{C}_B \geq \mathcal{C}_{AB} \qquad \text{(factorizable subsystems)} \tag{5.4}$$

Note that the inequalities (5.3) and (5.4) do not contradict each other. In fact it's conceivable that together they bound the span of purification complexity on general subsystems:

$$C_{AB} \leq C_A + C_B \leq 2C_{AB} \qquad \text{(not proven!!!)} \tag{5.5}$$

However neither of these inequalities is proven in general, rather each is proven for a different corner of state space (factorizable subsystems and completely non-factorizable subsystems, respectively). It is natural to ask whether either of these classes can violate the opposing inequality and whether intermediate classes of states obey either inequality. We return to these question shortly, but pause here to relate these statements to the work of [1] and the decomposition of purification complexity into spectrum and basis components.

5.2.3 Basis and Spectrum decomposition

Given an arbitrary mixed state and a large enough ancillary Hilbert space (e.g., a duplicate Hilbert space is always sufficient), it's always possible to construct a purification through a two-part process: first prepare a state with the appropriate spectrum on the reduced system, then from this state rearrange the subsystem basis until the target density matrix is achieved. There is an optimal circuit which performs each of these tasks, and their complexities

define the spectrum complexity C^S and the basis complexity C^B respectively [7]. In sequence these operations prepare the full mixed state; there may be more efficient routes to prepare a purification, but the sum of these circuit complexities upper bounds the purification complexity:

$$C^P \leq C^S + C^B \tag{5.6}$$

In [1], the authors consider the possibility that any one of these complexities (C^P, C^S, or C^B) might correspond to holographic subregion complexities as computed using the Complexity = Action (CA) or Complexity = Volume (CV) conjectures. The best tentative match aligned the CA subregion prescription with the full purification complexity C^P. This correspondence was particularly encouraged by the expectation that C^P should be subadditive, and among holographic prescriptions only CA includes bulk contributions which are not positive-definite, allowing that at least in the case considered CA was also subadditive. We will revisit this particular holographic example in section 5.5, but we here give a schematic outline of the reason for these expectations.

Consider a two-sided eternal black hole with the subregions being the full left and right boundaries (we will use subscripts L and R for "left" and "right" on a Penrose diagram, and subscript T for "total" or "thermofield

[7] In [1] what we call basis complexity is denoted $\tilde{C}^B$, while C^B denotes the exact difference $C^P - C^S$. We avoid using this exact difference to ensure that C^S and C^B are the complexities of circuits which can be applied in succession to prepare the correct mixed state

double state"). The individual subregions each decompose into a basis and spectrum part.

$$\begin{aligned} C_L^P &\leq C^S + C_L^B \\ C_R^P &\leq C^S + C_R^B \end{aligned} \tag{5.7}$$

Because the combined state is pure, the spectrum part is the same for left and right subsystems. To prepare the total state, we can presumably borrow the circuits utilized in the above decompositions, but importantly the spectrum part need only be prepared once at the beginning of this process:

$$C_T^P \leq C^S + C_L^B + C_R^B \tag{5.8}$$

Each of the preceding circuit decompositions only upper bounds the true purification complexity, but if we blithely suppose that the bounds are approximately saturated, then comparing (5.7) and (5.8) leads to the expectation that

$$C_T^P \leq C_L^P + C_R^P \leq 2C_T^P \tag{5.9}$$

These inequalities match those of Eq. (5.5). In the case considered here, with the subsystems being left and right halves of an eternal black hole, the rightmost inequality of (5.9) follows rigorously from (5.3) for fully entangled subsystems. The leftmost inequality is less certain. Particularly, in equation (5.8), we assume the total state can be prepared by "borrowing the circuits" used to prepare the subsystem density matrices. However, it is only guaranteed

that this combined circuit will prepare a state with the correct subsystem density matrices. There are many such states, and these can have vastly different complexities; preparing the correct total state may require complex operations which are effectively unnoticed by either subsystem and are not accounted for in any of the C^S, C_L^B, or C_R^B circuits of equation (5.7). To illustrate this point, recall the behavior of the thermofield double state evolved away from the $t_L = t_R = 0$ slice:

$$U(t_L, t_R)|TFD\rangle = e^{-iE_n(t_L+t_R)}e^{-\beta E_n/2}/\sqrt{Z}|n\rangle_L|n\rangle_R \tag{5.10}$$

where $U(t_L, t_R) = U_L(t_L)\otimes U_R(t_R) = e^{-iH_L t_L}\otimes e^{-iH_R t_R}$ implements time evolution independently on each boundary (with times set to increase 'upward' on both sides of a Penrose diagram). The effects of this operation, apparent in the leading phase factor of (5.10), go unnoticed by either subsystem and of course, it is precisely these effects which lead to the famed late-time linear growth of the pure state complexity. Away from the time symmetric slice of the two-sided black hole, the growth of the total state complexity will inevitably break the left-hand side inequality in (5.9).

If we consider the $t_L = t_R = 0$ boundary state only, the total state complexity is minimal among the family of states in 5.10, and so expected to obey $C_T \leq C_L^P + C_R^P$. Indeed this is the chief expectation which found a match in the Complexity=Action subregion calculations of [1]. However, there is a subtlety related to the degeneracy of the energy spectrum which

may muddle even this expectation. It was pointed out in [132] that when a subsystem density matrix has a degenerate spectrum, it has interesting implications for purification complexity. Unitaries which enact rotations or phase shifts within such a degenerate subspace act trivially on the subsystem density matrix (effectively limiting the basis complexity of the density matrix), so they never contribute to the purification complexity. However the same unitaries can affect the pure state on the combined system, sometimes increasing the complexity of the target state[8].

If we consider the most extreme case of a fully degenerate spectrum (or the $T \to \infty$ limit), we have maximally mixed subsystems. Preparing both subsystems is equivalent to preparing N bell pairs. This can be thought of as minimizing complexity over a huge family of states which all prepare the appropriate subsystem density matrices:

$$|\psi\rangle = U_L \otimes U_R \left(\frac{1}{\sqrt{N}} \sum_{i=1}^{N} |i\rangle_L |i\rangle_R \right) \tag{5.11}$$

Any state among these is a valid purification, and the subsystem purification complexities are upper bounded by minimizing state complexity overall U_L and U_R. The total state, on the other hand, will be some particular state among (5.11) with particular U_L and U_R. If the total state happens to be the minimally complex state among these, then $C_L^P = C_R^P = C_T$ and weak

[8]The unitaries enacting time evolution on the thermofield double state are a special case among this class of unitaries. Even if the spectrum is entirely non-degenerate, there are phase rotations within each energy subspace which go unnoticed by either subsystem density matrix but contribute non-trivially to the total state complexity.

superadditivity is saturated. On the other hand, by choosing U_R, U_L to make the total state maximally complex we can engineer the total state to violate subadditivity.

If we consider again the thermofield double state at finite temperature on a time-symmetric slice, the total state complexity is at least minimal among

$$|\psi\rangle_T = e^{-iH_L t_L} \otimes e^{-iH_R t_R} \left(\frac{1}{\sqrt{N}} \sum_{i=1}^{N} |i\rangle_L |i\rangle_R \right) \tag{5.12}$$

However, if there is some degeneracy in the energy spectrum, then in preparing the subsystem density matrices we can minimize over a larger class of unitaries (all those which do not intermix degenerate subspaces, but not all U_A and U_B). This class of unitaries is still potentially much larger than minimization over the time evolution unitaries which occurs at the $t_L = t_R = 0$ slice. It is not immediately clear how much the "extra minimization" over a larger class of unitaries affects the subsystem complexity in comparison to the total state complexity in the case of the thermofield double state. It would seem to depend on the specifics of the energy eigenstates and the gate set involved.

Unfortunately, through these considerations, we are only able to cast doubt on the expectation that the $t_L = t_R = 0$ thermofield double state ought to have purification complexity which is subadditive on the left and right factors, and not provide a rigorous alternative. We will nevertheless consider this example (specifically the BTZ case) holographically in section 5.5 and subject it to other consistency checks.

5.2.4 Expectations for Holographic States

The additivity relationships discussed in subsection 5.2.2 hold for different types of quantum states. Under what circumstances are these relationships relevant to holographic quantum states? We here consider this question, and then give a short list of consistency checks which must be satisfied by any holographic dual to purification complexity.

A pure state which factorizes between subsystems has no entanglement between those subsystems. On the other hand, the smoothness and connectedness of a holographic spacetime indicate that the state on any boundary subregion is fully entangled with its complement. We, therefore, consider the smoothness and connectedness of the classical geometry as the necessary and sufficient condition preventing factorization of the boundary pure state. Holographic states dual to connected spacetimes are therefore of the 'fully entangled' type in subsection 5.2.2.

Though connected geometries are dual to fully entangled states, we may still consider factorizable holographic pure states. To do so we merely treat multiple independent holographic geometries as product states, living in separate Hilbert spaces with boundary theories decoupled. This thought experiment provides at least one valuable lesson. Any of the geometric prescriptions for subregion complexity will be exactly additive on such factorizable subsystems. While utilizing gates which couple the combined Hilbert space could in principle allow for increased efficiency in preparing the combined state, evidently the notion of complexity dual to bulk action or volume

does not take advantage of such gates. Either holographic states are always of the sort that they are never optimally constructed utilizing these gates, or such gates should be excluded from the outset. This latter possibility stands in tension with naive prescriptions for choosing the gate set to vary only with the size of the Hilbert space with no other concern for locality or the entanglement structure of the state (such as the k-local gate set prescription outlined in section 5.2.1). This also indicates that if we consider only holographic purifications, the validity constraint excluding unentangled factors is redundant, because evidently including such factors never results in a 'speed up.'

Turning again to connected holographic spacetimes, if we consider only such systems we can apply our expectations about fully entangled states (see subsection 5.2.2). Along with the basic requirement that purification complexity is positive definite, we have a primitive list of consistency checks to perform on any proposed holographic dual to purification complexity. For any boundary subregion A and neighboring (connected, but not necessarily small) extension of that boundary subregion δA, we expect

$$\begin{aligned} \text{Positivity:} \qquad & C_A^P > 0 \\ \text{Monotonicity:} \qquad & C_{A+\delta A}^P > C_A^P \\ \text{Weak Superadditivity:} \qquad & C_A^P + C_{\delta A}^P < 2C_{A+\delta A}^P \end{aligned}$$

The monotonicity property, which is symmetric on A and δA, implies weak superadditivity. The same applies to the case already discussed in section 5.2.3, the two sides of an eternal black hole solution. In this case δA is replaced

with A^c, the boundary region complement to A. This is not a 'neighboring' boundary subregion (they are only connected through the bulk), but they form a partitioning of the total boundary (T) and the subsystems are fully entangled.

$$\text{Weak Superadditivity:} \quad C_A^P + C_{A^c}^P < 2C_T$$

5.3 Holographic Purification Complexity

In this section, we consider in detail the conjecture(s) that volume or action on a subsystem entanglement wedge in holographic geometries might be dual to the purification complexity of the corresponding boundary mixed state. We first motivate the relationship to purification complexity, as opposed to some other notion of mixed state complexity, by considering what the total state complexity conjecture may already imply about the meaning of subregion complexity. We do so through an analogy with the concept of 'entanglement of purification,' explained in subsection 5.3.1.

In 5.3.2 we make the case that the volume prescription for subregion complexity is computing a type of purification complexity. To be precise, if the class of purifications considered is all holographic purifications, then the prescription computes precisely the minimum complexity among these. Over any less restricted class of purifications, the subregion prescription merely bounds from above the purification complexity so defined. The same arguments applied to the action prescription do not lead so inexorably to the notion of

purification complexity. They imply that the prescription computes the complexity of a particular purification, but it is not clear that it is the optimal one. We defer more explicit holographic tests of this idea for subregion action to section 5.5.

The considerations of this section imply that the volume prescription matches our general expectations for purification complexity more or less automatically, but in 5.3.3 we discuss a puzzle with this interpretation and use it to motivate a modification of the bulk volume prescription to include a boundary term on the HRT surface.

5.3.1 Motivation from Entanglement of Purification

.

We would like to test the conjecture that subregion complexity is dual to purification complexity by finding a holographic estimate of the purification complexity (independent of the usual subregion complexity prescription). For guidance on how to construct such a holographic estimate, we turn to discussions *entanglement of purification* in holography. Entanglement of purification is defined as follows: Given a bipartite system consisting of subsystems A and B, and a state ρ_{AB} on that system, the entanglement of purification between A and B of ρ_{AB} is the minimum entanglement entropy $S(\rho_{A\bar{A}})$ of the reduced state $\rho_{A\bar{A}}$ minimized over all purifications $|\psi\rangle_{A\bar{A}B\bar{B}}$ of ρ_{AB} and all partitions of the purifying system into $\bar{A}$ and $\bar{B}$. If ρ_{AB} is pure, then the entanglement of purification is simply the entanglement entropy of the reduced state ρ_A and

ρ_B. Recent work [133, 134, 135], has discussed a conjectured holographic dual to this quantity for holographic CFTs, which is given as follows: Consider subregions A and B on the boundary, and the joint entanglement wedge of AB. The holographic entanglement of purification is then given by the area of the minimal surface in the entanglement wedge which divides A from B (refer to figure 5.1). In the case where there is no mutual information between A and B, and so the entanglement wedge is disjoint, we have that A and B are already divided, and so the entanglement of purification is zero. In the case of two disjoint intervals with non-zero mutual information, the minimal surface goes between the two disconnected pieces of the RT surface, and we need only minimize over which points on the RT surface it will intersect.

The intuition behind this definition is as follows: There is an optimal purification, which lives on the subregion AB on the boundary, as well as the on the RT surface of AB. The auxiliary states on the RT surface can be partitioned into an $\bar{A}$ system and $\bar{B}$ system in different ways, and for each partition, we may compute the entropy of $A\bar{A}$ using the RT prescription. By minimizing over such partitions, we arrive at the entanglement of purification, as given above. But how did we arrive at the fact that the purifying auxiliar system 'lives' on the RT surface? This is supported by intuition from tensor networks, but we can justify it as follows:

In minimizing over purifications, we certainly know that the state on the full boundary is a purification of the state on AB. However, this state contains much more information than is needed to purify the reduced state

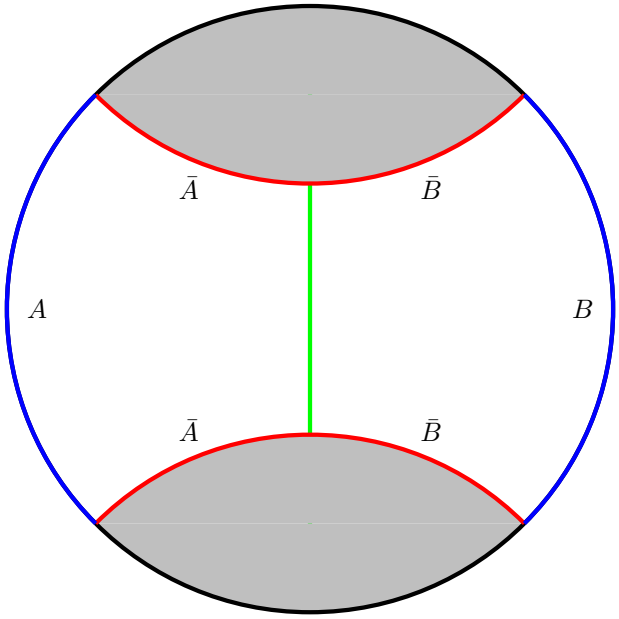

Figure 5.1: Entanglement of purification between two interval subregions with non-zero mutual information. The minimal surface whose area gives the entanglement of purification is shown in green.

ρ_{AB} on AB. As a consequence, for any partition, there more entropy than we needed. We can fix this by renormalizing the state, thereby getting rid of the extra information. These renormalized states correspond to putting different cutoffs in the bulk, which agree with our original cutoff in the entanglement wedge of AB, but which outside that wedge can be different. Each of these cutoffs corresponds to a different renormalization of the global state, and as

such a different purification of ρ_{AB} (see figure 5.2). Clearly then, the cutoff which will give the smallest RT surface, and likewise the one that corresponds to course graining away all the information not needed to purify ρ_{AB}, is the one which hugs the RT surface of AB. We then get the prescription above.

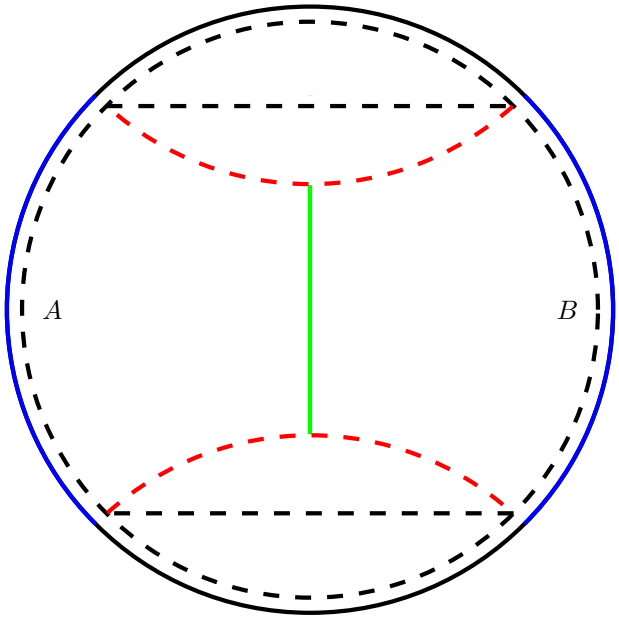

Figure 5.2: We may purify the state on AB to states with different course grainings, corresponding to different cutoffs, shown here as a dashed line. The optimal purification will correspond to cutoff which hugs the RT surface, shown here as a red dashed line.

Of course, there are potentially other holographic purifications of ρ_{AB}.

Suppose there is an isometric embedding of the entanglement wedge of AB into a geodesically complete asymptotically AdS spacetime, such that the entanglement wedge of the image $\tilde{A}\tilde{B}$ of AB is the image of the entanglement wedge of AB. Then according to subregion duality, the reduced state on $\tilde{A}\tilde{B}$ simply is ρ_{AB}, since both states are dual to geometries which are identical up to isometry. We may then repeat the above procedure on the new geometry. For entanglement of purification, we will inevitably be led to the same purification, by the arguments above. We will nevertheless term such geometries 'purifying geometries' for the holographic state ρ_{AB}.

We claim that this same procedure of minimizing over purifications by considering all purifying geometries, and all cutoffs on these purifying geometries compatible with our cutoff in the entanglement wedge, should be applied to find the purification complexity of a given reduced state holographically. We flesh out this claim in the following subsection.

5.3.2 Purification Complexity

Suppose we take for granted the original complexity=volume conjecture, that the maximal volume slice asymptoting to a fixed boundary Cauchy slice is dual to some notion of complexity for the total state on that boundary slice [9]. Consider all possible holographic geometries which geodesically

[9]In the complexity = volume conjecture, a choice of lengthscale is necessary to turn a proportionality into a true equality. Traditionally this length scale has simply been taken to be the AdS scale, but recent work [2] has suggested that a variable scale determined by features of the total geometry may be more appropriate. It is not clear how such a variable

complete a fixed entanglement wedge. The states dual to these 'purifying geometries' provide a set of purifications of the density matrix on the original boundary subregion (any pure state is, of course, a purification of all its subsystems). Further consider all possible cutoff surfaces in the complementary portion of these spacetimes, subject to the restriction that they can at least sustain a Cauchy slice for the original entanglement wedge. The corresponding set of coarse-grained states provides an even larger class of purifications to consider.

Trusting the total state complexity conjecture, we can compute all the complexities of these purifications and find the minimum. With the complexity=volume prescription, we are inevitably led to the conclusion that the minimum pure state complexity among all holographic purifications corresponds to choosing a cutoff surface which traces just outside (see next section) the HRT surface for the subregion; deviation from this choice results in either an increase in volume and a higher complexity, or in the exclusion of some portion of the entanglement wedge, which invalidates the state as a purification of the original density matrix. The first statement follows intuitively from the positive-definiteness of volume, and more rigorously from the super-

lengthscale should be set for the arbitrary subregions considered in this paper. For simplicity, we first consider the case where the length scale is the AdS scale. For our conclusions about additivity to hold for complexity and not just volume in a proposal with variable lengthscale, we at least require that the length scale is the same for the subregion, the total state, and the complement subregion. In a hypothetical scheme where the length scale changes even with the cutoff surface, the minimization procedures described in this section applies to complexity as well as volume only if variations in the cutoff surface which increase the max volume obey $\delta \log (V/V_0) \geq \delta \log (l/l_0)$, with l being the variable lengthscale, and V_0, l_0 being some reference values.

additivity relationship proven in the next section 5.4. The second statement relies on the specific duality between an entanglement wedge and the corresponding boundary mixed state. Any cutoff contour which cannot sustain a Cauchy slice for the original entanglement wedge will inevitably exclude some bulk operators which ought to be described by the original boundary subregion's mixed state. In so far as we consider only holographic purifications of a boundary mixed state, these considerations imply that the volume subregion prescription on an entanglement wedge is computing precisely the minimum complexity among purifications. The same claims follow analogously for the complexity=spacetime volume prescription.

Now consider the same series of statements for the complexity=action subregion prescription. We can consider purifying geometries of a fixed entanglement wedge, and we can vary over cutoff surfaces. The action on the entanglement wedge submanifold is just another pure state complexity, with the complementary degrees of freedom course-grained to the limiting case of the HRT surface itself. However, lacking in these considerations is the idea that computing this particular purification's complexity amounts to a minimization over holographic purifications. The action is not a positive-definite quantity, and other choices of cutoff surfaces in some purifying geometry may provide a purification of lower complexity. Finding any such state amounts to a disproof that the action subregion prescription can be called a purification complexity, in the usual sense of a minimization over the complexity of purifications. We find such counterexamples in 5.5.

We now provide an example of the procedure just outlined by considering the two-sided black hole (see figure 5.3). If our aim is to estimate the purification complexity of the left boundary mixed state with a certain cutoff $r = \delta_L$, and we are allowed to minimize over the purifying right cutoff, δ_R, an interesting result emerges: When one sets $\delta_R = r_+$, and regularizes the WDW patch by settings its 'corners' on the cutoff surfaces, one recovers (in this limit) the usual subregion complexity of the left side! Analogous procedures result in similar conclusions for other two-sided geometries, or for subregions of AdS_3. In fact, for a general boundary subregion A, allowing a minimization over possible cutoffs in the complement region, subject to certain consistency conditions (e.g., the total cutoff must be continuous), will lead to the inequality

$$C^P(A) \leq C^{\text{subregion}}(A) \tag{5.13}$$

whenever the entanglement wedges of a region and of its compliment meet on a single surface. By the HRT prescription, this should always happen for geodesically complete geometries.

Under either CV or CV2.0, superadditivity holds for any values of the left and right cutoff (we give a proof in section 5.4), and we thus have that

$$C(|\psi\rangle) \geq C^{\text{subregion}}(A) \tag{5.14}$$

for any holographic purification $|\psi\rangle$ of ρ_A. However, then this means that if we define a purification complexity only with respect to holographic states (which is perhaps appropriate at leading order in $\frac{1}{N}$), then we have that subregion

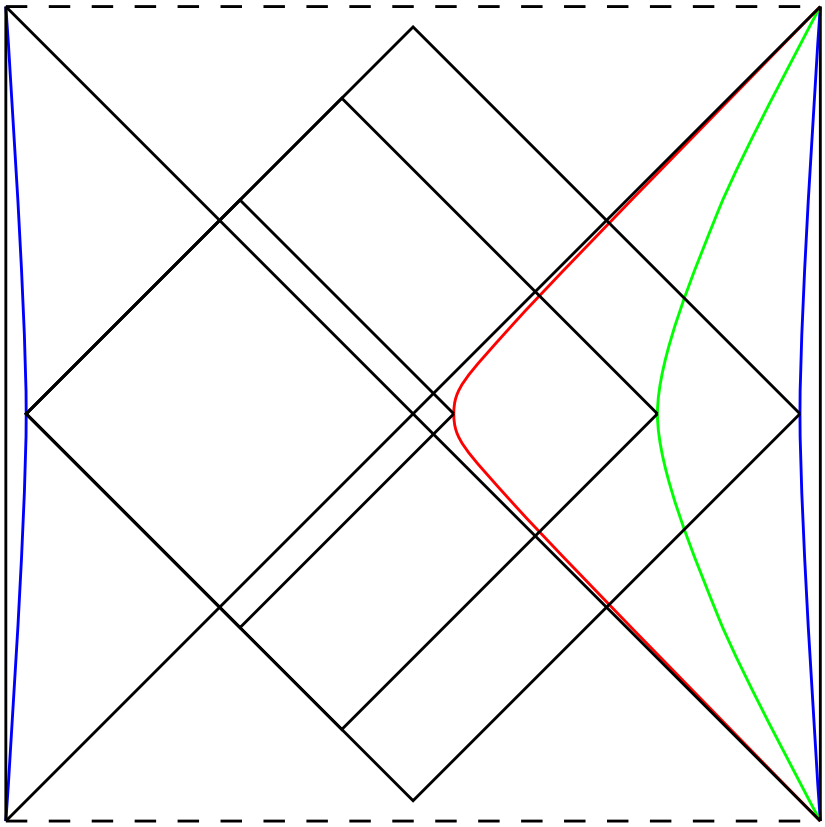

Figure 5.3: A two sided black hole, with different cutoff surfaces on the right side. For each cutoff surface, we have draw the corresponding regulated WDW patch.

complexity = holographic purification complexity. This strongly suggests that the duality proposed in [1] for CA works for both CV and CV2.0. The situation with CA is actually less clear, as the action is not positive definite and equation (5.14) does not apply. The inequality (5.13) does still hold for CA though, provided this minimization over the right cutoff is valid.

5.3.3 Adding a boundary term

One issue with this proposal to minimize over all cutoffs is that, for the optimal purification, the subregion complexity of the reduced state on the purifying right system vanishes. However, this reduced state must have a fixed entanglement entropy, as the state on the whole system is pure. Either we must have a mixed reference state (which seems unusual), or something else must be going on. We can resolve this issue by not allowing the cutoff surface to be pushed all the way to the horizon surface, instead taking it only to the stretched horizon. This too has a number of interesting consequences, the first of which is that it makes the purification complexity in CV subadditive on a slice about which there is time reflection symmetry. This is because the left and right purification complexities both include the volume of the slice between the left and right stretched horizon, and so this part of the volume gets counted twice when one adds the two purification complexities, and only once when one computes the total complexity. This is reminiscent of the argument in section 3.3 of [1] that the spectrum complexity gets double counted when adding the purification complexities, suggesting that perhaps this segment of the volume between the left and right stretched horizons should be identified with the spectrum complexity of the mixed state. We would then identify the part of the volume between the left cutoff and the left stretched horizon as the basis complexity.

When considering the thermofield double state away from the $t_L = t_R = 0$ slice, the maximal slice will not pass through the HRT surface, and the simple

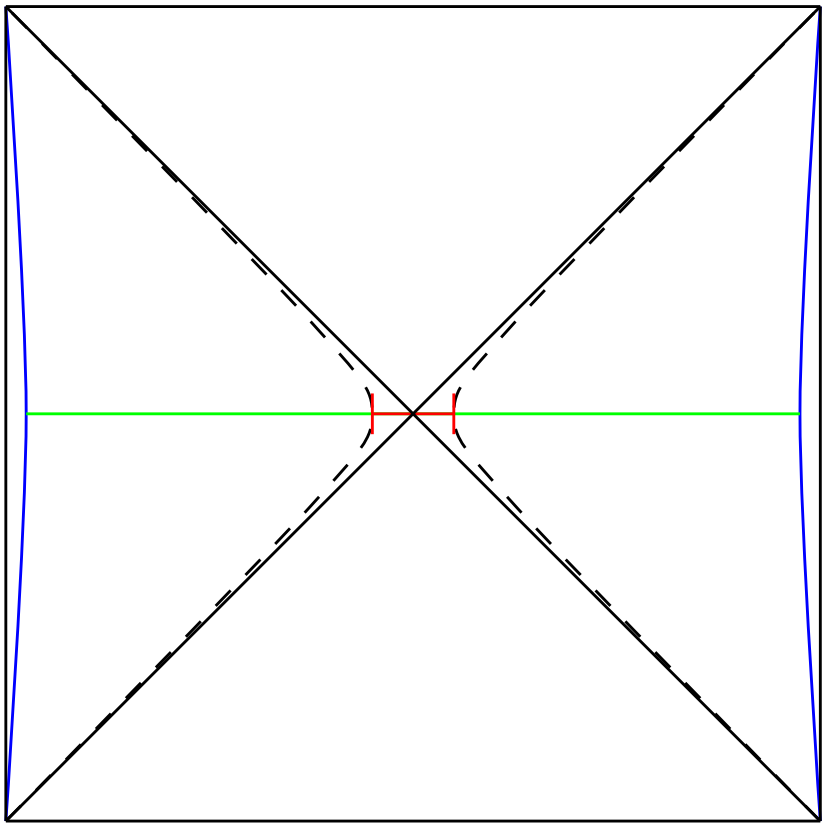

Figure 5.4: The dashed lines in this figure represent the stretched horizon. The purification complexity in CV of the left (right) reduced state is given by the volume of the left (right) green segment plus the red segment. The complexity of the total state is given by the volume of both green segments plus the volume of the red segment. We thus have that $C_L + C_R - C_T$ is given by the volume of the red segment, and as such is positive definite. We may identify the green segments with the basis complexity, and the red segment with the spectrum complexity, as per the discussion in section 3.3 of [1].

"double counting" mentioned in the above case does not apply. However, for these total states, we argued (see section 5.2.3) that the spectrum/basis decomposition of the subsystems is insufficient to parse total state complexity. In these cases, the behind-the-horizon region probed by the maximal slices

should roughly correspond to operators which mix degenerate subspaces and go unnoticed by either subsystem density matrix. See [136] for a recently proposed definition of a related quantity, the "binding complexity."

At this stage, one might be worried that we have ruined the upper bound of purification complexity by subregion complexity. However, our bound on purification complexity differs from subregion complexity by a term proportional to the area of the HRT surface (namely the volume between the true horizon and the stretched horizon), which could thus be thought of as an extra boundary term in the subregion complexity prescription. We will take the view that such a discrepancy likely should be corrected by altering the definition of subregion complexity in this way[10].

Such boundary terms could also be included for CV2.0, CA, and CA-2. In these cases, however, one does not automatically get subadditivity. For CV2.0 in particular, there will generally be a significant contribution to the total state complexity from behind the entanglement horizon which cannot be identified with either the spectrum or basis complexity (see figure 5.5). As suggested above for CV off of the $t = 0$ slice, this can perhaps be identified with the complexity in the total state due to gates acting within a degenerate eigenspace of the left and right density matrices, or even rotating the relative phase for a non-degenerate eigenspace. Discussions of this sort have occurred in [49], with proposals for decomposing a holographic spacetime into subregions

[10]We would like to thank Phuc Nguyen for suggesting including a boundary term in CV.

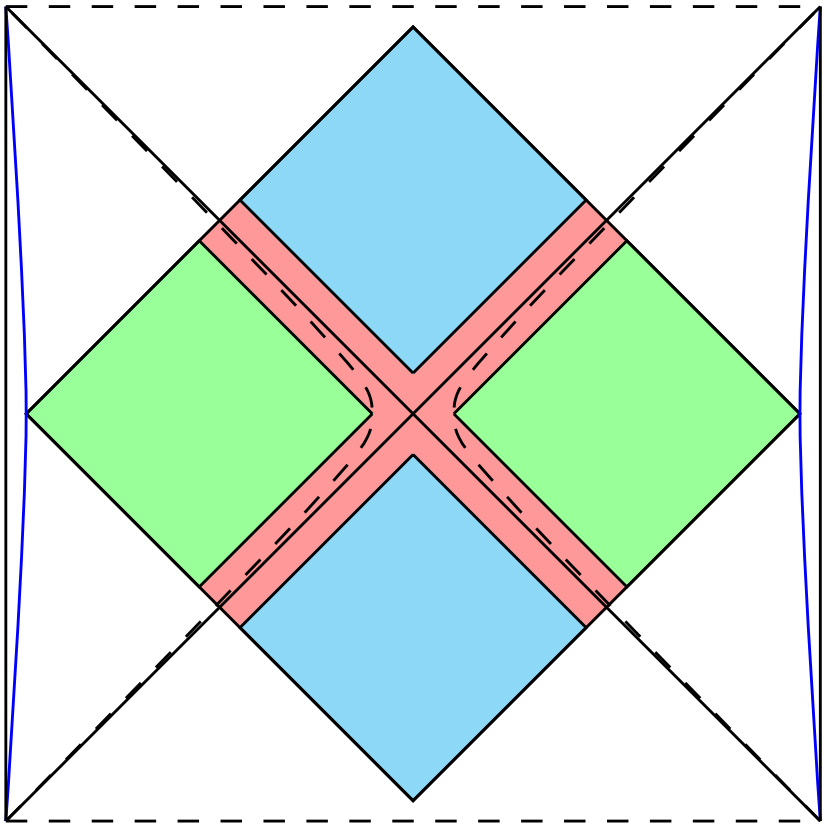

Figure 5.5: Similarly to CV, we may decompose the action in CA, CV2.0, or CA-2 by associating different parts of the WDW patch to the spectrum, basis, and degeneracy complexity. Roughly speaking, we suggest the green regions should correspond to the basis complexity, the blue regions to the degeneracy complexity, and the red to the spectrum complexity.

of particular significance for the quantity of "uncomplexity" (though those proposals did not strictly include a boundary term).

5.4 Superadditivity

It was noted in [1] that in CV, holographic subregion complexity obeys

$$C(\rho_{AB}) \geq C(\rho_A) + C(\rho_B). \tag{5.15}$$

when A and B partition a complete boundary Cauchy slice. Recently, a related property for "uncomplexity" was discussed in [132] for quantum systems. In this section we provide an independent discussion of this property, which we will call 'superadditivity.' We will give a proof that subregion complexity obeys this property for general subregions in CV, as well as in CV2.0, and discuss whether it may hold in CA.

Note that superadditivity implies that the subregion complexity of a given subregion must be less than or equal to the complexity of any of its holographic purifications. This will hold regardless of the cutoff imposed, as it is merely a statement about maximal volumes on Lorentzian manifolds with boundary. If we suppose (as is reasonable at leading order in $\frac{1}{N}$) that one need only consider holographic purifications, this result along with the discussion above is enough to guarantee the subregion complexity = purification complexity, provided one accepts complexity = volume or complexity = spacetime volume for geometries dual to pure states.

5.4.1 Maximal volumes of subregion wedges

Here we will give a proof of superadditivity of holographic subregion complexity in CV. Let w_X denote the entanglement wedge [137] of a given

boundary subregion X of a boundary time slice, and let Σ_X denote the maximal volume slice of w_X. By the maximal slice of w_X, we follow the proposal in [22], according to which we maximize over the volumes of slices anchored at both X and the HRT surface of this boundary subregion. Given non-overlapping subregions A and B on a Cauchy slice of the boundary, we have the inequality

$$\mathrm{Vol}(\Sigma_{AB}) \geq \mathrm{Vol}(\Sigma_A) + \mathrm{Vol}(\Sigma_B) \tag{5.16}$$

That this inequality is obeyed can be easily seen as follows: First, let us note that because A and B are non-overlapping, it is also true that w_A does not overlap w_B (see [128]). Now either Σ_A and Σ_B meet to form a spatial slice of w_{AB}, or there is a gap between them. An example of the first case is a two-sided black hole, with A and B taken to be the entire left and right boundary respectively (see figure 5.6 for an illustration). An example of the second case is two entanglement wedges in pure AdS, the union of which is not the whole bulk (see figure 5.7 for an illustration). In the case without a gap the inequality is immediate: Σ_{AB} is the *maximal* spatial slice over w_{AB}, so the slice formed by the union of Σ_A and Σ_B (whose volume is the sum of the individual volumes) must have a volume which does not exceed that of Σ_{AB}. In the case where there is a gap between Σ_A and Σ_B in w_{AB}, we may bridge this gap with a slice Σ_{bridge} of $w_{AB} - w_A - w_B$ which meets Σ_A and Σ_B at their boundaries. We will moreover require that Σ_{bridge} contains the HRT surface for AB. Then it is clear that the union of Σ_A, Σ_B, and Σ_{bridge} forms a Cauchy surface for w_{AB}.

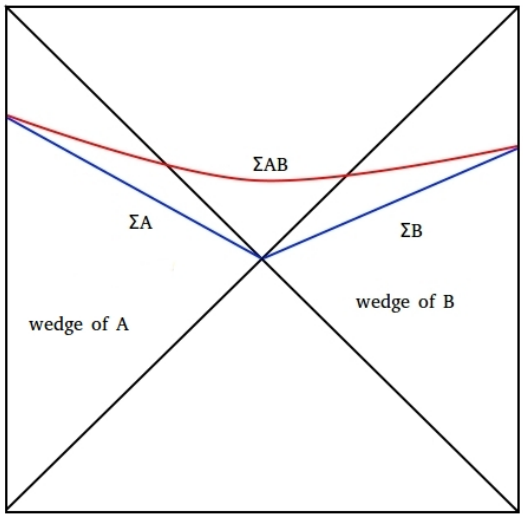

Figure 5.6: A slice through entanglement wedges who share an HRT surface, as in the case of a two-sided BH, or the wedges of two halves of the boundary of pure AdS.

But once again, since Σ_{AB} is maximal, we have that

$$\text{Vol}(\Sigma_{AB}) \geq \text{Vol}(\Sigma_A) + \text{Vol}(\Sigma_B) + \text{Vol}(\Sigma_{\text{bridge}}) \geq \text{Vol}(\Sigma_A) + \text{Vol}(\Sigma_B), \quad (5.17)$$

where the second inequality holds because volume is a non-negative quantity. This establishes the superadditivity property for maximal volumes of subregion wedges.

Notice that it is important to require that the bridge contains the HRT surface for AB. This is because the volume that computes the complexity is only maximal among Cauchy surfaces of the entanglement wedge, i.e. among surfaces anchored on this latter HRT surface (and also on AB). That Σ_{bridge} can be chosen in this way follows from the results in [138], according to which it is always possible to choose a spatial slice in the bulk containing simultaneous

the HRT surfaces for A, for B and for AB (assuming Einstein gravity together with the null energy condition).

5.4.2 CV 2.0

Superadditivity also holds for the spacetime volumes of Wheeler-DeWitt (WDW) patches, which has also been proposed as the dual quantity to state complexity in [4].

The super-additivity of WDW patch volumes follows trivially from the fact that given boundary regions A and B, the entanglement wedges w_A and w_B of these regions are both subsets of the entanglement wedge w_{AB} of the combined system. Hence, it is also true that the intersections of the WDW patch with w_A and w_B respectively are contained in the intersection with w_{AB}. Because spacetime volume is additive, this means the subregion complexity on A , B, and AB respectively, which are given by the volumes of the intersections of the WDW patch with w_A, w_B, and w_{AB}, obey inequality 5.15. This is illustrated for a two-sided black hole in figure 5.8, where region A is taken to be the whole left boundary and region B is likewise taken to be the right boundary. Then the subregion complexity of A is given by the spacetime volume of the region shaded in green, that of B by the spacetime volume of the region shaded in blue, and the complexity on AB is given by the spacetime volume of the whole WDW. The difference $\mathcal{C}_{AB} - \mathcal{C}_A - \mathcal{C}_B$ is thus given by the spacetime volume of the region shaded in red, which is clearly a positive definite quantity.

5.4.3 Additivity in CA?

Since we have not proved superadditivity in either CA or CA-2, it is natural to wonder under what conditions, if any, such a property holds for these conjectures. We do not pursue this question in depth here, but it is quick work to see that superadditivity is far from generic in either proposal. The spacetime regions considered under the complexity=spacetime volume proposal are identical to those considered in the action proposals, namely, the intersection of a region's entanglement wedge and the WDW patch of the boundary slice. The same nesting properties then hold here as in the previous section. However, the fact that volume and spacetime volume are positive-definite quantities led to the superadditivity conditions above. On the other hand, the bulk integral of the action is often negative. For instance the Einstein Hilbert term in pure AdS spacetimes gives a negative integrand ($R - 2\Lambda = \frac{-2(d-1)}{L^2}$ in d spacetime dimensions). There are also contributions from subregion boundaries and boundary intersections which may be of either sign. Some of these contributions have ambiguities which require stating a convention before the overall sign could be determined [74, 22, 1]. In the next section, we will look at specific instances where both subadditivity and superadditivity occur for the action.

5.5 Additional Purifications

In subsection 5.3.2 we argued that assuming the complexity=volume or complexity=spacetime volume prescription for pure states, then the corre-

sponding subregion prescription computes the purification complexity of the boundary mixed state, specifically minimizing complexity overall holographic purifications. The consistency conditions mentioned in 5.2.4 follow automatically for these proposals. Similar demonstrations for subregion action prescription are not forthcoming, so in this section, we put the action subregion prescription to the test holographically by considering what is perhaps the most canonical holographic mixed state, the thermal state dual to one size of a static eternal black hole.

5.5.1 Multisided Black Holes

In 2+1 spacetime dimensions, the entanglement wedge corresponding to the thermal mixed state under consideration amounts to one exterior region of a BTZ black hole. The most obvious purifying geometry is the two-sided eternal black hole solution, dual to the thermofield double state, and we will scrutinize this case more carefully in the next subsection. However, a much larger class of holographic purifying geometries exists, which we consider all together here: AdS_3 black holes with n sides and genus g. These geometries are an extension of the familiar BTZ black hole [40], obtained by quotienting pure AdS_3 by a discrete group of isometries, and they are studied in [139, 140, 141]. The states dual to these geometries were discussed in [142], and the entanglement structure was studied in [143]. The minimum complexity over all sides n and all genus g provides an upper bound on the purification complexity of the state on a single boundary.

The complexity of this family of black holes was computed for the $t_1 = t_2 = ... = t_n = 0$ spatial slice in [131] according to both the complexity = volume and complexity = action conjectures. The authors of that paper computed a quantity ΔC, which they defined as the difference in complexity between the solution of interest, and n copies of the one-sided $M = 0$ BTZ black hole. The results they found for an n sided black hole with a wormhole of genus g are

$$\Delta C_A = \tfrac{1}{6} c\chi \tag{5.18}$$

$$\Delta C_V = -\tfrac{4}{3}\pi c\chi \tag{5.19}$$

where $c = \frac{3L}{2G}$ is the central charge of the boundary CFT and $\chi = 2 - 2g - n$ is the Euler characteristic of the $t_1 = t_2 = ... = t_n = 0$ spatial slice. One immediate consequence of this result noted in [131], is that at any fixed n, ΔC_A decreases with increasing g. This already casts doubt on the idea that purification complexity should be identified with subregion complexity in CA, as for any value of the subregion complexity (which certainly does not depend on the genus, a property of the purification), we may find a genus such that the corresponding 2-sided purification has a lower complexity. This would seem to be a problem for 'complexity = action' generally, in so far as it implies the purification complexity of our state in CA is $-\infty$. The authors of [131] suggest that perhaps this merely indicates an upper bound on the allowed genus of such black holes. In order to remain consistent with purification complexity = subregion complexity, however, one would need an even stricter bound than

that implied by the positivity of complexity, or else our upper bound on the purification complexity will fall below the subregion complexity, the presumed true value.

By contrast, we see that for complexity = volume, increasing either the genus or the number of sides will only increase the complexity of the corresponding purification, and so our upper bound is provided by the ordinary BTZ case where $n = 2$ and $g = 0$. We see that in that case that χ vanishes, and so the total complexity is twice that of the $M = 0$ black hole (this calculation, of course, did not include any boundary term as suggested in section 5.3.3). On the other hand, due to the mass independence of the subregion complexity of one side of BTZ, the subregion complexity is identical to that of one side of the $M = 0$ black hole, and so for CV we have that our upper bound on purification complexity is still larger than the subregion complexity, consistent with the conjecture that purification complexity = subregion complexity in CV.

This comes as no surprise, as this result was guaranteed by superadditivity. Given any subregion A of any asymptotically AdS geometry, we may partition the total boundary into A and its complement. Then superadditivity of CV, along with the positivity of volume, guarantees us that the holographic complexity of the total state (as computed in CV) is greater than the subregion complexity of A (or equal to, in the limiting case where A is the full boundary). Thus, given a state ρ on a subregion A of a CFT, and all classical geometries dual to purifications of ρ, i.e. all geodesic completions of the entanglement wedge W of A which preserve W as the entanglement wedge of A,

we will always find that according to CV, our holographic estimation of the purification complexity of ρ is no greater than the subregion complexity of A.

Because the spacetime volume is also strictly positive, and because complexity according to CV2.0 is also superadditive, the same logic applies. Whether it applies to CA-2 in cases where it disagrees with CV2.0 is left to future work.

5.5.2 Two sided BTZ black hole: detailed treatment

Though the action results for the genus-g black hole solutions may cast doubt on the idea that subregion action is dual to purification complexity, they could alternatively be teaching us nontrivial information about limits on the genus which can be described holographically at a certain cutoff, or these solutions might be disallowed for some other unknown reason. With these possibilities in mind, we examine in more depth the standard case of a two-sided (genus zero) BTZ black hole. The metric is given by

$$ds^2 = \frac{L^2}{z^2}\left(-f(z)dt^2 + f(z)^{-1}dz^2 + L^2 d\theta\right)$$
$$f(z) = 1 - \left(\frac{z}{z_H}\right)^2$$

with $z \to 0$ representing the AdS boundary and z_H being the z coordinate of the horizon.

Subregion action calculations for this case were computed in [1], but we here report results which include an additional term[11] associated with null

[11] As this work was being prepared, we learned in private correspondence with the authors

boundaries required to make the action reparameterization invariant [74]. Utilizing this term, the on-shell action of the Wheeler-DeWitt patch depends on an undetermined lengthscale, which we denote $\tilde{L}$. We additionally allow the cutoff surfaces (of constant $z < z_H$) on right and left to vary independently as $z_{\text{L,min}} = \delta_L$ and $z_{\text{R,min}} = \delta_R$. We report the action result for the $t_L = t_R = 0$ slice here, abbreviating $\bar{L} = \tilde{L}/L$ where $L = L_{AdS}, \bar{\delta}_L = \delta_L/z_H$, and $\bar{\delta}_R = \delta_R/z_H$:

$$\frac{\mathcal{A}^T(\bar{\delta}_L, \bar{\delta}_R)}{16\pi G} = \frac{2L^2}{z_H}\left(-\frac{2\left(s_L s_R - 1\right)\log\left(\frac{4\bar{L}^2 s_L s_R}{(s_L s_R - 1)^2}\right)}{s_L s_R + 1} + \frac{\log\left(\left(1-\bar{\delta}_L^2\right)\bar{L}^2\right)}{\bar{\delta}_L} + \frac{\log\left(\left(1-\bar{\delta}_R^2\right)\bar{L}^2\right)}{\bar{\delta}_R}\right) \tag{5.20}$$

where $s_L = \sqrt{\frac{1+\bar{\delta}_L}{1-\bar{\delta}_L}}$ and $s_R = \sqrt{\frac{1+\bar{\delta}_R}{1-\bar{\delta}_R}}$. If the cutoffs are taken to be symmetric, this simplifies to

$$\frac{\mathcal{A}^T(\bar{\delta}, \bar{\delta})}{16\pi G} = \frac{4L^2}{z_H}\left(-\bar{\delta}\log\left(\bar{L}^2\left(\frac{1}{\bar{\delta}^2} - 1\right)\right) + \frac{1}{\bar{\delta}}\log\left(\bar{L}^2\left(1-\bar{\delta}^2\right)\right)\right) \tag{5.21}$$

The subregion action associated with either left or right side (restricted to the entanglement wedge[12]) is given by

$$\frac{\mathcal{A}^{L,R}(\bar{\delta})}{16\pi G} = \frac{2L^2}{z_H}\left(-\log\left(4\bar{L}^2\frac{(1-\bar{\delta})}{(1+\bar{\delta})}\right) + \frac{1}{\bar{\delta}}\log\left(\bar{L}^2\left(1-\bar{\delta}^2\right)\right)\right) \tag{5.22}$$

of [1] that they have also computed this term and will include it in work to appear soon.

[12]Joint contributions in the subregion action diverge if naively evaluated on the black hole horizon. We followed [1] by computing the action on an exterior region bounded by null surfaces just outside the future and past horizons and taking the limit that they coincide with the future and past horizons.

Comparing these results to expectations is complicated by the existence of the undetermined length scale $\tilde{L}$, which lacks a clear interpretation in relation to complexity in the boundary theory. Demanding that the complexity is a positive quantity in the strict UV limit ($\delta_L \to 0, \delta_R \to 0$) simply requires that we choose $\tilde{L} > L_{AdS} \implies \bar{L} > 1$. If the interpretations of section 5.3.2 are correct, however, and letting the cutoffs on both sides approach the horizon ($\delta \to z_H$ or $\bar{\delta} \to 1$) amounts to coarse-graining the state on both boundaries, then positive complexity should be imposed over the whole range of allowed cutoffs. We find that $\bar{L}$ greater than but of order 1 easily results in negative complexity as the cutoffs are pushed inward (away from $z = 0$). For $\bar{L} \gg 1$, both cutoffs must approach the horizon itself before there is a problem with negative complexity. For any choice of cutoffs, there is some $\bar{L}$ sufficiently large to avoid negative complexity. This is especially true if at least one cutoff remains in the deep UV (e.g., $\bar{\delta}_R \ll 1$).

If we ignore positivity requirements and allow any combination of fixed-z cutoffs, then we can find regions of subadditivity ($C_T < C_L + C_R$), as well as regions where the total state complexity is lower than one or the other of the subregion complexities ($C_T < C_L$ or $C_T < C_R$), which would violate the purification complexity interpretation of the corresponding subregion action. Neither of these properties occurs, however, if we restrict to regimes where the total state complexity as well as both subregion complexities are positive. See figure 5.9 for illustration of how requiring positivity excludes cases of subadditivity, for example.

To summarize the action results for this case, if we treat positivity as a strict condition for all complexities, then the choice of lengthscale $\tilde{L}/L_{AdS}$ can impose nontrivial restrictions on the allowable cutoff surfaces (especially for $\tilde{L}/L_{AdS}$ greater than but of order one). Over any combination of $\tilde{L}/L_{AdS}, \delta_L, \delta_R$ which gives positive complexities, we find that the total state complexity is always larger than either subsystem complexity, avoiding contradiction with the purification complexity = subregion action conjecture as could occur for the genus-g solutions of the previous section. In the parameter space consistent with positivity, the action behaves superadditively. As reviewed in section 5.2.3, this differs from the subadditivity expectation coming from the basis and spectrum decomposition utilized in [1]. The discussion of that section cast some doubt on the subadditivity expectation, but we nevertheless found it plausible. The mixed results of this section do not give any strict violation of the purification complexity interpretation of subregion action, but without a reason to expect superadditivity as the generic behavior for these states it remains a puzzle facing that interpretation. The significance of $\tilde{L}$ is an important piece in that puzzle.

If we consider instead the subregion volume prescription for the same spacetime decomposition, including the boundary term on the HRT surface suggested in 5.3.3), then at least our most immediate expectations follow naturally. All complexities are manifestly positive, and subadditivity is always obeyed on the $t_L = t_R = 0$ slice. The sum of the subregion complexities "double counts" the boundary term, which the total state slice effectively counts

only once. Because the boundary term is proportional to the area of the HRT surface (and therefore the entanglement entropy) and it does not vanish under any course graining, we loosely interpret it as the 'basis complexity' portion of the subregion complexity.

The volume prescription also incorporates the case we puzzled over after equation 5.11, where the total state happens to be exactly the minimal complexity purification of both subsystems, and we saturate the weak superadditivity limit $C_L + C_R = 2C_T$. This would not ordinarily occur for the thermofield double state unless it happened to be the minimally complex purification for both left and right factors. This can be realized as a limiting case, saturated by taking both cutoffs down to their limiting values around the HRT surface (equivalently, sending the volume portion to zero and leaving only the HRT boundary term, refer to figure 5.4). This could perhaps be thought of as effectively course grains the 'basis complexity' on both sides to zero and leaves only the spectrum part, necessary to maintain the entanglement structure and give a pure state.

5.5.3 Subregions of pure AdS_3

Finally, we will consider the reduced state on interval subregion of pure AdS. Actually, the subregion complexity of general subregions of AdS_3 was computed according to CV in [144]. It remains, however, to repeat that computation for CA, and to compute the purification complexity of such subregions, by considering all (or at least a large family of) geodesic completions

of the entanglement wedge. The state on any particular interval subregion in pure AdS_3 is related to the state on other interval subregions, whether of the global boundary or the Poincaré boundary, by boundary conformal transformations, and the entanglement wedge to which it is dual can be related to other entanglement wedges by bulk isometries. The entanglement wedge may also be isometrically mapped to an entanglement wedge of a subregion of the boundary of the BTZ black hole, or more generally to a subregion of a single side of the n sided genus g black hole. These transformations, however, will not, in general, preserve the cutoff, and so we must keep track of how the cutoff transforms under such transformations.

To begin with, we will consider an interval of length $2R$ along with a cutoff defined by constant Poincaré bulk coordinate z, namely, we will put a hard cutoff at $z = \delta$. The metric in this scenario is the familiar

$$ds^2 = \frac{L^2}{z^2}\left(-dt^2 + dx^2 + dz^2\right). \tag{5.23}$$

One purifying geometry is of course the entire Poincaré patch, the complexity of which can be computed to be (according to CA)

$$C = \frac{V_x L}{4\pi^2 \hbar G \delta}\left[\log\left(\frac{\tilde{L}}{\delta}\right) - 3\right] \tag{5.24}$$

where L is the AdS length scale and $\tilde{L}$ is an arbitrary length scale. Periodically identified Poincaré space, where we identify x with $x + a$, also provides a purifying geometry for our interval, provided the periodic identification does not change the RT surface. This requires that the length of our interval must

not be greater than half the length of the periodically identified boundary. One may see this as follows: Consider a region of length a on the Poincaré patch periodically identified as $x \sim x + R$. Clearly, for $\frac{a}{R}$ sufficiently small, the entanglement wedge of the region is the same as in the full Poincaré patch. How small though does $\frac{a}{R}$ need to be? In the periodically identified geometry, our interval from $x = 0$ to $x = a$ is homologous to the interval from $x = a$ to $x = R$. As a consequence, there are two surfaces competing to be the global minimum, one which lifts in the full Poincaré patch to the usual RT surface for the interval of interest, and one which lifts instead to the RT surface of the interval from $x = a$ to $x = R$. Clearly, the 'usual' RT surface wins out whenever $a < R - a$, i.e. when $\frac{a}{R} < \frac{1}{2}$. Because it is clear that the complexity of such a purification grows monotonically with R, the lowest complexity in this family will be given by $R = 2a$, right at the point of transition between the two minima. The complexity of this periodically identified geometry will be the same as for the non-identified case, but with the infinite transverse volume simply replaced by $2R$, yielding

$$C^P(R) \leq \frac{LR}{2\pi^2 \hbar G \delta} \left[\log\left(\frac{\tilde{L}}{\delta}\right) - 3 \right] \tag{5.25}$$

Notice now that if we scale all the coordinates, as well as the size of our region and our cutoff, by a uniform constant α, that is an isometry, such that the image of our original cutoff entanglement wedge is the new cutoff entanglement wedge (with the new cutoff). If one does this while holding $\tilde{L}$ fixed, one may, in fact, cause the complexity of the regulated complexity to

become negative. This may be avoided, however, if we scale $\tilde{L}$ along with the coordinates too, and the purification complexity bound found above is fixed under such rescalings.

We may also embed such regions as subregions of a single side of a BTZ black hole, or even to an entire side of a planar BTZ black hole (although the corresponding cutoff will not appear natural). To see this, first, consider that the entanglement wedge of an interval on the Poincaré patch may be mapped by a simple change of coordinates to one side of AdS-Rindler. By applying the map corresponding to our region of interest, we can get our entanglement wedge as one side of AdS-Rindler, and by considering a larger interval containing ours, we may get our interval as a subregion of the boundary of one side of AdS-Rindler. Notice that the AdS-Rindler metric may be written as

$$ds^2 = \frac{L^2}{z^2}\left[-f(z)dz^2 + \frac{dz^2}{f(z)} + L^2 d\chi^2\right] \tag{5.26}$$

where $f(z) = 1 - \frac{z^2}{L^2}$. This is exactly the same metric as the planar BTZ black hole with $z_h = L$. Replacing $f(z)$ by $f(z) = 1 - \frac{z^2}{z_h^2}$ then, we have AdS-Rindler when $z_h = L$, but the metric is invariant under scaling all the coordinates along with z_h (but not the AdS length scale L) by any constant α. The rescaling gives us an isometry between AdS-Rindler and a BTZ black hole of any temperature. Composing the two isometries we have found, we may then embed our regulated entanglement wedge either as a full side of a BTZ black hole or as the entanglement wedge of a subregion of a single boundary. We may also see that the entanglement wedge of our interval may be embedded into

BTZ by recalling that BTZ black holes (as a specific example of the n-sided genus g construction discussed above) may be obtained by a quotient of pure global AdS_3. Clearly then, any interval subregion of the boundary of AdS_3 may be mapped by a conformal transformation to an interval lying entirely inside a fundamental domain of our quotient space. Because such subregion lies entirely in a fundamental domain, that interval may be thought of as a subregion on the boundary of the quotient space. Either way, we may minimize the resulting embedding over a number of parameters, such as the size of the BTZ subregion or the BTZ temperature, but first, let us come back to the n sided genus g solutions discussed above. Clearly, for any embedding into a single side of a BTZ geometry, these also form a family of geodesic completions of the entanglement wedge of our interval. However, the conclusion from considering this family is no different from those we already saw for the BTZ thermal state. For CV and CV2.0, the complexity increases both with the number of sides n and the genus g. For CA, the complexity increases in n (at least for a sufficiently small choice of the cutoff), but decreases without bound with increasing g. This leads to the same problems as before and doesn't tell us anything particularly new.

5.6 Conclusion

In this paper, we have estimated the purification complexity of the reduced state on a boundary subregion holographically, by considering different geodesic completions of the dual entanglement wedge, and by considering

different cut-offs, corresponding to different course grainings of the purifying state. We have shown that according to CV and CV2.0, the optimal holographic purification is given by a geodesic completion of the entanglement wedge with a cutoff which skirts the HRT surface of the compliment of our region. As such, the minimum complexity among holographic purifications reproduces the usual subregion complexity (possibly up to an extra boundary term, as discussed in section 5.3.3). As such, we may conclude that at least to leading order in the $\frac{1}{N}$ expansion, subregion complexity = purification complexity if either CV or CV2.0 is correct for geometries dual to pure states.

For CA, we still find that the subregion complexity corresponds to the complexity of a particular holographic purification, though we have no guarantee that there is not some other purification of smaller complexity. In fact, we have several explicit examples in which what naively appears to be a holographic purification is found to have a smaller complexity than the subregion complexity in question, and even that the complexity can become negative. From this we must choose from the following conclusions, namely that these combinations of geometry and cutoff are not genuinely holographic (i.e., they are not dual to some state in a boundary CFT), that the complexity = action conjecture is simply wrong, or that the complexity = action is a special case of a more general conjecture, so that in these cases CA does not apply and we must use the generalization. As an example of the last situation, one might imagine adding a term which depends explicitly on the Euler characteristic in order to 'fix' CA in case of arbitrary behind the horizon genus.

These results are in some tension with those found in [1]. In the case of CV, this tension is not so strong. While it is true that CV is superadditive (as the authors of that paper had pointed out), we argue that in most circumstances this is to be expected due to the existence of operations which can raise the complexity of a pure state while going unnoticed by the density matrices arising from a decomposition into subsystems. In the particular case that preparing the total state does not require any such operations (as may be the case for the $t_L = 0, t_R = 0$ thermofield double state decomposed on right and left factors), then subadditivity can be realized modifying the prescription for subregion complexity in CV by adding the boundary term discussed in 5.3.3. Once this modification is made, the arguments made in [1] that subregion complexity in CA matches purification complexity applies equally well to CV. For CA, the tension is perhaps stronger, though it mostly arises from cases not considered by those authors.

5.7 Acknowledgments

We would like to thank Cesar Agón, Adam Brown, Shira Chapman, Matt Headrick, Ted Jacobson, Phuc Nguyen, Eliezer Rabinovici, Henry Stoltenberg, and Brian Swingle for useful discussions and feedback. In particular, part of this paper grew out of earlier work with Ted Jacobson and Phuc Nguyen. JC and SE would like to thank IAS for their hospitality during PITP 2018 and for thought-provoking talks and conversation. This work was supported by NSF grants PHY-1620610 and PHY-1820712.

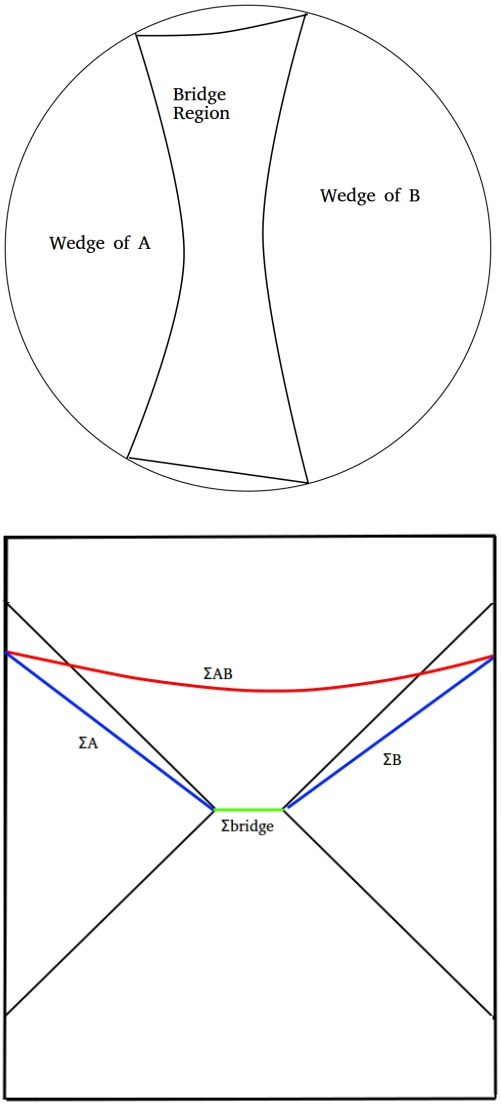

Figure 5.7: On the left is a spatial slice showing the wedge of a region A, the wedge of a region B, and a 'bridge region.' Here there is clearly a gap between a spatial slice on the A wedge and a spatial slice in the B wedge, as shown in the cross-section on the right. We can however always bridge this gap by an arbitrary spatial slice of the bridge region which meets the slices associated to A and B respectively at their boundaries

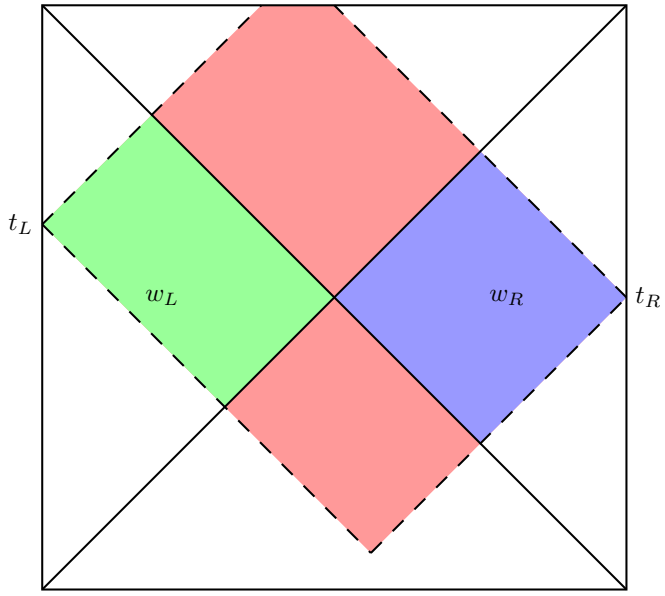

Figure 5.8: The WDW patch for a two-sided black hole, outlined with dashed lines. If we consider subregion A to be the left boundary and subregion B to be the right boundary, then the entire outside of the horizon on the left side, w_L, is the entanglement wedge of A, and likewise for the right side and B. The entanglement wedge of AB is the whole spacetime.

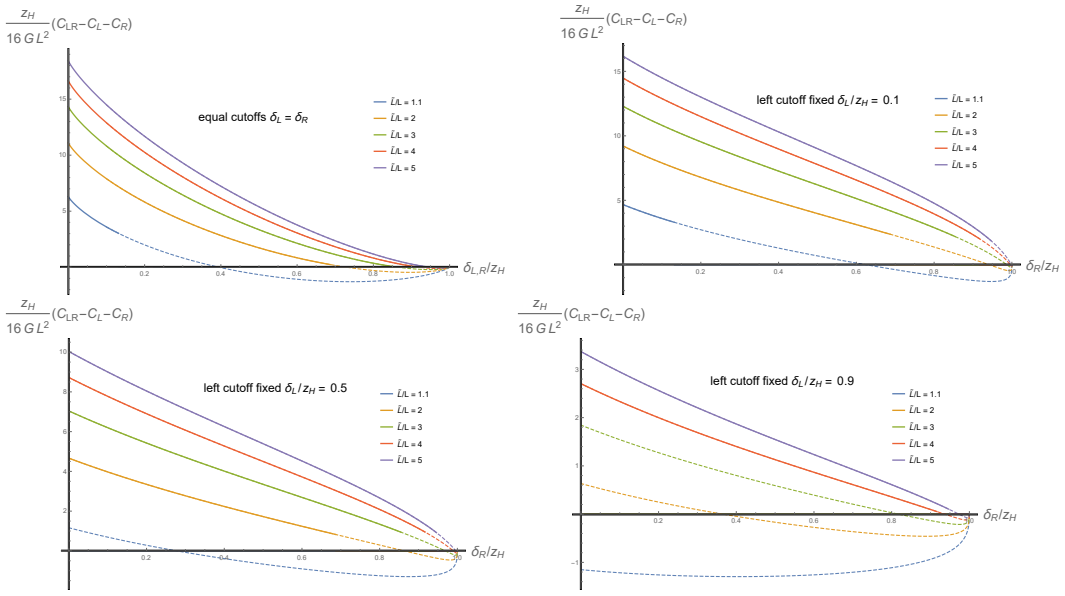

Figure 5.9: The above plots show the difference between the total state complexity $C_T = C_{LR}$ and the sum of left and right subregion complexities $C_L + C_R$ for the BTZ black hole at $t_L = t_R = 0$, computed using the complexity=action prescription. Positive values indicate that the left and right factors behave superadditively, and negative indicates subadditivity. The cutoffs are constant z surfaces $z_R = \delta_R$, $z_L = \delta_L$ and various choices of $\tilde{L}/L_{AdS}$ are displayed. Positivity in the strict UV limit ($\delta_L \to 0$ and $\delta_R \to 0$) requires that the lengthscale $\tilde{L}$ be chosen greater than L_{AdS}, so only such lines are displayed. The dashed portions of each line are excluded if we demand positivity of the total state complexity as well as both subregion complexities at the corresponding cutoffs. We find that in the remaining parameter space the system always behaves superadditively: $C_T > C_L + C_R$.

Appendices

Appendix A

Holographic Complexity and Volume

A.1 Boundary foliation induces maximal bulk foliation

We advertised in Section 2.3 that a foliation of the boundary of AdS induces a foliation by globally maximal volume slices in the bulk (assuming there exists such a slice terminating on each boundary slice). To establish this, we first show that, if two boundary slices do not intersect, then the corresponding bulk maximal slices[1] do not intersect. Next we argue that the (nonintersecting) bulk slices fail to be a foliation only if there are two distinct maximal slices anchored at the same boundary slice, and we prove, assuming the strong energy condition and the Einstein equation, that this cannot happen. In order to deal with finite volumes, we take the boundary to lie at a finite cutoff surface, which can be taken to infinity at the end.

The argument works by contradiction. Suppose the maximal slice anchored at the upper boundary slice dips down sufficiently low in the bulk that it intersects the maximal slice anchored at the lower boundary slice (see Figure A.1). Then we can write one maximal slice as the union of components a and b, and the other maximal slice as the union of components c and d

[1] In this appendix, "maximal" will always by default mean "globally maximal".

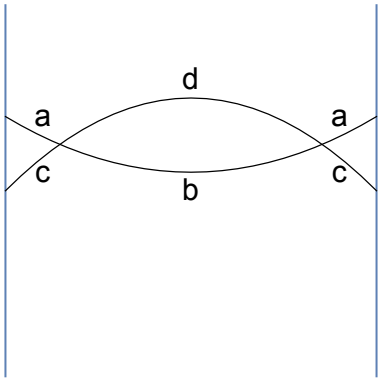

Figure A.1: Hypothetical situation where two maximal slices anchored on different boundary Cauchy slice intersect.

as in the figure. If $\mathrm{Vol}(b) < \mathrm{Vol}(d)$, then $\mathrm{Vol}(ab) < \mathrm{Vol}(ad)$, contradicting the maximality of the (ab) slice. If $\mathrm{Vol}(d) < \mathrm{Vol}(b)$, then $\mathrm{Vol}(cd) < \mathrm{Vol}(bc)$, contradicting the maximality of the (cd) slice. The only possibility remaining is $\mathrm{Vol}(b) = \mathrm{Vol}(d)$. If that is the case, then (ad) and (bc) would also have to be maximal slices. But they cannot be maximal, since they have corners, and by rounding off the corners their volume can be increased. If the slices are tangent, rather than intersecting transversally, this "rounding the corners" argument is not applicable, but by moving the boundary slices slightly closer together, one would expect that the tangency generically becomes a transversal intersection, which would be ruled out by the argument already given.[2] Although not quite a rigorous argument, this seems adequate for our present

[2]This argument is essentially an adaptation to Lorentzian signature of a similar argument presented in [138, 145] for Euclidean signature in the context of holographic entanglement entropy, establishing the property of "entanglement wedge nesting" on a static slice.

purposes.

Now if the bulk maximal slices do not intersect, then the boundary foliation will induce a bulk foliation unless there are gaps where the family of maximal volume slices jumps discontinuously across some spacetime region. Since the metric is assumed continuous, however, the maximal volume function itself cannot jump discontinuously as the boundary slice is pushed toward the future. Hence, if a gap does occur there must be two maximal slices with the same volume, anchored at the same boundary slice. We now argue that this cannot happen, given a causality assumption, the Einstein equation, and the strong energy condition. In fact, the argument will establish a stronger result: there cannot be two extremal bulk slices with the same boundary.

Suppose there are two such slices, Σ_1 and Σ_2, with Σ_2 to the future of Σ_1, with the same, co-dimension-2 boundary, and both with $\mathrm{Tr}K = 0$. While the domains of dependence $\mathcal{D}_1$ and $\mathcal{D}_2$ of Σ_1 and Σ_2 are each automatically globally hyperbolic, we need to assume that $\Sigma_2 \subset \mathcal{D}_1$ and $\Sigma_1 \subset \mathcal{D}_2$, which amounts to assuming that the domains of dependence coincide, $\mathcal{D}_1 = \mathcal{D}_2$. This condition "obviously" holds for "normal" causal structures. Under this causality assumption, we can invoke Theorems 9.4.3 and 9.4.5 and Lemma 8.3.8 of Ref.[42] to infer that every point p on Σ_2 lies on a geodesic that maximizes the proper time from p to Σ_1, meets Σ_1 orthogonally, and has no conjugate points between p and Σ_1. The congruence of these geodesics maps (possibly a subset of) Σ_1 onto all of Σ_2. The expansion θ of the congruence at Σ_1 is equal to $\mathrm{Tr}K$, which vanishes by assumption. The Raychaudhuri equation together

with the timelike convergence condition or, assuming the Einstein equation, the strong energy condition, then implies that θ is decreasing everywhere along the congruence.[3] Moreover, θ cannot go through $-\infty$ before reaching Σ_2 since, as stated above, the time-maximizing curve has no conjugate points between p and Σ_1. It follows that θ is negative everywhere, which implies that the geodesic flow is volume-decreasing. That is, the volume of a small ball carried along by the flow will *decrease*, as measured in the local rest frame of the flow. Furthermore, since the geodesics do not generally meet Σ_2 orthogonally, the volume of a small patch of Σ_2 on which the flow lands will be *less* than the volume of the small ball carried by the flow. It follows that the volume of Σ_2 is less than the volume of the pre-image of Σ_2 in Σ_1 under this flow, and *a fortiori* the volume of Σ_2 is less than that of Σ_1. Similarly, we can argue the opposite, and thus we reach a contradiction, since the volume of Σ_2 cannot be both less than and greater than that of Σ_1. The initial assumption is therefore false: there cannot be two extremal slices with the same boundary. Together with the previous results, this implies that a boundary foliation determines a maximal bulk foliation without gaps. Note that the latter need not completely cover the bulk, however. For example, as discussed in the text, the maximal slices for a two-sided black hole do not extend beyond a final slice, located inside the event horizon.

We established the uniqueness property of extremal slices with a given

[3]Strictly speaking, we need here to assume the generic condition, that $R_{ab}u^a u^b \neq 0$ somewhere along each geodesic, where u^a is the geodesic tangent. In the case with a (negative) cosmological constant, this is automatic.

boundary using a global argument in which the existence of time maximizing curves without conjugate points played a key role. However, it was briefly mentioned by Witten, in a conference talk [146], that uniqueness can be proved in a different fashion, namely, by (i) showing that the volume of any extremal slice is a local maximum with respect to small deformations, and (ii) arguing that if there were two local maxima, there would necessarily also be a saddle point of the volume, contradicting the fact that all extremal slices are local maxima of the volume. The reasoning for point (i) is simple and local: the expansion of the congruence of timelike geodesics orthogonal to any extremal slice starts out zero at the slice, and the strong energy condition (together with the Einstein equation) implies that it is negative and decreasing off the slice. The transversal spatial volume therefore decreases along the congruence, and non-orthogonality of the congruence to the deformed slice implies that the latter has even smaller volume, so the extremal slice is a local maximum of volume. The reasoning for (ii), the existence of the saddle point, was not as explicit in the talk, but it was pointed out in a picture that there would necessarily be a local minimum along some one-parameter family of slices joining them. This is of course a necessary condition for the existence of a saddle point, but it is not clear to us that a saddle point is guaranteed to exist.

We end this appendix with an example where the strong energy condition does *not* hold, and consequently there can be more than one extremal hypersurface with the same boundary, and the extremal slices are *not* local

maxima of volume: de Sitter spacetime. The constant time slices of a static patch of de Sitter spacetime are all anchored at the same location on the boundary of the patch, all are extremal, and all have the same volume. To visualize this, consider the two dimensional de Sitter hyperboloid embedded in three dimensional Minkowski spacetime. The constant-time slices of the static patch are equatorial semicircles on the de Sitter hyperboloid, and are related to one another by Lorentz boosts in the embedding spacetime.

A.2 Techniques to evaluate the maximal volume

In this appendix, we demonstrate the use of the flux picture of complexification as a technical tool for explicit computation. The techniques presented here complement existing studies in the literature such as [21], where the maximal volume was computed by maximizing the volume functional directly. In subsection (A.2.1), we evaluate the volume flux for the BTZ black hole. In subsection (A.2.2), we present a variation of this technique when the cutoff is null, in which case the flux density is given by the lapse function.

A.2.1 Direct evaluation of flux

In this appendix, we present the derivation of the volume current and the volume flux for the BTZ black hole. The boundary foliation is the symmetrical one $t_L = t_R$.

Let us start with the BTZ black hole. We work in (r, v) coordinates,

which are regular across the horizon:

$$ds^2 = -f(r)dv^2 + 2dvdr + r^2 d\phi^2 \tag{A.1}$$

$$f(r) = \frac{r^2 - r_+^2}{L^2} \tag{A.2}$$

The function $v(r)$ describing the shape of the maximal slices was essentially worked out in [21]. Its derivative is given by:

$$\frac{dv}{dr} = \frac{\sqrt{f(r)r^2 + C^2} - C}{f(r)\sqrt{f(r)r^2 + C^2}} \tag{A.3}$$

where C is a positive constant.[4] The constant C labels the particular maximal slice in the foliation, and it ranges from 0 (for the slice anchored at $t_L = t_R = 0$) to $r_+^2/2L$ (for the final slice).[5] The unit normal 1-form to the slice labeled by C is:

$$n_\mu dx^\mu = -\sqrt{f + \frac{C^2}{r^2}}dt - \frac{C}{rf}dr \tag{A.4}$$

To get the volume current v^μ, we glue together the unit normal to all the slices labeled by different values of C. This amounts to promoting C to the function of v and r implicitly given by integrating (A.3) from the midpoint (also called the "throat" in the numerical relativity literature) outward:

$$v = -\frac{1}{r_+}\text{arctanh}\left(\frac{r_C}{r_+}\right) + \int_{r_C}^{r} \frac{\sqrt{f(x)x^2 + C^2} - C}{f(x)\sqrt{f(x)x^2 + C^2}}dx \tag{A.5}$$

[4] C is the negative of the "energy" E in [21]. From the viewpoint of that paper, the constant C arises as a "conserved quantity" associated with the v-independence of the volume functional.

[5] To see this, note that $\frac{dv}{dr} = \frac{1}{f}$ on the slice $t_L = t_R = 0$ (since this slice is at $t = 0$). As for the final slice, symmetry dictates that it is a slice of constant r, and $\frac{dv}{dr}$ diverges. Both of these facts are verified by plugging in $C = 0$ and $C = \frac{r_+^2}{2L}$ respectively.

The first term on the right-hand side is the tortoise coordinate of the throat, and r_C is the radius of the throat given by:

$$r_C = \sqrt{\frac{1}{2}(r_+^2 + \sqrt{r_+^4 - 4C^2L^2})} \tag{A.6}$$

The two equations above define $C(r, v)$. We then find the volume current:

$$v^\mu \partial_\mu = \frac{1}{f(r)} \left(\sqrt{f(r) + \frac{C(r,v)^2}{r^2}} - \frac{C(r,v)}{r} \right) \partial_v - \frac{C(r,v)}{r} \partial_r \tag{A.7}$$

It can be checked that both components of v^μ are regular at the horizon. The volume element is $\epsilon = r dv \wedge dr \wedge d\phi$. Computing the interior product $v \cdot \epsilon$ and restricting to the cutoff at constant $r = r_c$ yields:

$$v \cdot \epsilon \Big|_{r_c} = C(r_c, v) dv \wedge d\phi \tag{A.8}$$

Note that r_c is allowed to be the horizon since our formalism can handle null surfaces. Evaluating the flux, we then find the change in the volume between v_1 and v_2 to be:

$$\Delta V = 2\pi \int_{v_1}^{v_2} C(r_c, v) dv \tag{A.9}$$

In the usual near-boundary cutoff $r_c \to \infty$, the v coordinates becomes the boundary time coordinate t and the function $C(r_c, v)$ is nothing but the flux density, or the complexification rate. The main lesson from this computation is that the flux density coincides with a certain time function C for the maximal slicing.

We also note that it is possible to work with Schwarzschild coordinates (r, t) instead of (r, v), despite the coordinate singularity at the horizon. In

Schwarzschild coordinates, the shape of the maximal slice reads:

$$t = -\int_{r_C}^{r} \frac{C}{f(x)\sqrt{f(x)x^2 + C^2}} dx \tag{A.10}$$

To integrate across the horizon, we should understand the integral above in the sense of the Cauchy principal value [147]. In fact, the plot (2.3) of the volume flow was generated by working in Schwarzschild coordinates and using the Cauchy principal value to continue the maximal slice across the horizon.

Finally, it might appear surprising that the flux of the volume flow yields a finite answer when the cutoff is taken to the boundary, especially if we think about the flow direction near the boundary. The maximal slice should become tangential to the constant Killing time slices near the boundary, and since the volume current is orthogonal to the maximal slices, it may seem that the volume flux across a constant-r cutoff is zero as $r \to \infty$. That this is not the case can be understood as follows: at a finite but large cutoff in the bulk, the flow direction has a small component not orthogonal to the constant Killing time slice. As the cutoff is sent to the boundary, this small component tends to zero, but the volume element on the cutoff also diverges in the same time. This divergence cancels the vanishing of the subleading component in a way to yield a finite answer.

A.2.2 Flux across a null surface

In this appendix, we elaborate on the particular case of the volume flux across a null surface, and relate this flux to the lapse function for a time

function τ defining the maximal foliation. Recall that to a time function τ we can associate a *lapse function* N defined by:

$$n = N d\tau \tag{A.11}$$

where n is the unit normal 1-form to a constant τ slice, with sign chosen so that $N > 0$. Since the volume current vector v is the unit normal vector to the maximal slices, we have $v \cdot n = 1$. Now let k be the null normal 1-form to the horizon, normalized so that $v \cdot k = 1$, and let $\mathcal{A}$ be the area form of the intersection of the maximal slice with the horizon, so that $\epsilon = k \wedge n \wedge \mathcal{A}$. The volume current is then $v \cdot \epsilon = n \wedge \mathcal{A} - k \wedge A$, whose pullback to the null surface is $n \wedge A = N d\tau \wedge \mathcal{A}$, since the pullback of k vanishes. The 2-form $N\mathcal{A}$ thus serves as the volume flux density.

This fact can be seen more geometrically as depicted in Figure (A.2). We pick two slices in the foliation labelled by τ and $\tau + \Delta\tau$, with $\Delta\tau$ small. Let A be the intersection between slice τ and the horizon, and let C be the intersection between slice $\tau + \Delta\tau$ and the horizon. Moreover, consider a volume flow worldline passing through A, and let B be the intersection of that worldline with the slice $\tau + \Delta\tau$. Since $\Delta\tau$ is infinitesimal, the geometry of the triangle ABC is like in flat space. Since AB is orthogonal to BC, we conclude that $AB = BC$, where AB denotes the proper time elapsed along the worldline between A and B, and BC denotes the proper length of the segment of the slice $\tau + \Delta\tau$ between B and C.

Now consider the increment in the volume ΔVol between τ to $\tau + \Delta\tau$.

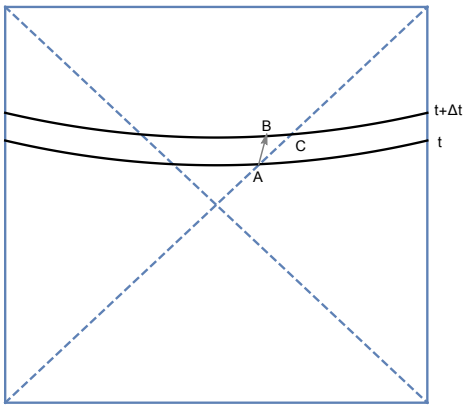

Figure A.2: Illustration of the derivation of (A.13).

We have $\Delta\text{Vol} = 4\pi r_+^2 BC = 4\pi r_+^2 AB$, where we work in 3+1 dimensions for concreteness, and in the second equality we used the relation derived in the previous paragraph. (There is also an identical contribution from the left-side of the Penrose diagram, which we ignored.) On the other hand, we have $AB = N(A)\Delta\tau$. Thus, we can relate the volume increment to the lapse as follows:

$$\Delta\text{Vol} = 4\pi r_+^2 N(A)\Delta\tau. \tag{A.12}$$

For a finite time difference, we integrate the lapse:

$$\Delta\text{Vol} = 4\pi r_+^2 \int_{\mathcal{H}} N d\tau. \tag{A.13}$$

This is the formula we are after: the volume flux across the horizon is also the integral of the lapse along the horizon. In other words, the lapse on the horizon serves as the volume flux density.

A.3 Stationarity of maximal foliation and volume flow in the late-time regime

In this appendix, we focus on the AdS-Schwarzschild in 3+1 dimensions, and explicitly check that the maximal foliation and volume flow are stationary at late times. To do this, we first write the Schwarzschild-AdS black hole in the "maximal slicing" gauge:

$$ds^2 = -\alpha^2 d\tau^2 + \gamma^2 (dr + \beta d\tau)^2 + r^2 d\Omega_2^2, \tag{A.14}$$

in which the slices of constant τ are the left-right symmetric maximal slices that asymptote to constant Schwarzschild time slices at the two boundaries. The radial coordinate r and the angles θ and ϕ on the sphere can be chosen to be the same as the usual Schwarzschild coordinates. The functions α, β and γ are functions of τ and r, given by:

$$\gamma^{-2} = 1 - \frac{2M}{r} + \frac{C(\tau)^2}{r^4} - \frac{\Lambda}{3} r^2 \tag{A.15}$$

$$\alpha = \gamma^{-1} \left[1 + C_{,\tau} \int_r^\infty \frac{\gamma^3(\tau, r')}{r'^2} dr' \right] \tag{A.16}$$

$$\beta = \frac{\alpha C(\tau)}{r^2} \tag{A.17}$$

for some function $C(\tau)$. To derive equations (A.15), (A.16) and (A.17), we can, for example, feed the metric (A.14) into Einstein's equation. Analogous calculations for black holes in flat space have been done in the numerical relativity literature (see for example [147]). In writing (A.16) we have imposed the boundary condition $\alpha\gamma \to 1$ as $r \to \infty$, so that τ will agree asymptotically with the standard AdS global time coordinate.

The function $C(\tau)$ is determined by regularity of the maximal slice at the "middle". According to (A.14), the metric induced on the maximal slice is $\gamma^2 dr^2 + r^2 d\Omega_2^2$, so in particular γdr is a unit 1-form on the slice. Since r reaches a minimum at the middle of each slice, the pullback of dr to the slice vanishes at the middle, so γ must diverge there. This implies

$$C^2 = 2Mr_m^3 - r_m^4 + \frac{\Lambda}{3} r_m^6, \tag{A.18}$$

where $r_m = r_m(\tau)$ is the r coordinate at the middle of each constant τ slice. In the late time limit, $r_m(\tau)$ approaches a constant, namely r_f, the radial coordinate of the "final slice". Therefore $C(\tau)$ too approaches a constant. It follows that the metric functions α, β, and γ all become constant in the late τ limit, which implies that the coordinate vector field ∂_τ approaches the Schwarzschild time Killing field. The unit normal 1-form $\alpha d\tau$ therefore becomes invariant under the Killing flow, as does the volume current

$$v = \alpha^{-1}(\partial_\tau - \beta \partial_r), \tag{A.19}$$

which is minus the contravariant form of $\alpha d\tau$.

A.4 Maximal slices in Vaidya: a closer look

Consider a maximal slice anchored at boundary time t_b in the double shell Vaidya/AdS spacetime in $2+1$ dimensions, (2.20), (2.25)). For $t_b < 0$, the slice stays entirely inside the AdS part of the geometry and is given by a constant t slice (where t denotes the global time in AdS). When $0 < t_b < b$,

the slice crosses the first shell and has two portions, one in the AdS region (still a constant t slice) and one outside the shell. The volume functional for the part outside the shell reads:

$$\text{Vol} = 2\pi \int r\sqrt{2r' - f}dv \tag{A.20}$$

where we write the slice as a function $r(v)$. Since the functional is independent of v, we have a conserved energy:

$$E = r'\frac{\partial L}{\partial r'} - L = \frac{r(f - r')}{\sqrt{2r' - f}} \tag{A.21}$$

Similarly, there is a conserved energy in the AdS region, which can be shown to vanish by smoothness at the center ($r = 0$). The maximal slices consist of locally maximal slices apart from on the shells, where they satisfy a Weierstrass-Erdmann corner condition [148]. Since the shells are located at a constant value of v, the corner condition simplifies to the requirement that the "conjugate momentum"

$$p_r = \frac{\partial L}{\partial r'} = \frac{r}{\sqrt{2r' - f}} \tag{A.22}$$

be continuous across the junction, which amounts to requiring that the jump in r' is $1/2$ the jump in f. Together with the fact that the portion of the maximal slice in the AdS region must be constant global time slice, this determines the derivative of $r(v)$ at the junction on the BTZ side:

$$\left.\frac{dr}{dv}\right|_{r_{1,+}} = 1 + r_1^2 - \frac{a}{2}(1 + r_+^2) \tag{A.23}$$

where r_1 is the r-coordinate of this junction, and $r_{1,+}$ means an r value slightly larger. Similarly, for $t_b > b$, the maximal slice crosses both shells and the junction condition has to be imposed at each junction. At the outer junction, located at $r = r_2$, the discontinuity of the derivative of $r(v)$ is found to be:

$$\left.\frac{dr}{dv}\right|_{r_{2,-}} - \left.\frac{dr}{dv}\right|_{r_{2,+}} = \frac{1-a}{2}(1+r_+^2). \tag{A.24}$$

Appendix B

Holographic Complexity and Noncommutative Gauge Theory

B.1 Calculation of $\dot{S}_{WDW}$

To minimize clutter in expressions, in this appendix we set $2\kappa^2 = (2\pi)^7\alpha^4 = 1$ and reinstate κ dependence only at the end. Following the systematic treatment of [74], the action on a bulk subregion is divided into contributions as follows:

$$\begin{aligned} S_{\mathcal{V}} = &\int_{\mathcal{V}} \big(\mathcal{R} + \mathcal{L}_m\big)\sqrt{-g}dV \\ &+ 2\Sigma_{T_i}\int_{\partial\mathcal{V}_{T_i}} K d\Sigma + 2\Sigma_{S_i}\text{sign}(S_i)\int_{\partial\mathcal{V}_{S_i}} K d\Sigma - 2\Sigma_{N_i}\text{sign}(N_i)\int_{\partial\mathcal{V}_{N_i}} \kappa d\sigma d\lambda \\ &+ 2\Sigma_{j_i}\text{sign}(j_i)\int_{B_{j_i}} \eta_{j_i} d\sigma + 2\Sigma_{m_i}\text{sign}(m_i)\int_{B_{m_i}} a_{m_i} d\sigma \end{aligned} \tag{B.1}$$

The first line we call the bulk contribution. The second line contains boundary contributions along timelike ($\mathcal{T}$), spacelike ($\mathcal{S}$), and null boundaries ($\mathcal{N}$), respectively. The final line contains joint contributions, divided into those which result from intersections of timelike and/or spacelike boundaries, and those which include one or more null boundaries. Sign conventions and notation for integrand quantities will be explained as needed in what follows.

While the action on a WDW patch is obviously of interest for its conjectured relation to Quantum Complexity, its time derivative is simpler to compute and interesting for diagnostic purposes. Due to the spacetime symmetries, this quantity reduces to the difference of two volume contributions ($\mathcal{V}_1$ and $\mathcal{V}_2$ in figure 3.1), one boundary surface contribution ($\mathcal{S}_\epsilon$ in figure 3.1), and two joint contributions (B_1 and B_2 in figure 3.1).

$$\begin{aligned}
\delta S_{\text{WDW}} &= \delta S_{\text{bulk}} + \delta S_{\text{boundary}} + \delta S_{\text{joints}} \\
\delta S_{\text{bulk}} &= S_{\mathcal{V}_1} - S_{\mathcal{V}_2} \\
\delta S_{\text{boundary}} &= -2\int_{\mathcal{S}_\epsilon} K d\Sigma \\
\delta S_{\text{joints}} &= 2\int_{B_1} a_1 d\sigma - 2\int_{B_2} a_2 d\sigma
\end{aligned} \tag{B.2}$$

B.1.1 Bulk Contribution

The bulk integral contributions are of the form:

$$S_{\text{bulk}} = \int_{\mathcal{V}} \sqrt{-g_E}\big(\mathcal{R} + \mathcal{L}_m\big) d\mathcal{V}, \tag{B.3}$$

where Einstein frame metric is used. For the action eq(3.7) and field content eq(3.3) we have

$$\mathcal{R} = \frac{-2\sqrt{\hat{g}_s}\big(2a^4 r_H^4 + a^8 r^4 (r^4 + r_H^4)\big)}{\alpha' R^2 (1 + a^4 r^4)^{9/4}}, \tag{B.4}$$

$$\mathcal{L}_m = \frac{2\sqrt{\hat{g}_s}\big(4a^4 r_H^4 + a^8 r^4 (3r^4 + r_H^4)\big)}{\alpha' R^2 (1 + a^4 r^4)^{9/4}}. \tag{B.5}$$

We let the integral over x_1, x_2, and x_3 give V_3 and the five-sphere Ω_5. Also abbreviate $C = \dfrac{\alpha'^4 \Omega_5 V_3}{\hat{g}_s^2}$. Further let $\rho(u,v)$ and $\bar{\rho}(u,v)$ denote the radial

value r as implicit functions of advanced/retarded coordinates u and v from the appropriate quadrant (here the left and bottom quadrants, respectively). The form of these functions is not important here.

The bulk contribution for $\mathcal{V}_1$ can be written in (u, r) coordinates with radial limits expressed implicitly.

$$S_{\mathcal{V}_1} = C \int_{u_L}^{u_L+\delta t} du \int_{r=\epsilon}^{r=\rho_L(u-v_L)} dr \frac{4r^3(a^8r^8 + a^4r_H^4)}{(1+a^4r^4)^2}, \tag{B.6}$$

Here $r = \epsilon$ is a surface close to the singularity which will be sent to zero. A similar expression can be written for $\mathcal{V}_2$ in (v, r) coordinates, and after the radial integration we have:

$$\frac{1}{C}(S_{\mathcal{V}_1} - S_{\mathcal{V}_2}) = \int_{u_L}^{u_L+\delta t} du \big(G(\rho_L(u-(v_L+\delta t))) - G(\epsilon)\big) - \int_{v_L}^{v_L+\delta t} dv \big(G(\rho_L(u_L - v))) - G(\bar{\rho}(u_R, v))\big) \tag{B.7}$$

Changing variables $u \to u_L + v_L - v + \delta t$ leads to a cancellation of terms such that for small δt we are left with

$$\begin{aligned} S_{\mathcal{V}_1} - S_{\mathcal{V}_2} &\approx C\bigg(G\big(\bar{\rho}(u_R, v_L) = r_B\big) - G\big(\epsilon\big)\bigg)\delta t, \\ G(r) &= \frac{a^4(2r^4 + a^4L^8 - r_H^4) - 2(1+a^4r^4)\log(1+a^4r^4)}{(a^4 + a^8r^4)}. \end{aligned} \tag{B.8}$$

This cancellation is expected from the boost symmetry of the left wedge of the spacetime, and also indicates the cutoff independence of our calculation. We

denote the radial value at the bottom corner of the WDW patch $\bar{\rho}(u_R, v_L) \equiv r_B$. As $\epsilon \to 0$ we find a bulk contribution of

$$\dot{S}_{\text{bulk}} = \lim_{\delta t \to 0} \frac{S_{v_1} - S_{v_2}}{\delta t} = \frac{\alpha^4 \Omega_5 V_3}{\hat{g}_s^2} \left(\frac{a^4 r_B^4}{1 + a^4 r_B^4} (r_H^4 - r_B^4) + 2 r_B^4 - \frac{2 \log(1 + a^4 r_B^4)}{a^4} \right) \tag{B.9}$$

Note that r_B is related to t_L in the manner that as $t_L \to \infty$, $r_B \to r_H$. Therefore, the late time limit can be obtained by taking $r_B \to r_H$ limit.

B.1.2 Boundary Contributions

We adopt the convention that the null boundary geodesics are affinely parameterized: $k^\mu \nabla_\mu k^\nu = \kappa k^\nu$ with $\kappa = 0$, which simplifies the action computation considerably because all but one boundary surface ($\mathcal{S}_\epsilon$) make no contribution. The boundary $\mathcal{S}_\epsilon$ is the spacelike surface $r = \epsilon \to 0$. The contribution is of the form

$$\delta S_{\text{boundary}} = -2 \int_{\mathcal{S}_\epsilon} K d\Sigma \tag{B.10}$$

where $d\Sigma$ is the induced volume element on the boundary hypersurface and K is the extrinsic curvature: $K = g^{\mu\nu} \nabla_\mu s_\nu$ with the unit normal s^ν chosen to be future directed, away from the WDW patch. This convention for choosing the direction of the surface normal is responsible for the minus sign on this term [74].

For our metric eq(3.6) we have

$$K = \left(\frac{\hat{g}_s}{\alpha^2} \right)^{1/4} \frac{4 r h(r) f'(r) + f(r) \left(32 h(r) - r h'(r) \right)}{8 R h(r)^{7/8} \sqrt{-f(r)}}, \tag{B.11}$$

which as $\epsilon \to 0$ leads to

$$\dot{S}_{\text{boundary}} = 4r_H^4 \frac{\alpha^4 \Omega_5 V_3}{\hat{g}_s^2} \tag{B.12}$$

B.1.3 Joint Contributions

There are two joints (B and B') which contribute to the complexification rate. Each of these is comprised of the intersection of two null surfaces, so their contributions are of the form

$$S_J = 2\Sigma_{m_i} \text{sign}(m_i) \int_{B_{m_i}} a_{m_i} d\sigma \tag{B.13}$$

$$a_{m_i} = \log \left| -\frac{1}{2} k_L \cdot k_R \right|$$

where dS is the volume element on the joint. Here k_L and k_R are future-pointing null generators along the left-moving and right-moving boundaries, respectively. Both of the joints in question lie at the past of the corresponding null segments, which together form the past boundary of a WDW patch. Together these facts determine that the sign of each joint's contribution to the WDW patch action is positive [74], and so taking a difference of two patches leads to the signs given in equation B.2.

In addition to the affine parameterization of boundary generators, a convention must be chosen to fix their normalization. It may be possible to associate the freedom allowed by this choice with corresponding conventions which must be established in the definition of quantum complexity (e.g.,

choice of reference state and gate set). Indeed, progress has been made in this direction [24]. For our purposes, establishing a normalization convention is necessary to make meaningful comparisons between different WDW patch actions (such as that implicit in our "time derivative") as parameters of the theory are adjusted.

We normalize according to $k_L \cdot t_L = -c$ and $k_R \cdot t_R = -\bar{c}$, where $\hat{t}_R$ and $\hat{t}_L$ are normalized generators of time-translation on each boundary. With this in mind we choose

$$\begin{aligned}(k_L)_\mu &= -c(\delta^t_\mu - \sqrt{\frac{-g_{rr}}{g_{tt}}}\delta^r_\mu) \\ (k_R)_\mu &= \bar{c}(\delta^t_\mu + \sqrt{\frac{-g_{rr}}{g_{tt}}}\delta^r_\mu).\end{aligned} \tag{B.14}$$

For small δt, the joints B_2 and B_1 are at fixed radii $r = r_B$ and $r = r_B + \frac{1}{2}\sqrt{\frac{-g_{tt}}{g_{rr}}}\delta t$, respectively. The quantities a_m in equation B.13 are easily evaluated at each joint and the combined contribution is found to be:

$$\begin{aligned}S_{B_1} - S_{B_2} &= 2\frac{\alpha^4 V_3 \Omega_5}{\hat{g}_s^2}\left(r^3 \log\big[-\bar{c}c\frac{R^2(\hat{g}_s^2 h(r))^{1/4}}{\alpha r^2 f(r)}\big]\Big|_{r=r_{B_2}}^{r=r_{B_1}}\right) \\ &\approx \delta t \frac{\alpha^4 V_3 \Omega_5}{\hat{g}_s^2}\left(\frac{2r_H^4 + r_B^4(2 + a^4(3r_B^4 + r_H^4))}{1 + a^4 r_B^4} + 3(r_H^4 - r_B^4)\log\left|\frac{c\bar{c}\sqrt{\hat{g}_s}R^2 r_B^2}{\alpha(1 + a^4 r_B^4)^{1/4}(r_H^4 - r_B^4)}\right|\right.\end{aligned} \tag{B.15}$$

B.1.4 Combined Contributions

We can combine contributions B.9, B.12, and B.15 to arrive at the full time rate change of the WDW patch action (reinstating explicit κ dependence and immediately using $2\kappa^2 = (2\pi)^7\alpha^4$):

$$\dot{S}_{WDW} = \frac{\Omega_5 V_3}{(2\pi)^7 \hat{g}_s^2}\left(\frac{-2\log(1+a^4 r_B^4)}{a^4} + 4r_B^4 + 6r_H^4 + 3(r_H^4 - r_B^4)\log\left|\frac{c\bar{c}\sqrt{\hat{g}_s}R^2 r_B^2}{\alpha(1+a^4 r_B^4)^{1/4}(r_H^4 - r_B^4)}\right|\right) \tag{B.16}$$

B.2 Thermodynamics and the Lloyd Bound

It is interesting that the thermodynamic quantities for these systems exhibit no dependence on the noncommutativity parameter a (see [66] for discussion). We find that for general p[1]

$$\begin{aligned} E &= \frac{(9-p)r_H^{(7-p)}}{2(2\pi)^7\hat{g}_s^2} V_p \Omega_{(8-p)} \\ T &= \frac{(7-p)r_H^{(5-p)/2}}{4\pi R^{(7-p)/2}} \\ S &= \frac{4\pi R^{(7-p)/2} r_H^{(9-p)/2}}{(2\pi)^7 \hat{g}_s^2} V_p \Omega_{(8-p)} \end{aligned} \tag{B.17}$$

with E being the ADM mass. The first law $dE = TdS$ is easily confirmed.

In the original CA duality conjecture [18, 19] the proportionality constant in Complexity $= k \times$ Action was fixed by an expectation that black holes are the fastest computers in nature, and that at late times they would saturate a bound from Lloyd [62, 63]. Matching $\dot{C} = \frac{2M}{\pi}$ at late times for Schwarzschild

[1]Note that for $p = 5$ equations B.17 would indicate zero specific heat. We take this as further evidence that results for $p \geq 5$ should be viewed skeptically.

AdS black holes sets the constant at $k = \frac{1}{\pi}$. The relevance of the Lloyd bound to these considerations is questionable [64], but in the interest of comparison we note that the systems studied in this work would require different constants to meet the same criterion: for the commutative black holes to saturate the bound at late times, $k = \lim_{t\to\infty} \frac{2M}{\pi \dot{S}}$ would be given by

	$p = 2$	$p = 3$	$p = 4$	$p = 5$	$p = 6$
k	$\frac{7}{12\pi}$	$\frac{3}{4\pi}$	$\frac{1}{\pi}$	$\frac{1}{\pi}$	$\frac{1}{\pi}$

Furthermore, if the proportionality k were fixed with reference to commutative black holes, the bound would still be violated by highly noncommutative black holes. Rather than proposing novel bounds or searching over all systems for a minimum necessary $k = \lim_{t\to\infty} \frac{2M}{\pi \dot{S}}$ (giving the weakest bound on $\dot{S}$) to be the true proportionality in $\mathcal{C} = kS$, we suspect that the precise proportionality cannot be universally generalized between systems, at least under the established conventions for computing the WDW action.

Appendix C

Holographic Purification Complexity

C.1 Calculation of two-sided BTZ Action

We here calculate the on shell action for the BTZ black hole with metric described by

$$ds^2 = \frac{L^2}{z^2}\left(-f(z)dt^2 + f(z)^{-1}dz^2 + L^2dx^2\right)$$
$$f(z) = 1 - \left(\frac{z}{z_H}\right)^2$$

We will allow the cutoffs on the left and right side to vary independently, though we still choose constant z surfaces, and we consider only the $t_L = t_R = 0$ slice. We denote these cutoffs as $z_L = \delta_L, z_R = \delta_R$, though they are not necessarily small.

We'll consider the total WdW patch action ($\mathcal{A}^T$), as well as that of the right subsystem ($\mathcal{A}^R$). The latter is obtained by restricting to the entanglement wedge of the subsystem, which is simply the right exterior of the black hole. The left subsystem action ($\mathcal{A}^L$) is the same as $\mathcal{A}_R$ with $\delta_R \to \delta_L$. Time reflection symmetry and additivity of the bulk action also allow for simple determination of the action on the behind-the-horizon regions to the future ($\mathcal{A}_F$) and past ($\mathcal{A}_P$) through $\mathcal{A}_F = \mathcal{A}_P = \frac{1}{2}(\mathcal{A}_T - \mathcal{A}_R - \mathcal{A}_L)$. These two bulk

subregions are not expected to correspond to boundary state complexities in their own right so we do not compute them here.

We'll first use the prescription summarized in appendix C of [74] with the generators of null boundaries affinely parameterized. This leaves a dependence on the overall normalization of these generators (see equation C.3). We'll also compute the boundary counterterms described in appendix B of [74], the inclusion of which makes the action result reparameterization invariant. In this appendix we report results with and without these terms.

C.1.1 Setup

Both the total state WdW patch and the left/right subregions we consider are "diamond shaped" on a conformal diagram, so we adopt a common labeling scheme for the boundaries and joints, shown in figure C.1. In each case, the action $\mathcal{A}$ consists of a bulk contribution on the relevant volume $\mathcal{V}$, four contributions on null boundaries $\mathcal{N}_i$ $(i = 1, 2, 3, 4)$, and four co-dimension two "joint" contributions[1]. We'll denote these joints as $\mathcal{J}_j$ $(j = 1, 2, 3, 4)$. We'll also use sometimes use j_1 and j_2 to label the leftgoing/rightgoing null boundaries who's intersection forms the jth joint. For example for $j = 1$ the joint is the intersection of $\mathcal{N}_1$ and $\mathcal{N}_4$, so $(j_1, j_2) = (1, 4)$.

Before adding the term for reparameterization invariance, the action

[1]Note that a prescription using variable cutoff surfaces to define a family of purifications is more naturally suited to a joint (constant t) cutoff scheme as opposed to a timelike boundary cutoff, see fig. C.2

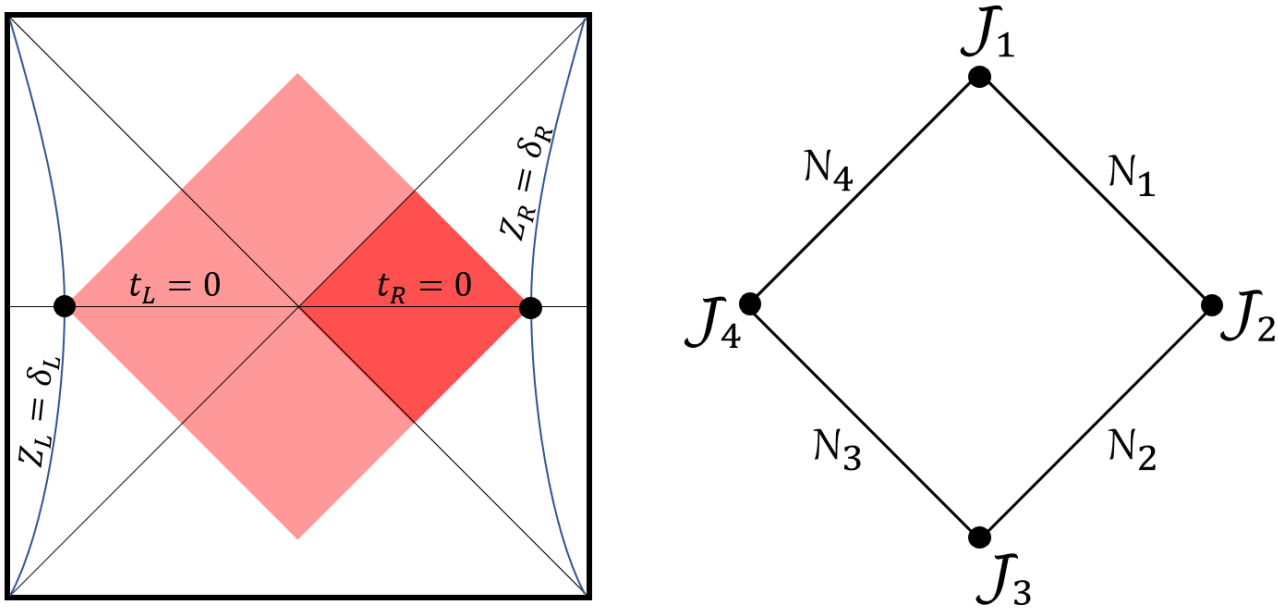

Figure C.1: A conformal diagram for the two-sided BTZ spacetime is shown in the left panel. The Wheeler-DeWitt patch corresponding to the total state is shaded in light red, while dark red indicates the subregion of interest for the right subregion computation. Both regions are "diamond shaped" so we adopt a shared labeling scheme for the joints and null boundaries, as illustrated in the right panel.

on such a bulk regions is given by

$$16\pi G\,\mathcal{A} = \mathcal{S} = \int_{\mathcal{V}} (\mathcal{R} - 2\Lambda)\sqrt{-g}\, dV \\ - 2\sum_i \text{sign}(\mathcal{N}_i) \int_{\mathcal{N}_i} \kappa dS d\lambda_i + 2\sum_j \text{sign}(\mathcal{J}_j) \int_{\mathcal{J}_j} \ln|k_{j_1} \cdot k_{j_2}/2| dS$$

Here λ_i parameterizes the ith null boundary through $k_i^\alpha = dx^\alpha/d\lambda_i$ with κ defined by $k_i^\beta \nabla_\beta k_i^\alpha = \kappa\, k_i^\alpha$. We first choose this parameter to be affine, and express results in terms of arbitrary normalization constants for the k_i: $k_i \cdot \hat{t} = c_i$ with $\hat{t}$ being the static time coordinate vector $\hat{t} = \partial_t$. This leaves only the

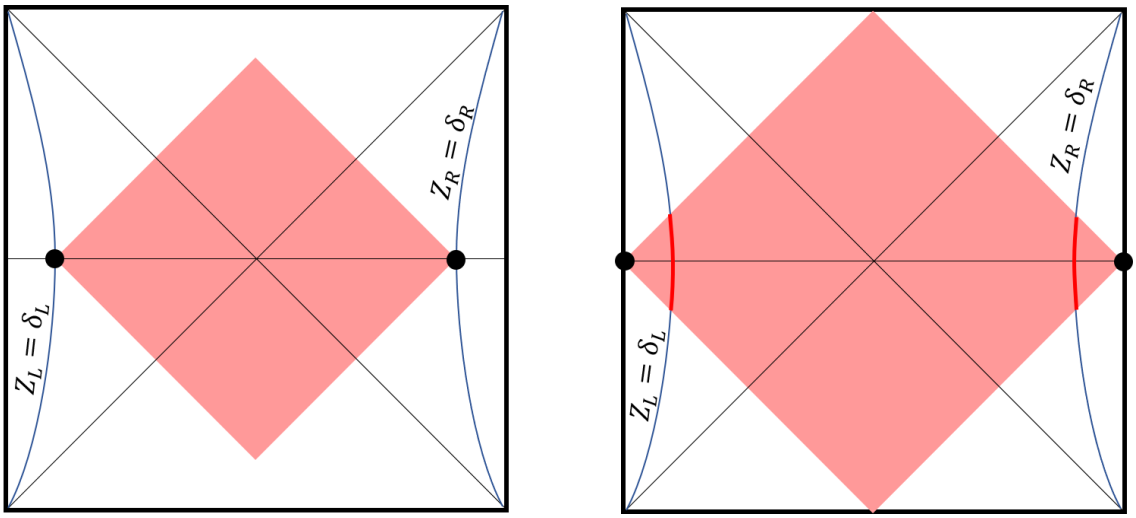

Figure C.2: The cutoff prescription utilized in this paper is that of the left diagram.

bulk and joint contributions, which we'll label $S_{\mathcal{V}}$ and $S_{\mathcal{J}}$.

$$S_{\mathcal{V}} = \int_{\mathcal{V}} (\mathcal{R} - 2\Lambda)\sqrt{-g}\, dV$$
$$S_{\mathcal{J}} = 2\sum_j \text{sign}(\mathcal{J}_j) \int_{\mathcal{J}_j} \ln|k_{j_1} \cdot k_{j_2}/2| dS$$

After computing these contributions we'll add counterterms associated with the null boundaries which make the action reparameterization invariant. These terms ultimately render the choices of the previous paragraph irrelevant (the affine parameterization and normalization of k_i^α), but they require the introduction of arbitrary lengthscale(s) which we'll denote $\tilde{L}_i$.

For the ith null boundary, the counterterm $\Delta S_{\mathcal{N}_i}$ is given by

$$\Delta S_{\mathcal{N}_i} = 2\,\text{sign}(\mathcal{N}_i) \int_{\mathcal{N}_i} \Theta_i \left(\ln|\tilde{L}\Theta_i|\right) dS d\lambda_i$$

where $\Theta_i = \frac{1}{\sqrt{\gamma}} \frac{d\sqrt{\gamma}}{d\lambda_i}$, the expansion parameter associated with λ_i. Here $\sqrt{\gamma}$ is the volume element induced on the space transverse to fixed λ_i.

The normalization constants c_i, and the lengthscales $\tilde{L}_i$ should be the same on future-directed left-going and right-going null boundaries (this ensures, for instance, that the action goes to zero when the "diamond" is squashed along either null direction). At the end we'll impose this but we'll first denote them independently to illustrate more explicitly the replacement of c_i dependence by $\tilde{L}_i$ dependence. The signs for both null boundary and joint contributions will be listed in their respective subsections below.

C.1.2 Bulk contribution

The bulk contributions on each subregion simply integrate over the constant value of $R - 2\Lambda = -4/L^2$. The spacetime volume of each wedge (Right/Left/Future/Past) can be written $\mathcal{V} = \Delta x L^4 \left| \frac{1}{z_c} - \frac{1}{z_H} \right|$, where z_c is the position of the joint furthest from the bifurcation surface in each quadrant. In the right and left quadrants, z_c is simply the cutoff $z_c = \delta_{L,R}$. In the future and past quadrants we denote these joints as z_F and z_P, though symmetry dictates that these are at the same coordinate z-value, determined by the two cutoffs as

$$z_F = z_P = z_H \frac{1 + \sqrt{\frac{(z_H+\delta_R)(z_H+\delta_L)}{(z_H-\delta_R)(z_H-\delta_L)}}}{-1 + \sqrt{\frac{(z_H+\delta_R)(z_H+\delta_L)}{(z_H-\delta_R)(z_H-\delta_L)}}} \tag{C.1}$$

The bulk contribution in each quadrant can therefore be written in the

unified form

$$S_{\mathcal{V}}^{\mathrm{R,L,F,P}} = -4\Delta x L^2 \left| \frac{1}{z_{R,L,F,P}} - \frac{1}{z_H} \right| \tag{C.2}$$

C.1.3 Joint contribution

Turning to the joint contributions, we utilize affinely parameterized future-directed boundary generators, normalized according to $k_i \cdot \hat{t} = -c_i$ where $\hat{t} = \partial_t$. For example in the right quadrant we choose future-directed ingoing and outgoing generators on $\mathcal{N}_1$ and $\mathcal{N}_2$ to be given by

$$\begin{aligned} (k_1)_\mu &= c_1\, \partial_\mu(-t + z^*(z)) \\ (k_2)_\mu &= c_2\, \partial_\mu(-t - z^*(z)) \end{aligned} \tag{C.3}$$

where $z^*(z)$ is a BTZ 'tortoise' coordintate:

$$z^*(z) = \frac{z_H}{2} \log \left| \frac{z + z_H}{z - z_H} \right| \tag{C.4}$$

Analogous expressions apply for all k_i. For every joint we will consider, we have $\log |k_{j_1} \cdot k_{j_2}/2| = \log \left(\frac{c_{j_1} c_{j_2}\, z^2}{L^2 |f(z)|} \right)$ and $dS = L^2/z\, dx$, so the total joint contributions can be written

$$S_{\mathcal{J}} = 2\Delta x \sum_j \left(\mathrm{sign}(\mathcal{J}_j) \frac{L^2}{z_j} \ln \left(\frac{c_{j_1} c_{j_2}\, z_j^2 z_H^2}{L^2 |z_j^2 - z_H^2|} \right) \right) \tag{C.5}$$

The signs of the joint contributions given by (see [74], appendix C) $\mathrm{sign}(\mathcal{J}_1) = 1$, $\mathrm{sign}(\mathcal{J}_2) = -1$, $\mathrm{sign}(\mathcal{J}_3) = 1$, $\mathrm{sign}(\mathcal{J}_4) = -1$.

C.1.4 Counterterm

Lastly, we compute the counterterms required for reparameterization invariance. This requires the introduction of a lengthscale which we'll denote $\tilde{L}_i$ on the null boundary $\mathcal{N}_i$. Once again these lengthscales should match for left-going and right-going boundaries, but we first denote them independently to keep track of contributions and cancellations with joints. For each null surface we have a contribution depending on Θ_i, the expansion parameter associated with λ_i:

$$\Delta S_{\mathcal{N}_i} = 2\,\mathrm{sign}(\mathcal{N}_i)\int_{\mathcal{N}_i}\Theta_i\left(\ln|\Theta_i\tilde{L}|\right)dSd\lambda_i$$

For each of the four null surfaces in question, $\sqrt{\gamma} = (L^2/z)$ and so $\Theta_i = -\frac{1}{z}\frac{dz}{d\lambda_i}$. For the generators parameterized as in equation (C.3), we have $dz/d\lambda_i = \pm c_i\, z^2/L^2$. This allows us to write each contribution in the form:

$$\begin{aligned}\Delta S_{\mathcal{N}_i} =& -2\,\mathrm{sign}(\mathcal{N}_i)\Delta x\int_{z_i(\lambda_{\min})}^{z_i(\lambda_{\max})}\frac{L^2}{z^2}\log\big(\frac{c_i\tilde{L}_i z}{L^2}\big)dz \\ =& 2\,\mathrm{sign}(\mathcal{N}_i)\Delta x\frac{L^2}{z}\left(1+\log\left(\frac{c_i\tilde{L}_i z}{L^2}\right)\right)\Bigg|_{z_i(\lambda_{\min})}^{z_i(\lambda_{\max})}\end{aligned} \tag{C.6}$$

With λ integrated to the future, parameterization invariance requires $\mathrm{sign}(\mathcal{N}_i) = -1$ for null boundaries which are to the future of the bulk subregion, and $+1$ for past null boundaries.

C.1.5 $\mathcal{A}^T$: full WdW patch action

We first compute the full action on the WdW patch. Summing the bulk contributions from each quadrant we have

$$S_{\mathcal{V}}^T = -4\Delta x L^2 \left(\frac{1}{\delta_L} + \frac{1}{\delta_R} - \frac{1}{z_F} - \frac{1}{z_P} \right)$$

where $z_F = z_P$ are the futuremost and pastmost joint location, given by eq. (C.1). The joint contributions amount to

$$\begin{aligned} S_J^T = 2\Delta x L^2 \Bigg(& \frac{1}{z_F} \log \left(\frac{c_1 c_4 \, z_F^2 z_H^2}{L^2 (z_F^2 - z_H^2)} \right) + \frac{1}{z_P} \log \left(\frac{c_2 c_3 \, z_P^2 z_H^2}{L^2 (z_P^2 - z_H^2)} \right) \\ & - \frac{1}{\delta_R} \log \left(\frac{c_1 c_2 \, \delta_R^2 z_H^2}{L^2 (z_H^2 - \delta_R^2)} \right) - \frac{1}{\delta_L} \log \left(\frac{c_3 c_4 \delta_L^2 z_H^2}{L^2 (z_H^2 - \delta_L^2)} \right) \Bigg) \end{aligned}$$

and the counterterms together give

$$\begin{aligned} \Delta S_{\mathcal{N}}^T = & \, 4\Delta x L^2 \left(\frac{1}{\delta_L} + \frac{1}{\delta_R} - \frac{1}{z_F} - \frac{1}{z_P} \right) \\ & + 2\Delta x L^2 \Bigg(\frac{1}{\delta_R} \log \left(\frac{c_1 c_2 \tilde{L}_1 \tilde{L}_2 \delta_R^2}{L^4} \right) + \frac{1}{\delta_L} \log \left(\frac{c_3 c_4 \tilde{L}_3 \tilde{L}_4 \delta_L^2}{L^4} \right) \\ & - \frac{1}{z_F} \log \left(\frac{c_1 c_4 \tilde{L}_1 \tilde{L}_4 z_F^2}{L^4} \right) - \frac{1}{z_P} \log \left(\frac{c_2 c_3 \tilde{L}_2 \tilde{L}_3 z_P^2}{L^4} \right) \Bigg) \end{aligned}$$

The cancellation of c_i constants from the joint terms after the inclusion of counterterms is evident from the above expressions. In the combined answers we impose that $c_1 = c_3 = c$, $c_2 = c_4 = \bar{c}$, $\tilde{L}_3 = \tilde{L}_1$, $\tilde{L}_4 = \tilde{L}_2$, as well as $z_P = z_F$. The total action, reported without ($\mathcal{A}^T$) and with ($\tilde{\mathcal{A}}^T$) the counterterms is therefore as follows.

$$\mathcal{A}^T = \frac{\Delta x L^2}{8\pi G}\left[\frac{2}{z_F}\left(2+\log\left(\frac{c\bar{c}\, z_F^2 z_H^2}{L^2(z_F^2-z_H^2)}\right)\right) - \frac{1}{\delta_R}\left(2+\log\left(\frac{c\bar{c}\,\delta_R^2 z_H^2}{L^2(z_H^2-\delta_R^2)}\right)\right) - \frac{1}{\delta_L}\left(2+\log\left(\frac{c\bar{c}\,\delta_L^2 z_H^2}{L^2(z_H^2-\delta_L^2)}\right)\right)\right]$$

$$\tilde{\mathcal{A}}^T = \frac{\Delta x L^2}{8\pi G}\left[\frac{2}{z_F}\log\left(\frac{L^2 z_H^2}{\tilde{L}_1\tilde{L}_2(z_F^2-z_H^2)}\right) - \frac{1}{\delta_R}\log\left(\frac{L^2 z_H^2}{\tilde{L}_1\tilde{L}_2(z_H^2-\delta_R^2)}\right) - \frac{1}{\delta_L}\log\left(\frac{L^2 z_H^2}{\tilde{L}_1\tilde{L}_2(z_H^2-\delta_L^2)}\right)\right] \tag{C.7}$$

C.1.6 Subregion Action

We now compute the right subregion action, defined by restricting the Wheeler-deWitt patch to the entanglement wedge of the boundary subregion, which for the right boundary is simply the full right-side exterior of the black hole. In most respects the right subregion computation follows the same procedure as the previous section. The bulk contribution is given by equation (C.2) as

$$S_{\mathcal{V}}^R = -4L^2\Delta x\left(\frac{1}{\delta_R}-\frac{1}{z_H}\right)$$

However, evaluating joints directly on the horizon would naively give divergent results. We follow [1], by first setting null surfaces just outside the past and future horizons and taking the limit that they coincide with the horizons. More precisely, we define null boundaries $\mathcal{N}_3$ and $\mathcal{N}_4$ to pass through a joint just off the bifurcation surface: $t = 0, z = zH - \epsilon$ in the right quadrant (a different t would not affect the result). We then let $\epsilon \to 0$, which ultimately leaves a finite result for the total joint contribution. Because of the simplicity of the

$z^*(z)$ function in equation (C.4), this procedure can be carried out exactly for any δ_R.

Before setting the c_i constants to c and $\bar{c}$, the contribution from joints $\mathcal{J}_1$, $\mathcal{J}_3$, and $\mathcal{J}_4$ is

$$S^R_{\mathcal{J}_1} + S^R_{\mathcal{J}_3} + S^R_{\mathcal{J}_4} = \frac{2L^2\Delta x}{z_H}\left(\log\left(\frac{c_1 c_2 z_H^2(z_H+\delta_R)}{4L^2(z_H-\delta_R)}\right)\right)$$

. Adding the contribution from $\mathcal{J}_2$ and replacing $c_1 \to c$ and $c_2 \to \bar{c}$, the total joint contribution to the subregion action is

$$S^R_{\mathcal{J}} = 2L^2\Delta x\left(\frac{1}{z_H}\log\left(\frac{c\bar{c}\, z_H^2(z_H+\delta_R)}{4L^2(z_H-\delta_R)}\right) - \frac{1}{\delta_R}\log\left(\frac{c\bar{c}\,\delta_R^2 z_H^2}{L^2(z_H^2-\delta_R^2)}\right)\right)$$

The counterterm contributions from null boundaries $\mathcal{N}_3$ and $\mathcal{N}_4$ vanish and the remaining pieces give:

$\Delta S^R_{\mathcal{N}_1} + \Delta S^R_{\mathcal{N}_2} =$

$$4L^2\Delta x\left(\frac{1}{\delta_R} - \frac{1}{z_H}\right) + 2L^2\Delta x\left(\frac{1}{\delta_R}\log\left(\frac{c\bar{c}\,\tilde{L}_1\tilde{L}_2\delta_R^2}{L^4}\right) - \frac{1}{z_H}\log\left(\frac{c\bar{c}\,\tilde{L}_1\tilde{L}_2 z_H^2}{L^4}\right)\right)$$

.

Combining the previous expressions we find the total result for the subregion action without ($\mathcal{A}^R$) and with ($\tilde{\mathcal{A}}^R$) the counterterms:

$$\begin{aligned}
\mathcal{A}^R &= \frac{L^2\Delta x}{8\pi G}\left(\frac{1}{z_H}\left(2+\log\left(\frac{c\bar{c}\, z_H^2(z_H+\delta_R)}{4L^2(z_H-\delta_R)}\right)\right) - \frac{1}{\delta_R}\left(2+\log\left(\frac{c\bar{c}\,\delta_R^2 z_H^2}{L^2(z_H^2-\delta_R^2)}\right)\right)\right)\\
\tilde{\mathcal{A}}^R &= \frac{L^2\Delta x}{8\pi G}\left(\frac{1}{z_H}\log\left(\frac{L^2(z_H+\delta_R)}{4\tilde{L}_1\tilde{L}_2(z_H-\delta_R)}\right) - \frac{1}{\delta_R}\log\left(\frac{L^2 z_H^2}{\tilde{L}_1\tilde{L}_2(z_H^2-\delta_R^2)}\right)\right)
\end{aligned} \tag{C.8}$$

In the main text, our discussion centers on the result with counterterms included (reported there in a somewhat different form, see section **??**).

Bibliography

[1] C.A. Agón, M. Headrick and B. Swingle, *Subsystem Complexity and Holography*, 1804.01561.

[2] J. Couch, S. Eccles, T. Jacobson and P. Nguyen, *Holographic Complexity and Volume*, *JHEP* **11** (2018) 044 [1807.02186].

[3] J. Couch, S. Eccles, W. Fischler and M.-L. Xiao, *Holographic complexity and noncommutative gauge theory*, *JHEP* **03** (2018) 108 [1710.07833].

[4] J. Couch, W. Fischler and P.H. Nguyen, *Noether charge, black hole volume, and complexity*, *JHEP* **03** (2017) 119 [1610.02038].

[5] E. Cáceres, J. Couch, S. Eccles and W. Fischler, *Holographic Purification Complexity*, *Phys. Rev.* **D99** (2019) 086016 [1811.10650].

[6] J.M. Maldacena, *The Large N limit of superconformal field theories and supergravity*, *Int. J. Theor. Phys.* **38** (1999) 1113 [hep-th/9711200].

[7] S.S. Gubser, I.R. Klebanov and A.M. Polyakov, *Gauge theory correlators from noncritical string theory*, *Phys. Lett.* **B428** (1998) 105 [hep-th/9802109].

[8] E. Witten, *Anti-de Sitter space and holography*, *Adv. Theor. Math. Phys.* **2** (1998) 253 [hep-th/9802150].

[9] O. Aharony, O. Bergman, D.L. Jafferis and J. Maldacena, *N=6 superconformal Chern-Simons-matter theories, M2-branes and their gravity duals*, *JHEP* **10** (2008) 091 [0806.1218].

[10] A. Hashimoto and N. Itzhaki, *Noncommutative Yang-Mills and the AdS / CFT correspondence*, *Phys. Lett.* **B465** (1999) 142 [hep-th/9907166].

[11] S. Ryu and T. Takayanagi, *Holographic derivation of entanglement entropy from AdS/CFT*, *Phys. Rev. Lett.* **96** (2006) 181602 [hep-th/0603001].

[12] S. Ryu and T. Takayanagi, *Aspects of Holographic Entanglement Entropy*, *JHEP* **08** (2006) 045 [hep-th/0605073].

[13] V.E. Hubeny, M. Rangamani and T. Takayanagi, *A Covariant holographic entanglement entropy proposal*, *JHEP* **07** (2007) 062 [0705.0016].

[14] L. Susskind, *Entanglement is not enough*, *Fortsch. Phys.* **64** (2016) 49 [1411.0690].

[15] L. Susskind, *Computational Complexity and Black Hole Horizons*, *Fortsch. Phys.* **64** (2016) 44 [1403.5695].

[16] D. Stanford and L. Susskind, *Complexity and Shock Wave Geometries*, *Phys. Rev.* **D90** (2014) 126007 [1406.2678].

[17] L. Susskind and Y. Zhao, *Switchbacks and the Bridge to Nowhere*, 1408.2823.

[18] A.R. Brown, D.A. Roberts, L. Susskind, B. Swingle and Y. Zhao, *Holographic Complexity Equals Bulk Action?*, *Phys. Rev. Lett.* **116** (2016) 191301 [1509.07876].

[19] A.R. Brown, D.A. Roberts, L. Susskind, B. Swingle and Y. Zhao, *Complexity, action, and black holes*, *Phys. Rev.* **D93** (2016) 086006 [1512.04993].

[20] Wikipedia contributors, *Word metric — Wikipedia, the free encyclopedia*, 2020.

[21] D. Carmi, S. Chapman, H. Marrochio, R.C. Myers and S. Sugishita, *On the Time Dependence of Holographic Complexity*, 1709.10184.

[22] D. Carmi, R.C. Myers and P. Rath, *Comments on Holographic Complexity*, *JHEP* **03** (2017) 118 [1612.00433].

[23] S. Chapman, H. Marrochio and R.C. Myers, *Complexity of Formation in Holography*, *JHEP* **01** (2017) 062 [1610.08063].

[24] R.A. Jefferson and R.C. Myers, *Circuit complexity in quantum field theory*, 1707.08570.

[25] D. Harlow and P. Hayden, *Quantum Computation vs. Firewalls*, *JHEP* **06** (2013) 085 [1301.4504].

[26] M. Headrick and V.E. Hubeny, *Riemannian and Lorentzian flow-cut theorems*, 1710.09516.

[27] R. Cleve, *An introduction to quantum complexity theory*, quant-ph/9906111.

[28] J. Watrous, *Quantum Computational Complexity*, *ArXiv e-prints* (2008) [0804.3401].

[29] S. Aaronson, *The Complexity of Quantum States and Transformations: From Quantum Money to Black Holes*, 7, 2016 [1607.05256].

[30] M. Moosa, *Evolution of Complexity Following a Global Quench*, 1711.02668.

[31] M. Moosa, *Divergences in the rate of complexification*, 1712.07137.

[32] R. Laflamme, *Geometry and Thermofields*, *Nucl. Phys. B* **324** (1989) 233.

[33] A.O. Barvinsky, V.P. Frolov and A.I. Zelnikov, *Wavefunction of a Black Hole and the Dynamical Origin of Entropy*, *Phys. Rev. D* **51** (1995) 1741 [gr-qc/9404036].

[34] J.M. Maldacena, *Eternal black holes in anti-de Sitter*, *JHEP* **04** (2003) 021 [hep-th/0106112].

[35] A.R. Brown, L. Susskind and Y. Zhao, *Quantum Complexity and Negative Curvature*, *Phys. Rev.* **D95** (2017) 045010 [1608.02612].

[36] A.R. Brown and L. Susskind, *The Second Law of Quantum Complexity*, 1701.01107.

[37] I. Bengtsson and J.M.M. Senovilla, *The Region with trapped surfaces in spherical symmetry, its core, and their boundaries*, *Phys. Rev.* **D83** (2011) 044012 [1009.0225].

[38] V. Balasubramanian, A. Bernamonti, J. de Boer, N. Copland, B. Craps, E. Keski-Vakkuri et al., *Thermalization of Strongly Coupled Field Theories*, *Phys. Rev. Lett.* **106** (2011) 191601 [1012.4753].

[39] V. Balasubramanian, A. Bernamonti, J. de Boer, N. Copland, B. Craps, E. Keski-Vakkuri et al., *Holographic Thermalization*, *Phys. Rev.* **D84** (2011) 026010 [1103.2683].

[40] M. Banados, C. Teitelboim and J. Zanelli, *The Black hole in three-dimensional space-time*, *Phys. Rev. Lett.* **69** (1992) 1849 [hep-th/9204099].

[41] R. Emparan, *AdS / CFT duals of topological black holes and the entropy of zero energy states*, *JHEP* **06** (1999) 036 [hep-th/9906040].

[42] R.M. Wald, *General Relativity*, Chicago Univ. Pr., Chicago, USA (1984), 10.7208/chicago/9780226870373.001.0001.

[43] S. Chapman, H. Marrochio and R.C. Myers, *Holographic Complexity in Vaidya Spacetimes I*, 1804.07410.

[44] S. Chapman, H. Marrochio and R.C. Myers, *Holographic Complexity in Vaidya Spacetimes II*, 1805.07262.

[45] R. Bousso and N. Engelhardt, *New Area Law in General Relativity*, *Phys. Rev. Lett.* **115** (2015) 081301 [1504.07627].

[46] R. Bousso and N. Engelhardt, *Proof of a New Area Law in General Relativity*, *Phys. Rev.* **D92** (2015) 044031 [1504.07660].

[47] N. Engelhardt and A.C. Wall, *Decoding the Apparent Horizon: A Coarse-Grained Holographic Entropy*, 1706.02038.

[48] N. Engelhardt and A.C. Wall, *Coarse Graining Holographic Black Holes*, 1806.01281.

[49] Y. Zhao, *Uncomplexity and Black Hole Geometry*, 1711.03125.

[50] V.E. Hubeny and H. Maxfield, *Holographic probes of collapsing black holes*, *JHEP* **03** (2014) 097 [1312.6887].

[51] S.W. Hawking, C.J. Hunter and M. Taylor, *Rotation and the AdS / CFT correspondence*, *Phys. Rev. D* **59** (1999) 064005 [hep-th/9811056].

[52] I. Bengtsson and E. Jakobsson, *Black holes: Their large interiors*, *Mod. Phys. Lett.* **A30** (2015) 1550103 [1502.01907].

[53] M.J. Duncan, *Maximally slicing a black hole with minimal distortion*, *Physical Review D.* **31** (1985) 1267.

[54] B. Czech, J.L. Karczmarek, F. Nogueira and M. Van Raamsdonk, *Rindler Quantum Gravity*, *Class. Quant. Grav.* **29** (2012) 235025 [1206.1323].

[55] M. Parikh and P. Samantray, *Rindler-AdS/CFT*, 1211.7370.

[56] H. Casini, M. Huerta and R.C. Myers, *Towards a derivation of holographic entanglement entropy*, *JHEP* **05** (2011) 036 [1102.0440].

[57] K. Hashimoto, N. Iizuka and S. Sugishita, *Time Evolution of Complexity in Abelian Gauge Theories - And Playing Quantum Othello Game* -, 1707.03840.

[58] P. Caputa, N. Kundu, M. Miyaji, T. Takayanagi and K. Watanabe, *Liouville Action as Path-Integral Complexity: From Continuous Tensor Networks to AdS/CFT*, 1706.07056.

[59] B. Czech, *Einstein's Equations from Varying Complexity*, 1706.00965.

[60] S. Chapman, M.P. Heller, H. Marrochio and F. Pastawski, *Towards Complexity for Quantum Field Theory States*, 1707.08582.

[61] R.-Q. Yang, *A Complexity for Quantum Field Theory States and Application in Thermofield Double States*, 1709.00921.

[62] S. Lloyd, *Ultimate physical limits to computation*, *Nature* **406** (2000) 1047.

[63] N. Margolus and L.B. Levitin, *The Maximum speed of dynamical evolution*, *Physica* **D120** (1998) 188 [quant-ph/9710043].

[64] W. Cottrell and M. Montero, *Complexity is Simple*, 1710.01175.

[65] N. Seiberg and E. Witten, *String theory and noncommutative geometry*, *JHEP* **09** (1999) 032 [hep-th/9908142].

[66] J.M. Maldacena and J.G. Russo, *Large N limit of noncommutative gauge theories*, *JHEP* **09** (1999) 025 [hep-th/9908134].

[67] R.-G. Cai and N. Ohta, *On the thermodynamics of large N noncommutative superYang-Mills theory*, *Phys. Rev.* **D61** (2000) 124012 [hep-th/9910092].

[68] M. Alishahiha, Y. Oz and M.M. Sheikh-Jabbari, *Supergravity and large N noncommutative field theories*, *JHEP* **11** (1999) 007 [hep-th/9909215].

[69] D.S. Berman, V.L. Campos, M. Cederwall, U. Gran, H. Larsson, M. Nielsen et al., *Holographic noncommutativity*, *JHEP* **05** (2001) 002 [hep-th/0011282].

[70] M. Edalati, W. Fischler, J.F. Pedraza and W. Tangarife Garcia, *Fast Scramblers and Non-commutative Gauge Theories*, *JHEP* **07** (2012) 043 [1204.5748].

[71] W. Fischler, A. Kundu and S. Kundu, *Holographic Entanglement in a Noncommutative Gauge Theory*, *JHEP* **01** (2014) 137 [1307.2932].

[72] J.L. Karczmarek and C. Rabideau, *Holographic entanglement entropy in nonlocal theories*, *JHEP* **10** (2013) 078 [1307.3517].

[73] W. Fischler, E. Gorbatov, A. Kashani-Poor, R. McNees, S. Paban and P. Pouliot, *The Interplay between theta and T*, *JHEP* **06** (2000) 032 [hep-th/0003216].

[74] L. Lehner, R.C. Myers, E. Poisson and R.D. Sorkin, *Gravitational action with null boundaries*, *Phys. Rev.* **D94** (2016) 084046 [1609.00207].

[75] M. Alishahiha, H. Ita and Y. Oz, *Graviton scattering on D6-branes with B fields*, *JHEP* **06** (2000) 002 [hep-th/0004011].

[76] T. Araujo, I. Bakhmatov, E.Ó. Colgáin, J. Sakamoto, M.M. Sheikh-Jabbari and K. Yoshida, *Yang-Baxter σ-models, conformal twists, and noncommutative Yang-Mills theory*, *Phys. Rev.* **D95** (2017) 105006 [1702.02861].

[77] T. Araujo, I. Bakhmatov, E.Ó. Colgáin, J.-i. Sakamoto, M.M. Sheikh-Jabbari and K. Yoshida, *Conformal Twists, Yang-Baxter σ-models & Holographic Noncommutativity*, 1705.02063.

[78] I. Bakhmatov, Ö. Kelekci, E.Ó. Colgáin and M.M. Sheikh-Jabbari, *Classical Yang-Baxter Equation from Supergravity*, 1710.06784.

[79] J.D. Bekenstein, *Black holes and entropy*, *Phys. Rev.* **D7** (1973) 2333.

[80] J.D. Bekenstein, *Generalized second law of thermodynamics in black hole physics*, *Phys. Rev.* **D9** (1974) 3292.

[81] S.W. Hawking, *Particle Creation by Black Holes*, *Commun. Math. Phys.* **43** (1975) 199.

[82] S.W. Hawking, *Black Holes and Thermodynamics*, *Phys. Rev. D* **13** (1976) 191.

[83] D. Kastor, S. Ray and J. Traschen, *Enthalpy and the Mechanics of AdS Black Holes*, *Class. Quant. Grav.* **26** (2009) 195011 [0904.2765].

[84] B.P. Dolan, *Where is the PdV term in the fist law of black hole thermodynamics?*, 1209.1272.

[85] D. Kubiznak and R.B. Mann, *Black hole chemistry*, *Can. J. Phys.* **93** (2015) 999 [1404.2126].

[86] A.M. Frassino, R.B. Mann and J.R. Mureika, *Lower-Dimensional Black Hole Chemistry*, *Phys. Rev.* **D92** (2015) 124069 [1509.05481].

[87] D. Kubiznak, R.B. Mann and M. Teo, *Black hole chemistry: thermodynamics with Lambda*, *Class. Quant. Grav.* **34** (2017) 063001 [1608.06147].

[88] C.V. Johnson, *Holographic Heat Engines*, *Class. Quant. Grav.* **31** (2014) 205002 [1404.5982].

[89] E. Caceres, P.H. Nguyen and J.F. Pedraza, *Holographic entanglement entropy and the extended phase structure of STU black holes*, *JHEP* **09** (2015) 184 [1507.06069].

[90] A. Karch and B. Robinson, *Holographic Black Hole Chemistry*, *JHEP* **12** (2015) 073 [1510.02472].

[91] E. Caceres, P.H. Nguyen and J.F. Pedraza, *Holographic entanglement chemistry*, *Phys. Rev.* **D95** (2017) 106015 [1605.00595].

[92] P.H. Nguyen, *An equal area law for holographic entanglement entropy of the AdS-RN black hole*, *JHEP* **12** (2015) 139 [1508.01955].

[93] D. Kastor, S. Ray and J. Traschen, *Extended First Law for Entanglement Entropy in Lovelock Gravity*, *Entropy* **18** (2016) 212 [1604.04468].

[94] D. Kastor, S. Ray and J. Traschen, *Chemical Potential in the First Law for Holographic Entanglement Entropy*, *JHEP* **11** (2014) 120 [1409.3521].

[95] P. Pradhan, *Thermodynamic Products in Extended Phase Space*, *Int. J. Mod. Phys.* **D26** (2016) 1750010 [1603.07748].

[96] V. Iyer and R.M. Wald, *Some properties of Noether charge and a proposal for dynamical black hole entropy*, *Phys. Rev.* **D50** (1994) 846 [gr-qc/9403028].

[97] V. Iyer and R.M. Wald, *A Comparison of Noether charge and Euclidean methods for computing the entropy of stationary black holes*, *Phys. Rev.* **D52** (1995) 4430 [gr-qc/9503052].

[98] T. Faulkner, M. Guica, T. Hartman, R.C. Myers and M. Van Raamsdonk, *Gravitation from Entanglement in Holographic CFTs*, *JHEP* **03** (2014) 051 [1312.7856].

[99] J. Lin, M. Marcolli, H. Ooguri and B. Stoica, *Locality of Gravitational Systems from Entanglement of Conformal Field Theories*, *Phys. Rev. Lett.* **114** (2015) 221601 [1412.1879].

[100] N. Lashkari and M. Van Raamsdonk, *Canonical Energy is Quantum Fisher Information*, *JHEP* **04** (2016) 153 [1508.00897].

[101] N. Lashkari, J. Lin, H. Ooguri, B. Stoica and M. Van Raamsdonk, *Gravitational positive energy theorems from information inequalities*, *PTEP* **2016** (2016) 12C109 [1605.01075].

[102] B. Mosk, *Holographic equivalence between the first law of entanglement entropy and the linearized gravitational equations*, *Phys. Rev.* **D94** (2016) 126001 [1608.06292].

[103] M. Alishahiha, *Holographic Complexity*, *Phys. Rev.* **D92** (2015) 126009 [1509.06614].

[104] D. Momeni, M. Faizal, S. Bahamonde and R. Myrzakulov, *Holographic complexity for time-dependent backgrounds*, *Phys. Lett.* **B762** (2016) 276 [1610.01542].

[105] D. Momeni, S.A. Hosseini Mansoori and R. Myrzakulov, *Holographic Complexity in Gauge/String Superconductors*, *Phys. Lett. B* **756** (2016) 354 [1601.03011].

[106] O. Ben-Ami and D. Carmi, *On Volumes of Subregions in Holography and Complexity*, *JHEP* **11** (2016) 129 [1609.02514].

[107] M. Miyaji, T. Numasawa, N. Shiba, T. Takayanagi and K. Watanabe, *Distance between Quantum States and Gauge-Gravity Duality*, *Phys. Rev. Lett.* **115** (2015) 261602 [1507.07555].

[108] T. Hartman and J. Maldacena, *Time Evolution of Entanglement Entropy from Black Hole Interiors*, *JHEP* **05** (2013) 014 [1303.1080].

[109] T. Jacobson, G. Kang and R.C. Myers, *On black hole entropy*, *Phys. Rev. D* **49** (1994) 6587 [gr-qc/9312023].

[110] M. Cvetic, G.W. Gibbons, D. Kubiznak and C.N. Pope, *Black Hole Enthalpy and an Entropy Inequality for the Thermodynamic Volume*, *Phys. Rev. D* **84** (2011) 024037 [1012.2888].

[111] B.P. Dolan, *The compressibility of rotating black holes in D-dimensions*, *Class. Quant. Grav.* **31** (2014) 035022 [1308.5403].

[112] J.D. Bekenstein, *A Universal Upper Bound on the Entropy to Energy Ratio for Bounded Systems*, *Phys. Rev. D* **23** (1981) 287.

[113] J.D. Bekenstein, *How does the entropy / information bound work?*, *Found. Phys.* **35** (2005) 1805 [quant-ph/0404042].

[114] Y. Sekino and L. Susskind, *Fast Scramblers*, *JHEP* **10** (2008) 065 [0808.2096].

[115] M.R. Dowling and M.A. Nielsen, *The geometry of quantum computation*, *arXiv e-prints* (2006) quant [quant-ph/0701004].

[116] J.D. Brown and M. Henneaux, *Central Charges in the Canonical Realization of Asymptotic Symmetries: An Example from Three-Dimensional Gravity*, *Commun. Math. Phys.* **104** (1986) 207.

[117] R.-G. Cai, S.-M. Ruan, S.-J. Wang, R.-Q. Yang and R.-H. Peng, *Action growth for AdS black holes*, *JHEP* **09** (2016) 161 [1606.08307].

[118] H.-S. Liu and H. Lü, *Thermodynamics of Lifshitz Black Holes*, *JHEP* **12** (2014) 071 [1410.6181].

[119] W.G. Brenna, R.B. Mann and M. Park, *Mass and Thermodynamic Volume in Lifshitz Spacetimes*, *Phys. Rev. D* **92** (2015) 044015 [1505.06331].

[120] B. Czech, L. Lamprou, S. McCandlish and J. Sully, *Integral Geometry and Holography*, *JHEP* **10** (2015) 175 [1505.05515].

[121] B. Czech, P. Hayden, N. Lashkari and B. Swingle, *The Information Theoretic Interpretation of the Length of a Curve*, *JHEP* **06** (2015) 157 [1410.1540].

[122] B. Czech, G. Evenbly, L. Lamprou, S. McCandlish, X.-L. Qi, J. Sully et al., *Tensor network quotient takes the vacuum to the thermal state*, *Phys. Rev. B* **94** (2016) 085101 [1510.07637].

[123] B. Swingle, *Entanglement Renormalization and Holography*, *Phys. Rev.* **D86** (2012) 065007 [0905.1317].

[124] L. Susskind, L. Thorlacius and J. Uglum, *The Stretched horizon and black hole complementarity*, *Phys. Rev.* **D48** (1993) 3743 [hep-th/9306069].

[125] G. 't Hooft, *On the Quantum Structure of a Black Hole*, *Nucl. Phys. B* **256** (1985) 727.

[126] J. Maldacena and L. Susskind, *Cool horizons for entangled black holes*, *Fortsch. Phys.* **61** (2013) 781 [1306.0533].

[127] Z.-Y. Fan and M. Guo, *On the Noether charge and the gravity duals of quantum complexity*, 1805.03796.

[128] B. Czech, J.L. Karczmarek, F. Nogueira and M. Van Raamsdonk, *The Gravity Dual of a Density Matrix*, *Class. Quant. Grav.* **29** (2012) 155009 [1204.1330].

[129] A. Almheiri, X. Dong and D. Harlow, *Bulk Locality and Quantum Error Correction in AdS/CFT*, *JHEP* **04** (2015) 163 [1411.7041].

[130] X. Dong, D. Harlow and A.C. Wall, *Reconstruction of Bulk Operators within the Entanglement Wedge in Gauge-Gravity Duality*, *Phys. Rev. Lett.* **117** (2016) 021601 [1601.05416].

[131] Z. Fu, A. Maloney, D. Marolf, H. Maxfield and Z. Wang, *Holographic complexity is nonlocal*, *JHEP* **02** (2018) 072 [1801.01137].

[132] H. Stoltenberg, *Properties of the (Un)Complexity of Subsystems*, 1807.05218.

[133] K. Umemoto and T. Takayanagi, *Entanglement of purification through holographic duality*, *Nature Phys.* **14** (2018) 573 [1708.09393].

[134] P. Nguyen, T. Devakul, M.G. Halbasch, M.P. Zaletel and B. Swingle, *Entanglement of purification: from spin chains to holography*, *JHEP* **01** (2018) 098 [1709.07424].

[135] N. Bao and I.F. Halpern, *Holographic Inequalities and Entanglement of Purification*, *JHEP* **03** (2018) 006 [1710.07643].

[136] V. Balasubramanian, M. DeCross, A. Kar and O. Parrikar, *Binding Complexity and Multiparty Entanglement*, 1811.04085.

[137] M. Headrick, V.E. Hubeny, A. Lawrence and M. Rangamani, *Causality & holographic entanglement entropy*, *JHEP* **12** (2014) 162 [1408.6300].

[138] A.C. Wall, *Maximin Surfaces, and the Strong Subadditivity of the Covariant Holographic Entanglement Entropy*, *Class. Quant. Grav.* **31** (2014) 225007 [1211.3494].

[139] D.R. Brill, *Multi - black hole geometries in (2+1)-dimensional gravity*, *Phys. Rev.* **D53** (1996) 4133 [gr-qc/9511022].

[140] S. Aminneborg, I. Bengtsson, D. Brill, S. Holst and P. Peldan, *Black holes and wormholes in (2+1)-dimensions*, *Class. Quant. Grav.* **15** (1998) 627 [gr-qc/9707036].

[141] D. Brill, *Black holes and wormholes in (2+1)-dimensions*, gr-qc/9904083.

[142] D. Marolf, H. Maxfield, A. Peach and S.F. Ross, *Hot multiboundary wormholes from bipartite entanglement*, *Class. Quant. Grav.* **32** (2015) 215006 [1506.04128].

[143] V. Balasubramanian, P. Hayden, A. Maloney, D. Marolf and S.F. Ross, *Multiboundary Wormholes and Holographic Entanglement*, *Class. Quant. Grav.* **31** (2014) 185015 [1406.2663].

[144] R. Abt, J. Erdmenger, H. Hinrichsen, C.M. Melby-Thompson, R. Meyer, C. Northe et al., *Topological Complexity in AdS3/CFT2*, 1710.01327.

[145] M. Headrick, *General properties of holographic entanglement entropy*, *JHEP* **03** (2014) 085 [1312.6717].

[146] E. Witten, "*Canonical Quantization in Anti de Sitter Space*, conference talk at 20 Years Later: The Many Faces of AdS/CFT." `http://pcts.princeton.edu/pcts/20YearsAdSCFT/slides+videos.html`, 2017.

[147] F. Estabrook, H. Wahlquist, S. Christensen, B. DeWitt, L. Smarr and E. Tsiang, *Maximally Slicing a Black Hole*, *Physical Review D.* **7** (1973) 2814.

[148] I. Gelfand and S. Fomin, *Calculus of Variations*, Dover Books on Mathematics, Dover Publications (2012).

Vita

Josiah Couch was born in 1990 to Brian and Jennifer Couch and grew up around Duncan, Oklahoma. He graduated in 2013 from Oklahoma State University with B.S. degrees in physics and mathematics. He began his Ph.D. studies in the Department of Physics at the University of Texas at Austin in August 2013. He met his wife Kimberley (UT Alumna, Bachelor of Journalism 2015, Masters of Science in Information Studies 2019) in 2015 at a café near campus. They were married in February of 2020. In January 2021, Josiah started a machine learning position under Professor Jose Bento in the computer science department at Boston College. After graduation, he plans to continue in that position as a postdoctoral research scholar.

Permanent address: 8112A Ceberry Drive, Austin, TX, 78759

This dissertation was typeset with LaTeX[†] by the author.

[†]LaTeX is a document preparation system developed by Leslie Lamport as a special version of Donald Knuth's TeX Program.